



HAL
open science

Contributions to the study of the unresolved resonance range of neutron-induced reactions

Gilles Noguere

► **To cite this version:**

Gilles Noguere. Contributions to the study of the unresolved resonance range of neutron-induced reactions. Nuclear Theory [nucl-th]. Université Bordeaux-1, 2014. tel-01858682

HAL Id: tel-01858682

<https://hal.science/tel-01858682>

Submitted on 21 Aug 2018

HAL is a multi-disciplinary open access archive for the deposit and dissemination of scientific research documents, whether they are published or not. The documents may come from teaching and research institutions in France or abroad, or from public or private research centers.

L'archive ouverte pluridisciplinaire **HAL**, est destinée au dépôt et à la diffusion de documents scientifiques de niveau recherche, publiés ou non, émanant des établissements d'enseignement et de recherche français ou étrangers, des laboratoires publics ou privés.

Mémoire présenté pour obtenir le

DIPLÔME D'HABILITATION À DIRIGER DES RECHERCHES

Spécialité : **Astrophysique, Plasmas, Nucléaire**

par

Gilles NOGUERE

préparé au sein du **SPRC / LEPH** du CEA de Cadarache
et de l'**École Doctorale 209 : Sciences Physiques et de l'Ingénieur**

Contributions à l'étude du domaine en énergie des résonances non résolues des réactions induites par neutrons

HDR soutenue publiquement le **24 juin 2014**,
devant le jury composé de :

Monsieur Igor TSEKHANOVICH

Professeur d'Université Bordeaux I, Président

Monsieur Gérard BARREAU

Directeur de Recherche émérite CNRS, Rapporteur

Monsieur Yaron DANON

Professor and Director Gaertner LINAC Center, Rapporteur

Monsieur Laurent TASSAN-GOT

Directeur de Recherche CNRS, Rapporteur

Monsieur Charles-Olivier BACRI

Directeur de Recherche CNRS

Monsieur Gérald RIMPAULT

Expert International, Professeur INSTN



REMERCIEMENTS

Les études que je réalise depuis une dizaine d'années au sein du groupe Données Nucléaires et Traitement (DNT) du Laboratoire d'Etudes Physiques (LEPh) du CEA de Cadarache, sont principalement consacrées à la mesure et à l'évaluation des sections efficaces des réactions induites par neutrons. La finalité de ces études est de répondre à certains problèmes liés au transport des neutrons dans les Réacteurs à Eau Légère (REL) et dans les Réacteurs à Neutrons Rapides (RNR). Les résultats obtenus contribuent à l'amélioration de la bibliothèque de données nucléaires évaluées JEFF.

Au LEPh, le travail d'évaluation des sections efficaces neutroniques consiste à établir un ensemble cohérent de paramètres de modèle permettant de décrire le domaine des résonances et le « continuum » jusqu'à quelques dizaines de MeV. Dans le domaine des résonances, l'évaluateur se doit de distinguer les domaines des résonances résolues (RRR) et non-résolues (URR). Le domaine des résonances résolues a déjà fait l'objet d'un mémoire présenté par Frank Gunsing à l'Université Paris 7. Aussi, dans ce document, je m'attache à synthétiser les travaux réalisés dans le URR. Ces derniers ont été réalisés avec la participation d'étudiants (stages, thèse, post-doctorat) et de collaborateurs étrangers provenant de différents instituts (Institute for Reference Materials and Measurements, Faculty of Physics of the Bucarest University, Horia Hulubei National Institute of Physics and Nuclear Engineering, Serco Assurance, Oak Ridge National Laboratory, NRG Petten).

Ce travail n'aurait jamais pu aboutir sans les discussions menées avec Olivier Bouland (collègue depuis une dizaine d'années après avoir été mon responsable de thèse), Cyrille De Saint Jean (responsable du LEPh et auteur du code CONRAD), Pascal Archier (codéveloppeur de CONRAD) et Luiz Leal (ORNL, USA). Je tiens particulièrement à remercier ce dernier pour son aide et sa disponibilité lors de la rédaction du manuscrit.

Je remercie chaleureusement Messieurs Yaron Danon (RPI, USA), Gerard Barreau (CENBG), Igor Tsekhanovich (CENBG), Charles-Olivier Bacri (IPNO), Laurent Tassan-Got (IPNO) et Gerald Rimpault (CEA Cadarache) de l'intérêt qu'ils ont porté à ce travail en acceptant d'être rapporteurs ou examinateur. Je leur suis très reconnaissant des remarques et discussions qui ont suivi la soutenance.

Je tiens également à adresser mes plus vifs remerciements à Arjan Koning et Dimitri Rochman (NRG Petten) pour les nombreux échanges tout au long de ces années autour du code TALYS et de la librairie TENDL.

Je souhaite exprimer ma gratitude à Anabella Tudora pour son aide et ses nombreux conseils pendant le Post-doctorat d'Emilie Rich et les travaux de thèse de Claudia Morariu. Je lui suis reconnaissant d'avoir partagé ses connaissances sur la modélisation des sections efficaces de fission dans le « continuum ».

Qu'il me soit permis d'adresser mes remerciements et ma reconnaissance à l'ensemble des membres du groupe DNT du LEPh. Je tiens particulièrement à remercier David Bernard, Pierre Leconte, Olivier Litaize, Yannick Penelieu et Olivier Serot pour leur aide régulière dans des domaines variés allant de la mesure à la qualification des données nucléaires.

J'ai également eu le soutien de ma hiérarchie. Je souhaite remercier chaleureusement Jean-Michel Ruggieri, précédent responsable du LEPh, qui m'a permis de lancer ce projet.

RESUME

Ce document présente la description statistique des sections efficaces neutroniques dans le domaine en énergie des résonances non résolues. La modélisation de la section efficace totale et de la section efficace "shape-elastic" est basée sur le formalisme de la "Matrice-R moyenne". Les sections efficaces partielles décrivant les réactions de captures radiatives, de diffusion élastique, de diffusion inélastique et de fission sont calculées à l'aide du formalisme Hauser-Feshbach avec fluctuations des largeurs. Dans le domaine des résonances non résolues, ces modèles dépendent des paramètres de résonances moyens ("neutron strength function" S_c , espacement moyen entre les résonances D_c , largeur moyenne de réaction partielle $\langle \Gamma_c \rangle$, rayon de voie a_c , rayon effectif R' et paramètre des niveaux distants \overline{R}_c^∞). Les codes (NJOY, CAL-ENDF ...) dédiés au traitement des bibliothèques de données nucléaires (JEFF, ENDF/B, JENDL, CENDL, BROND ...) utilisent les paramètres moyens pour prendre en compte le phénomène d'autoprotection des résonances non résolues, indispensable à la simulation du transport des neutrons par les codes stochastiques (MCNP, TRIPOLI ...) et déterministes (APOLLO, ERANOS ...). Le travail d'évaluation consiste à établir un ensemble cohérent de paramètres moyens dépendants du moment angulaire total du système J et du moment orbital du neutron incident l . Les travaux exposés dans ce document s'attachent à décrire les liens entre les formalismes de la Matrice-S et celui de la "Matrice-R moyenne" pour le calcul des paramètres S_c , \overline{R}_c^∞ , a_c et R' .

Contents

1	Introduction	10
2	The Unresolved Resonance Range of the neutron cross sections	13
2.1	Context	13
2.2	Theoretical framework	15
2.3	Microscopic and integral measurements	15
2.3.1	Post Irradiated Experiments	16
2.3.2	Time of flight technique	16
2.3.3	Measurements on Van Der Graaff accelerator	18
2.3.4	Surrogate measurements	18
3	Wave description of the nuclear scattering in the external region	20
3.1	Definition of the partial-wave channel	20
3.1.1	Conservation laws	20
3.1.2	"L-S" coupling scheme for the R-Matrix formalism	21
3.1.3	"j-j" Coupling scheme for Optical Model calculations	22
3.2	Notions of configuration space for nuclear reactions	23
3.2.1	The internal and external regions	23
3.2.2	The nuclear radius R of spherical nuclei	24
3.2.3	The channel radius a_c	25
3.2.4	The effective radius R'	25
3.3	Elementary wave description of the nuclear scattering	26
3.3.1	The forward scattering amplitude	26
3.3.2	The total and shape-elastic cross sections	28
3.3.3	The compound-nucleus cross section	29
3.4	Connections between the matching and channel radius	30
3.4.1	Diffuse-edge potential	30
3.4.2	Square-well potential approximation	33
3.4.3	Equivalent hard-sphere scattering	34
4	Theory of average cross section within the Reich-Moore approximation	39
4.1	Average R-Matrix approximation	39
4.1.1	Average collision function in the Bethe's assumptions	39
4.1.2	Average R-function in the uniform level approximation	41
4.1.3	Average cross sections	44
4.1.4	Neutron transmission coefficients	44
4.2	Average R-Matrix parameters	46
4.2.1	Generalization of the SPRT method	47
4.2.2	Neutron strength function	48

4.2.3	Low neutron energy approximations	50
5	Conclusions	56
6	Perspectives	57
6.1	Statistical nature of the neutron resonances	57
6.2	Extension of the Resolved Resonance Range	57
6.3	Systematic behavior of the average parameters	58
	Appendices	64
A	SPRT method	64
B	Average cross section of Neptunium	76
C	Average cross section of Hafnium	90

List of Tables

3.1	Equivalent hard-sphere channel radii obtained from the least squares fit of the phase shift calculated by ECIS for the nuclear system $^{241}\text{Am}+n$	38
3.2	Comparison of the equivalent hard-sphere radius for the nuclear system $^{241}\text{Am}+n$ with results obtained from Eqs. (3.16), (3.52) and (3.53).	38
4.1	Neutron strength functions S_l and distant level parameters \overline{R}_l^∞ obtained with the SPRT method (Eqs. (4.35) and (4.36)) for the nuclear system $^{241}\text{Am}+n$. The channel radii a_c are taken from Tables 3.1 and 3.2. The coupled channel calculations were performed with ECIS by using the parameters reported in the Japanese library JENDL-4. Results are compared with those reported in Refs. [28, 69].	54
4.2	Effective radius R' calculated with optical models described in Refs. [20–22] and reported in the Atlas of Neutron Resonances [28]. For $^{241}\text{Am}+n$, the given radius is a preliminary result.	55

List of Figures

1.1	Simplified representation of the compound and direct processes [4].	11
1.2	Capture cross sections of ^{238}U , ^{235}U and ^{239}Pu compared to SFR neutron spectrum.	12
2.1	Comparison of the Unresolved Resonance Range for ^{240}Pu in JEFF-3.0 and JEFF-3.1.1. The experimental data were retrieved from EXFOR.	14
2.2	^{151}Sm capture cross section deduced from the PROFIL experiment with the IDA technique of the CONRAD code. The theoretical calculations were performed with the ECIS and TALYS codes. The experimental data were retrieved from EXFOR.	16
2.3	capture yield and transmission data for ^{241}Am measured at the GELINA facility with the time of flight technique [69].	17
2.4	^{241}Am fission and capture cross sections calculated from the fission probability measured by the surrogate technique [31].	19
3.1	Coupling scheme used in the R-matrix formalism (left hand plot) and in optical model calculations (right hand plot).	21
3.2	Total, shape-elastic and reaction cross sections for $^{241}\text{Am}+n$ calculated with the ECIS code by using the optical model parameters reported in the Japanese library JENDL-4. The data for the total cross section were retrieved from EXFOR.	24
3.3	Illustration of the scattering of an incoming plane wave (top plot) by a localized repulsive centrifugal potential. The outgoing wave function (middle plot) beyond the range of the potential has the form given by Eq. (3.18).	27
3.4	Matter density distribution (top plot) and real part of the volume potential (bottom plot) for the nuclear system $^{241}\text{Am}+n$. The densities ρ_n and ρ_p are taken from the AMEDE data base [56]. The channel radius a_c is calculated with the ENDF convention (3.16).	32
3.5	Comparison of the channel radius calculated with the expressions (3.16) and (3.52). The reduced radius r_0 and the surface diffuseness a of the real part of the volume potential are calculated with Eqs (3.47) and (3.48).	34
3.6	Total, shape and reaction cross sections for $^{208}\text{Pb}+n$ calculated with the spherical optical model of CONRAD with parameters of Ref. [54] for different values of channel radius.	35
3.7	Energy dependence of the phase shift ($l = 0, 1, 2$) calculated with the optical model code ECIS for the nuclear system $^{241}\text{Am}+n$ in log-log and log-lin scales. The open circles represent the equivalent hard-sphere phase shift calculated with Eq. (3.63).	37

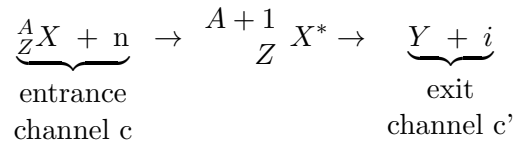
4.1	Modelisation of the ^{239}Pu capture cross section with non zero background s_c^{loc} .	42
4.2	Total cross sections for the hafnium isotopes obtained with the average R-Matrix formalism of the CONRAD code. The optical model calculations, performed with the ECIS code, are based on the parameters given in Ref [20]. Parameters β_2 and β_4 define the dipole and quadrupole deformation parameters. The data for the total cross section were retrieved from EXFOR.	45
4.3	Schematic description of the SPRT method established by Delaroche et al. [64]. The standard SPRT method provides an estimate of the neutron strength functions (S_0 and S_1) and potential scattering length R' via the neutron transmission coefficients and the shape-elastic cross section calculated by Optical Model.	47
4.4	Partial wave breakdown calculations performed with the generalization of the SPRT method on $^{131}\text{Xe}+n$ up to $l = 4$	48
4.5	Systematic behavior of the s- and p-wave neutron strength functions with the mass number of the compound nucleus. Values for Iodine, Xenon, Hafnium, Neptunium and Americium are compared with data compiled in the RIPL library.	50
4.6	Neutron strength functions (top plot) and distant level parameters (bottom plot) obtained with the SPRT method (Eqs. (4.35) and (4.36)) for the nuclear system $^{241}\text{Am}+n$. Channel radii calculated in the equivalent hard-sphere approximation and in the ENDF convention are reported in Tables 3.1 and 3.2. The coupled channel calculations were performed with ECIS by using the parameters reported in the Japanese library JENDL-4.	51
4.7	Distant level parameters obtained with the SPRT method (Eq. (4.35)) for the nuclear system $^{241}\text{Am}+n$ by using the channel radius of the ENDF convention (3.2). The coupled channel calculations were performed with ECIS by using the parameters reported in the Japanese library JENDL-4.	52
4.8	Comparison of the neutron transmission coefficients provided by the ECIS code and calculated with Eqs. (4.45) for the nuclear system $^{241}\text{Am}+n$. The equivalent hard sphere radii of Table 3.1 are used. The coupled channel calculations were performed with ECIS by using the parameters reported in the Japanese library JENDL-4.	53
6.1	^{135}Xe capture cross section from JEFF-311 (top plot) and reconstructed via average R-Matrix parameters calculated with the SPRT method under the Equivalent hard-sphere approximation (bottom plot). The optical model used for the SPRT calculations is described in Ref. [22].	58
6.2	Extension of the Resolved Resonance Range of ^{241}Am with ladders of resonances whose partial widths were calculated via the SPRT method and the equivalent hard-sphere radius formalism.	59

Chapter 1

Introduction

Whenever the nuclei of a given species are bombarded with neutrons, nuclear reactions can be observed with probabilities expressed as cross sections in units of barns. In the range of neutron reactions from thermal to MeV energies, two processes can be distinguished: the compound nucleus reactions and the direct reactions.

When neutrons collide with a nucleus, they may form long-lived compound states of very high complexity, decaying usually via particle production, γ -decay or fission. A resonance is observed when the energy of the compound system corresponds to that of an excited state. In the framework of the Bohr compound nucleus theory, a neutron induced reaction is considered as a two-step process:



The complex interactions between the nucleons lead to the independence hypothesis according to which the formation and the decay of the compound nucleus are independent. In some events, the incident neutron may be directly absorbed without intermediate state. The direct reaction is a one-step reaction in which the nucleons which do not participate to the reaction are left undisturbed. Direct reactions play a dominant role at neutron energies higher than few hundred of keV. Direct processes of interest for this work are the direct inelastic and shape-elastic cross sections. In the case where the target is in an excited state, the direct process to the ground state is often call superelastic (Fig. 1.1).

At intermediate energies, the resonances are not fully resolved owing to the limitation of the experimental resolution of the facility. Thus, two resonance regions can be distinguished, that of the resolved resonances (RRR) and that of the unresolved resonances (URR). The former is parameterized in terms of R-Matrix parameters (resonance energies and partial widths). The URR is analyzed on the basis of the statistical properties of the resonance parameters. Figure 1.2 shows the energy limits of the Unresolved Resonance Range for the capture cross sections of ^{238}U , ^{235}U and ^{239}Pu . The comparison with a neutron spectrum of sodium-cooled fast reactor (SFR) indicate the energy range of interest for fast reactor applications.

The URR is characterized by the coexistence of the compound nucleus and direct reactions.

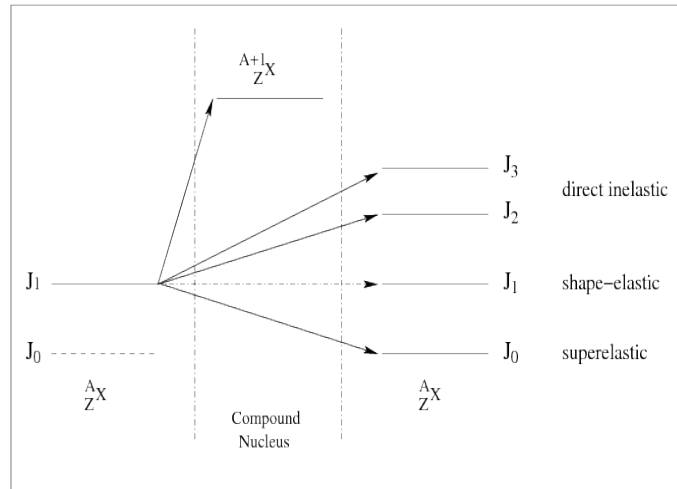


Figure 1.1: Simplified representation of the compound and direct processes [4].

This coexistence makes it difficult for the interpretation of the neutron cross sections in terms of average parameters. In the low energy range, the neutron cross sections are calculated with the Single-Level Breit-Wigner, Multi-Level Breit-Wigner or Reich-Moore approximations of the R-Matrix theory [1]. They involve arbitrary boundary condition parameters that do not play a very conspicuous role [2]. Direct reactions do not readily emerge from them. Usually, their contributions arise from unknown distant levels.

In the high neutron energy range, the neutron cross sections are calculated with optical and statistical models. The optical model calculations rely on the wave description of the nuclear scattering through the S-matrix theory. The aim of the present document is to accommodate such a wave description within the R-Matrix framework. This idea was introduced in the early 60s but never used to produce consistent sets of average parameters for Evaluated Nuclear Data Files in ENDF-6 format [3].

This document is structured as follows. The 2nd chapter will introduce the context of the present studies, the theoretical framework and the type of experimental data used for the analysis of the Unresolved Resonance Range. Chapter 3 will give elementary wave descriptions of the nuclear scattering in the S-Matrix formalism. The average R-Matrix formalism will be presented in chapter 4. Few perspectives and the overall conclusions will be given in chapters 5 and 6. Documents reported in appendix present relationships between the S-Matrix and the R-Matrix theories, thanks to the generalization of the SPRT method, and provide results for fissile (Neptunium) and non-fissile (Hafnium) isotopes.

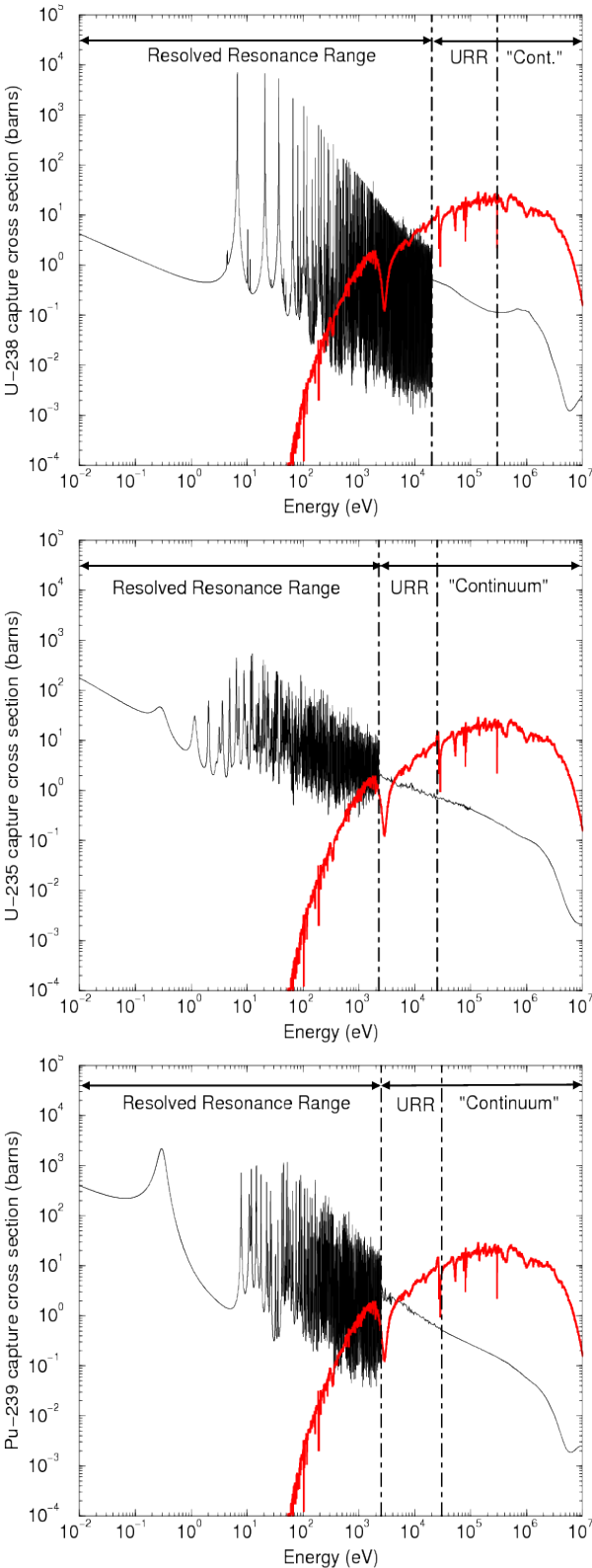


Figure 1.2: Capture cross sections of ²³⁸U, ²³⁵U and ²³⁹Pu compared to SFR neutron spectrum.

Chapter 2

The Unresolved Resonance Range of the neutron cross sections

The evaluation of the neutron cross sections aims to provide model parameters that describe the Resolved Resonance Range (RRR) and the "continuum" of the neutron induced reactions up to tens of MeV. Between the RRR and the "continuum", one has to distinguish the Unresolved Resonance Range (URR). This chapter summarizes the context of the studies carried out on the URR by the nuclear data group of Cadarache with the participation of students and collaborators from different institutes (Institute for Reference Materials and Measurements, Faculty of Physics of Bucarest, Horia Hulubei National Institute of Physics and Nuclear Engineering, Serco Assurance, Oak Ridge National Laboratory, Centre d'Etudes Nucleaires de Bordeaux Gradignan, Nuclear Research and Consultancy Group NRG). A short introduction of the theoretical background is given, followed by a presentation of the integral and microscopic data of interest for this work.

2.1 Context

The Unresolved Resonance Range is an energy range between the resolved resonances and the "continuum". In the URR, the spacing between the resonances and the time resolution of the time-of-flight spectrometers no longer allow the analysis of individual resonances. As a consequence, the evaluation work consists of modeling the average behavior of the neutron cross sections with "average resonance parameters". The average parameters of interest are the neutron strength function S_c , the mean level spacing D_c and the average value of the partial reaction widths $\langle \Gamma_c \rangle$.

Average parameters are essential for neutron transport simulations. Processing codes, such as CALENDAR and NJOY, use the average parameters for generating Probability Tables (PT) associated with the capture, fission elastic and inelastic reactions [5]. The PT are then used by the deterministic (APOLLO2, ERANOS) and stochastic (TRIPOLI, MCNP) codes to simulate the "natural" fluctuations of the cross sections.

There is an abundant literature exploring the formalism of the Probability Tables and its impact on neutronic calculations [6, 7]. A recent study was performed on well-defined assemblies of the MASURCA reactor in order to quantify the effect of the Probability Tables on the reactivity calculated by ERANOS, MCNP and TRIPOLI [8]. This study focuses on

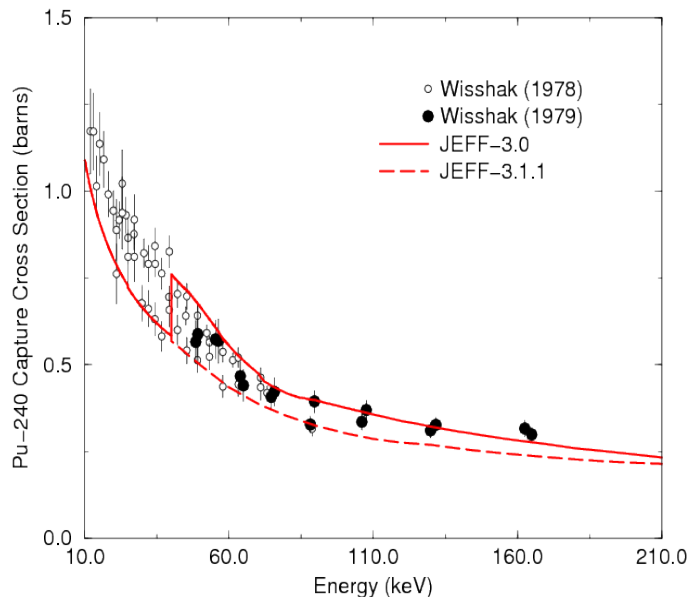


Figure 2.1: Comparison of the Unresolved Resonance Range for ^{240}Pu in JEFF-3.0 and JEFF-3.1.1. The experimental data were retrieved from EXFOR.

the Probability Tables of ^{238}U and ^{239}Pu . For benchmark systems where uranium is present, non-negligible changes on the multiplication factor ranging from 300 pcm to 1000 pcm are observed. The magnitude of the calculated effects depends on the shape of the neutron flux and on the energy bounds of the URR (Fig. 1.2).

A better understanding of the URR was motivated by several problems found in the evaluated nuclear data files. One of the recurrent problems can be illustrated with the URR of ^{240}Pu recommended in a previous version of the European library JEFF-3.0, released in the early 2000s. Integral results reported in Ref. [9, 10] showed a systematic overestimation greater than 4% of the experimental ratio $^{241}\text{Pu}/^{240}\text{Pu}$ by the ERANOS calculations. Sensitivity studies indicated that the origin of the overestimation was the inconsistent description of the unresolved resonance and "continuum" ranges around 40 keV for ^{240}Pu (Fig. 2.1).

More recently, works performed in the frame of the international working group WPEC/SG-32 have confirmed several inconsistencies in the modeling of the Unresolved Resonance Range of ^{239}Pu [11]. One of them was identified with a simplified simulation of a plutonium sphere and with a more realistic simulation of a ZONA2 assembly of MASURCA [8, 12]. Significant differences close to 300 pcm between MCNP and TRIPOLI calculations showed the inconsistent interpretation of the average parameters by the processing codes CALENDF and NJOY.

Some of the observed problems were corrected in the latest version of the European library. However, few questions still remain concerning the representation of the fluctuations of the neutron cross sections between the RRR and the "continuum".

2.2 Theoretical framework

The statistical theory is the basic principle of the analytical treatment of the Unresolved Resonance Range. In the late 80s, this treatment was implemented by Frohner in his FITACS code in the analyze of the ^{238}U neutron cross sections below 200 keV [13]. FITACS uses the average R-Matrix theory to describe the total and shape-elastic cross sections. The Hauser-Feshbach formalism with Moldauer's prescriptions for the width fluctuations is used to describe the partial cross sections (radiative capture, fission, elastic and inelastic scattering). For the fission reaction, the transmission coefficients through a parabolic barrier are calculated with the Hill-Wheeler formula. The average parameters introduced in the FITACS calculations are the mean level spacing D_l , the neutron strength function S_l , the average radiation width $\langle\Gamma_\gamma\rangle$, the channel radius a_c and the distant level parameter R_l^∞ .

The treatment of the Unresolved Resonance Range of the neutron cross sections has changed little since the 90s. More than 10 years after the work of Frohner on ^{238}U , a similar analysis was carried out by introducing FITACS in the nuclear data code SAMMY [14]. Recently, the work of Frohner has also been introduced in the CONRAD code in order to investigate marginalization techniques for the propagation of the uncertainties in the URR [15]. In 2001, Koyumdjieva proposed a new modeling of the URR based on the characteristic function of the R-matrix [16]. In 2003, Leal analyzed the Unresolved Resonance Range of ^{235}U by using the principle of the Probability Tables [17]. More recently, Sirakov proposed to use optical model calculations to analyze the Unresolved Resonance Range of ^{232}Th [18]. A similar approach was developed by the nuclear data group of Cadarache [19].

The methodology consists in replacing FITACS by optical and statistical model calculations. Parameters of the high energy models are determined from the least square fit of experimental data with constraints on s -wave average parameters. The latter constraints are deduced from the statistical analysis of the resolved resonance parameters. This approach facilitates the modeling of the URR and enhances the long and tedious Neutron Resonance Shape Analysis. However, the agreement between the low and high energy ranges is not always achieved. This requires further studies to understand and eliminate the discontinuities. Several iterations are needed to find a satisfactory compromise between the average parameters. Studies carried out on non-fissile and fertile isotopes have shown the relevance of the existing approaches [20–22]. However, the systematic behavior with the target mass of the average parameters cannot be improved without reliable and accurate experimental data.

2.3 Microscopic and integral measurements

The evaluation of the neutron cross sections requires a precise knowledge of the experimental conditions and of the main sources of uncertainties, which affect the accuracy of the data. For these reasons, the nuclear data group of Cadarache is often involved in experimental programs through collaborations with national or European institutes (Institut Laue-Langevin, Centre d'Etudes Nucléaire de Bordeaux Gradignan, Institute for Reference Materials and Measurements, Institute of Isotopes Hungarian Academy of Sciences).

Among measurements of interest for the modelling of the Unresolved Resonance Range, we have to distinguish the integral and microscopic measurements (differential data). For the integral data, the evaluation work can take into account results provided by the CEA facilities (PHENIX, MINERVE, EOLE and MASURCA reactors). For the microscopic data, we often

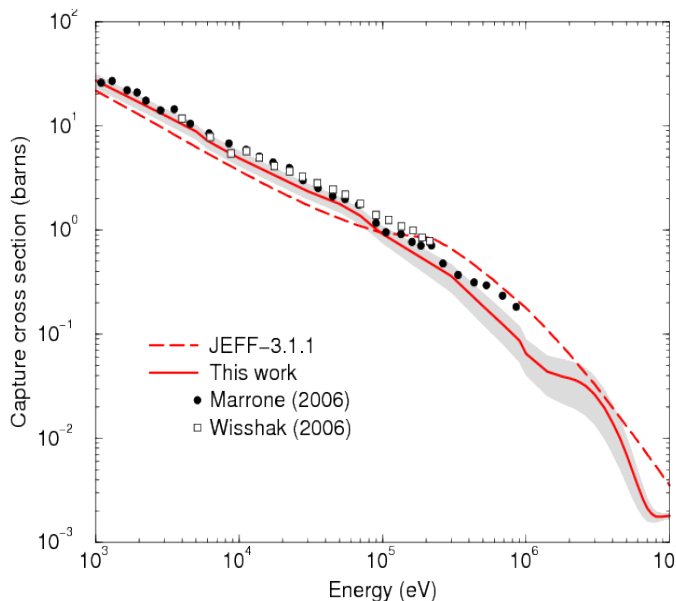


Figure 2.2: ^{151}Sm capture cross section deduced from the PROFIL experiment with the IDA technique of the CONRAD code. The theoretical calculations were performed with the ECIS and TALYS codes. The experimental data were retrieved from EXFOR.

use time of flight measurements performed on the GELINA facility and results provided by the Van der Graaff facility of FZK. In the latest evaluation work on ^{241}Am , we also take into account fission probabilities measured on the Tandem accelerator of Orsay thanks to the transfer reaction technique.

2.3.1 Post Irradiated Experiments

The evaluation procedure of the neutron cross sections requires integral results which are sensitive to a limited number of nuclear data. Post Irradiated Experiments performed on separate samples, such as PROFIL and PROFIL-2 in the PHENIX reactor of CEA Marcoule, represent valuable sources of information to determine reliable average parameters over a large number of isotopes [9, 10].

The PROFIL results have already been used to improve the ^{242}Pu capture cross sections with a standard evaluation procedure [23]. The procedure consists in optimizing the values of the model parameters on microscopic measurements and to test the final evaluation with integral data. In order to simplify such a procedure, the Integral Data Assimilation technique (IDA) has been developed in the CONRAD code [24]. The IDA allows analyzing simultaneously or sequentially integral and microscopic experiments. Figure 2.2 shows the ^{151}Sm capture cross sections deduced from the PROFIL data with the IDA technique [25].

2.3.2 Time of flight technique

The time of flight technique is the experimental method used to measure energy dependent cross-section data. In Europe, experimental results are produced at the nTOF facility (CERN) and at the GELINA facility of the IRMM (Geel, Belgium). In the early 2000s, major upgrades of the GELINA facility allowed to achieve excellent level of accuracy on fission

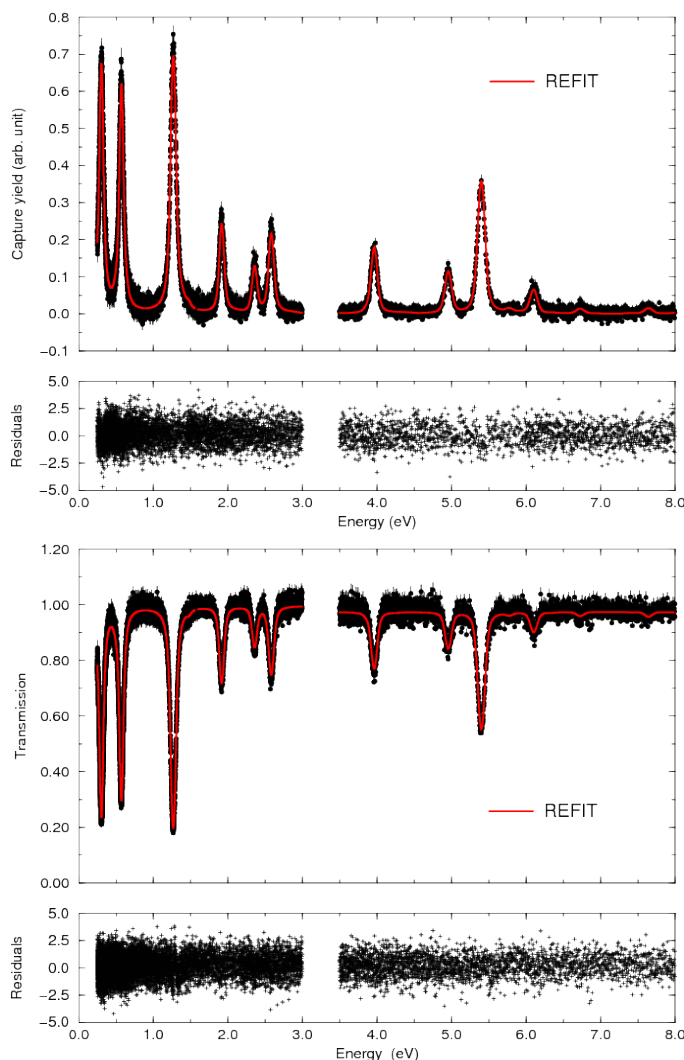


Figure 2.3: capture yield and transmission data for ^{241}Am measured at the GELINA facility with the time of flight technique [69].

and capture cross sections and transmission measurements. These high-resolution data are crucial in the data evaluation process.

Neutron Resonance Shape Analysis (NRSA) consists of determining the energies and the partial widths of the observed structures with the R-Matrix theory. Numerous experimental corrections have to be included in the analysis. The main corrections are related to the Doppler effect, the time resolution of the spectrometer, the normalization, the background and the sample composition. The resonance evaluation code REFIT [27] is the reference code for the analysis of the data measured at the GELINA facility (Fig. 2.3). One goal of the nuclear data group of Cadarache is to produce equivalent results with the CONRAD code.

2.3.3 Measurements on Van Der Graaff accelerator

Beyond the threshold of the inelastic cross section, GELINA are not suitable for precise measurements of radiative capture cross sections. It is thus preferable to use data measured with accelerators such as the Van der Graaff facility of Karlsruhe (see Figs. 2.1 and 2.2). Many experimental results covering the needs of sodium fast reactors have been measured in the context of stellar nucleosynthesis studies. Indeed, the temperatures of interest for the existing models range from $kT = 5$ keV to 1 MeV. Such measures have been used in the compilations of the neutron resonances in order to recommend capture cross sections at 30 keV for a large number of isotopes [28, 29]. These recommended values are of great interest to determine reliable values for the γ -ray transmission coefficients involved in the statistical modeling of the capture cross sections.

2.3.4 Surrogate measurements

The experimental databases have many shortcomings. Some of them are mainly due to technical difficulties related to the direct measurement of neutron cross sections of radioactive isotopes. The experimental activities conducted at the Centre d'Etudes Nucleaires de Bordeaux Gradignan (CENBG) have shown that these difficulties could be overcome for the fission cross sections with transfer reactions induced by light charged particles. The validity of such measurements is still under investigation [30].

One of the latest experimental campaign [31] provided fission probabilities which were used for the modeling of the ^{241}Am neutron induced reactions. Figure 2.4 shows the fission and capture cross sections calculated in CONRAD with "bin-by-bin" correction factors given the fission probability of ^{242}Am .

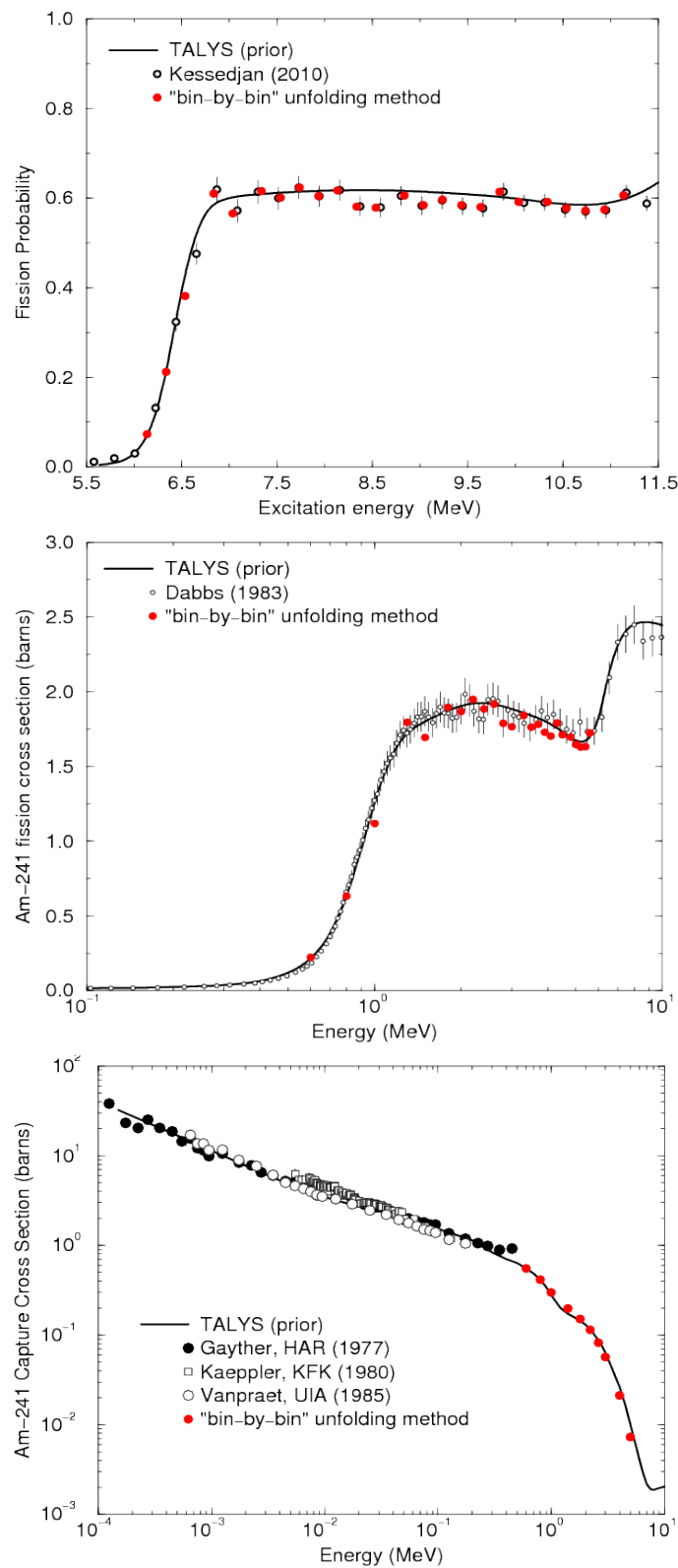


Figure 2.4: ^{241}Am fission and capture cross sections calculated from the fission probability measured by the surrogate technique [31].

Chapter 3

Wave description of the nuclear scattering in the external region

Before introducing the theory of average cross sections used to establish the average resonance parameters, a short description of the wave description of the nuclear scattering is presented in this chapter. The main expressions of interest for the modeling of the Unresolved Resonance Range in terms of partial-wave channels are given with a special emphasis on the connections between the channel radius a_c , nuclear radius R , potential scattering length R' , matching radius r_m and distant level parameter \overline{R}_c^∞ .

3.1 Definition of the partial-wave channel

The neutron cross section formalisms presented in this document give a phenomenological description of binary reactions between a projectile and a target nucleus in terms of wave functions for the entrance and exit channels. This presentation guesses the definition of what we call a "partial-wave" channel c . As indicated in Ref. [32], the concept of reaction channel was first introduced by Wigner and Eisenbud (unpublished) and Breit [33]. It corresponds to the identification of a pair of particles characterized by a total angular momentum J and a parity π .

3.1.1 Conservation laws

In the definition of the entrance channel c (incoming particle+target nucleus), it is convenient to include the spin I (and the parity π_I) of the target nucleus, the spin i (and the parity π_i) of the incident particle and features of their relative motion via the orbital momentum l . The same set of quantum numbers with a prime are commonly used to define the exit channel c' (outgoing particle+residual nucleus).

An interaction may occur if the total angular momentum and parity $J^{\pi'}$ of the exit channel c' is equal to the J^π value of the entrance channel c . According to the conservation laws $\vec{J} = \vec{J}'$ and $\pi = \pi'$. The parity and the total angular momentum of the compound system are given, respectively, by:

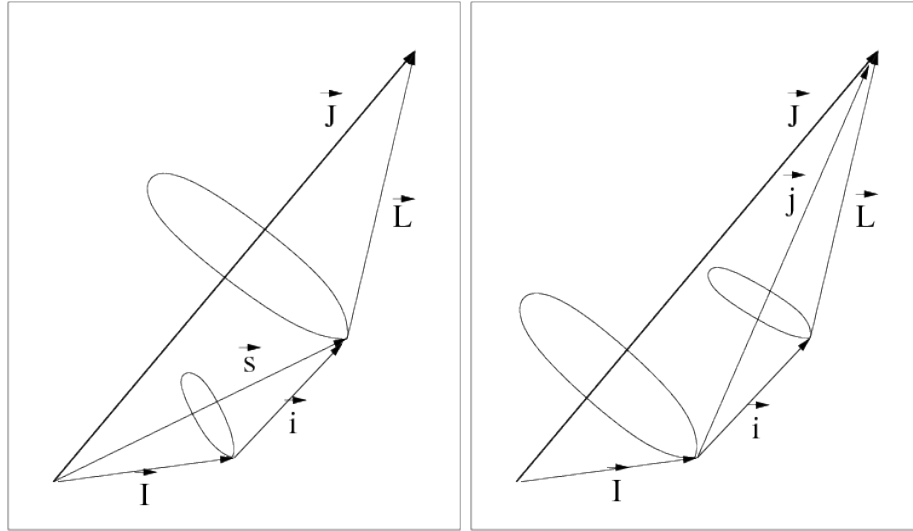


Figure 3.1: Coupling scheme used in the R-matrix formalism (left hand plot) and in optical model calculations (right hand plot).

$$\pi = \begin{cases} (-1)^l \pi_I \pi_i, \\ (-1)^{l'} \pi_{I'} \pi_{i'}, \end{cases} \quad (3.1)$$

and

$$\vec{J} = \begin{cases} \vec{l} + \vec{i} + \vec{I}, \\ \vec{l}' + \vec{i}' + \vec{I}'. \end{cases} \quad (3.2)$$

As introduced by Lane and Thomas [1], two extreme vector combinations can be applied to reach the total angular momentum J of the compound system. By analogy with the spectroscopic notations in atomic physics [34], a coupling scheme which is nearly equivalent to the "L-S" coupling shell-model is historically used to solve the vector combination problem at low incident energies while the "j-j" coupling shell-model is adopted for high bombarding energies (Fig. 3.1).

3.1.2 "L-S" coupling scheme for the R-Matrix formalism

The "L-S" coupling scheme is suitable for the R-Matrix representation of the compound nucleus in the Resolved Resonance Range where a limited number of angular momenta can contribute to a neutron induced reaction. At low neutron energies, it is convenient to presume that the individual spin of the target and projectile are coupled to produce the channel spin s [35]. In this case, the total angular momentum J is formed by combining l and s as follows:

$$\vec{J} = \vec{l} + \vec{s}, \quad (3.3)$$

where

$$\vec{s} = \vec{I} + \vec{i}. \quad (3.4)$$

Their vectorial combinations lead to the following expressions:

$$|I - i| \leq s \leq I + i, \quad (3.5)$$

and

$$|l - s| \leq J \leq l + s. \quad (3.6)$$

In the resonance range, it is impossible in most experimental cases to distinguish between channels which differ only in their channel spins s . As a consequence, the channel spin can be arbitrarily removed from the set of quantum numbers and the index c will refer simply to the pair $\{l, J\}$.

3.1.3 "j-j" Coupling scheme for Optical Model calculations

At high energy, the spin-orbit interactions become as strong as the interactions between the individual spins of the target and projectile. In this case, we can couple vectorially the spin i of the projectile to its orbital angular momentum l and define a total angular momentum j . The channel c is defined by the set of quantum numbers $\{l, j, J\}$. The total angular momentum J of the whole system is defined by:

$$\vec{J} = \vec{I} + \vec{j}, \quad (3.7)$$

where

$$\vec{j} = \vec{l} + \vec{i}. \quad (3.8)$$

For neutron induced reactions, j can take two different values:

$$\begin{cases} j = l - \frac{1}{2}, \\ j = l + \frac{1}{2}, \end{cases} \quad (3.9)$$

and the total angular momentum can take values between:

$$|j - I| \leq J \leq j + I, \quad (3.10)$$

In the ground state channel, for target nucleus with $I = 0$, we have $J = j$. In that case, the "L-S" and "j-j" coupling schemes become equivalent.

3.2 Notions of configuration space for nuclear reactions

3.2.1 The internal and external regions

Central to the R-Matrix and Optical Model frameworks is the division of the configuration space at an appropriate matching radius chosen to match the solution of the Schrodinger equation with its corresponding asymptotic expression.

The notions of "internal" (or "interior") and "external" regions were introduced by Kapur and Peierls [36] and re-formulated by Wigner and Eisenbud in the 1940s. In this early picture, the compound nucleus in which all of the nucleons are in a resonance state is assumed to exist within the volume defined by the "internal" region. So that, the total cross section $\sigma_t^{(n)}$ for the interaction between a neutron and a nucleus in the ground state ($n = 0$), or in an excited state ($n > 0$), can be viewed as being partitioned as [4]:

$$\sigma_t^{(n)}(E) = \sigma_C^{(n)}(E) + \sum_{n'} \sigma_D^{(n,n')}(E). \quad (3.11)$$

The cross section $\sigma_C^{(n)}$ for formation of the compound nucleus corresponds to the contribution of the various partial-wave channels c through which the compound nucleus can be formed when the target is at the n -th level.

The combined cross sections $\sigma_D^{(n,n')}$ denote the reactions which proceed through direct and pre-equilibrium mechanisms from the n -th to the n' -th levels. Suitable expressions for the cross sections of the nuclear reactions, that take place outside the "internal" region, emerge from the partial wave analysis of the scattering process (see section 3.3).

In the present work, we limit ourselves to consider neutron-induced reactions in channels corresponding to the ground-state of the target ($n = 0$) for incident energies below the excitation energy of the second inelastic level ($n' = 0, 1$). The expression (3.11) becomes:

$$\sigma_t^{(0)}(E) = \sigma_C^{(0)}(E) + \sigma_D^{(0,0)}(E) + \sigma_D^{(0,1)}(E). \quad (3.12)$$

If the emission of charged light particles are not energetically possible, the special cases $n' = 0$ and $n' = 1$ are the shape-elastic (σ_e) and the direct inelastic-scattering (σ_D) cross sections, respectively. The former is defined as the cross section for scattering without change of the quantum state of the nucleus [37]. In that case, the total cross section is given by:

$$\sigma_t(E) = \sigma_r(E) + \sigma_e(E), \quad (3.13)$$

where the reaction cross section σ_r is defined as:

$$\sigma_r(E) = \sigma_C(E) + \sigma_D(E), \quad (3.14)$$

in which the absence of index n is equivalent to the notation $n = 0$. Figure 3.2 displays the total, shape-elastic and reaction cross sections calculated with the optical model code

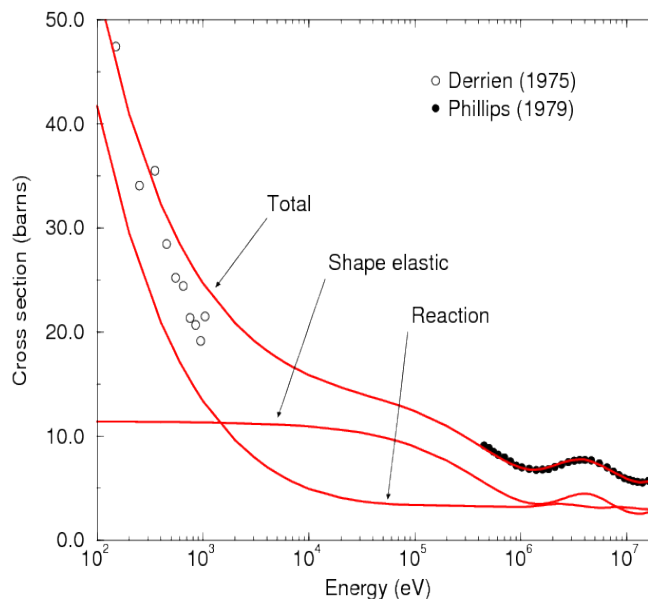


Figure 3.2: Total, shape-elastic and reaction cross sections for $^{241}\text{Am}+n$ calculated with the ECIS code by using the optical model parameters reported in the Japanese library JENDL-4. The data for the total cross section were retrieved from EXFOR.

ECIS [38] for the nuclear reaction $^{241}\text{Am}+n$.

3.2.2 The nuclear radius R of spherical nuclei

The division of the configuration space is based on the condition that all particles are relatively close together. In other words, the physical reason why the space can be divided into such external and internal regions is that the strong nuclear forces between nucleons are rather short range. For practical reasons, the internal region of many nuclei can be described by independent particle motion in a mean field potential that has spherical symmetry. In the 50s, optical model calculations showed that the experimental neutron total cross sections as well as the angular dependence of the elastic scattering data were well reproduced in the MeV energy range assuming that the A nucleons are uniformly distributed throughout a sphere of radius:

$$R = r_0 A^{1/3}. \quad (3.15)$$

Wrong values of nuclear radius were often reported because the earlier models had an unrealistic amount of wave reflexion [39]. Therefore, the attenuation of absorption was probably compensated by an increase of r_0 . First values found in the literature range between 1.4 fm to 1.5 fm, while values lower than 1.3 fm are expected with the latest optical model calculations [40].

3.2.3 The channel radius a_c

The abrupt separation between the internal and external region is made by a choice of an imaginary closed surface of radius a_c which is not necessarily equal to the nuclear radius R [41]. The quantity a_c is called the "interaction radius" by Lane and Thomas [1] or the "matching radius" when it explicitly refers to a boundary condition parameter between the internal and external regions [42]. Here, we adopt the widely accepted definition of "channel radius".

The size of the internal region is not defined. Kapur and Peierls suggest making the internal region as small as possible but slightly larger than the radius of the nucleus to ensure that all nuclear effects are confined to the internal region [36]. Similar prescriptions were given by Wigner and Eisenbud [35] and recalled by Vogt in Ref. [43]. In many applications the values of a_c are chosen more or less arbitrarily. In the community of the evaluated nuclear data, the channel radius a_c is defined as a simple function of the target mass plus a constant term [3]:

$$a_c = 1.23m_A^{1/3} + 0.8 \quad (\text{in fm}). \quad (3.16)$$

Such a phenomenological representation dates back to 1950. Values of the parameters equal to 1.26 fm and 0.75 fm were reported by Drell in Ref. [44]. The order of magnitude of the constant term (0.8 fm) could also be explained by using the Droplet Model nuclear density distribution proposed by Myers [45] with a parameterization given in Ref. [46]. It takes into account the dilatation due to several effects such as the surface tension, the neutron excess and the Coulomb repulsion that occurs for finite nuclei.

The relationship between a_c and the nuclear radius R is clarified in section 3.4 assuming that the nuclear mean-field has a diffuse-edge of the Wood Saxon type with a mid-point radius equal to R .

3.2.4 The effective radius R'

At low neutron energies, the shape-elastic cross section σ_e of Eq. (3.13) becomes the potential scattering cross section σ_p [47] whose expression is similar to the scattering of a hard sphere of radius R' :

$$\sigma_p = 4\pi R'^2, \quad (3.17)$$

The so-called potential scattering length R' mimics the classical radius of an impenetrable sphere described by a hard-sphere potential that is infinitely repulsive for $r < R'$ and zero outside.

The relationship between the effective radius R' and the channel radius a_c is established in section 4.2.3 via the distant level parameter \overline{R}_c^∞ involved in the average R-Matrix formalism.

3.3 Elementary wave description of the nuclear scattering

Usually, the index c (entrance channel) and c' (exit channel) are used to label the generic quantities involved in the mathematical description of the nuclear reactions. In the present work, we are interested only on the angle-integrated probability of getting the final results for c' given c . Therefore, in the following expressions, the subscript c' is dropped.

3.3.1 The forward scattering amplitude

Many of the literatures and lecture notes on the scattering theory give a short review of the ingredients involved in the description of the neutron cross sections. Some of them are presented below. For our purpose, we consider the idealized situation where a "free" neutron with a well defined energy and momentum is scattered by a single nucleus which is fixed in position. A solution of this simple scattering process is given by solving the time-independent Schrodinger equation for a plane wave $\exp(i\vec{k}\cdot\vec{r})$ impinging on a localized repulsive centrifugal potential. The potential refers to the motion of particles under the influence of central forces "directed" away from the origin [34]. The asymptotic form of the external wave function far away the scattering region ($r \rightarrow \infty$) is the sum of the incident plane wave plus an outgoing spherical wave (Fig. 3.3):

$$\psi(E, r, \theta, \phi) \propto e^{ikr \cos(\theta)} + f(E, \theta, \phi) \frac{e^{ikr}}{r}. \quad (3.18)$$

The scattering amplitude $f(E, \theta, \phi)$ has the dimension of length and the angles (θ, ϕ) are measured with respect to the ingoing direction. The wave nature of the neutron is defined by the neutron wave number of length k . For non-relativistic neutrons, the wave number is given by:

$$k = \sqrt{\frac{2m_n E}{\hbar^2}}. \quad (3.19)$$

If the neutron energy E is in eV, k is calculated as follows:

$$k = 2.1968 \times 10^{-3} \left(\frac{A}{A+1} \right) \sqrt{E} \quad (3.20)$$

If we consider a spherically symmetric potential $V(r)$, the scattering amplitude $f(E, \theta, \phi)$ of Eq. (3.18) becomes independent of the azimuthal angle ϕ :

$$f(E, \theta, \phi) = f(E, \theta), \quad (3.21)$$

and the partial wave expansion of the original plane wave in Legendre polynomials allows to break the scattering amplitude $f(E, \theta)$ into partial wave components

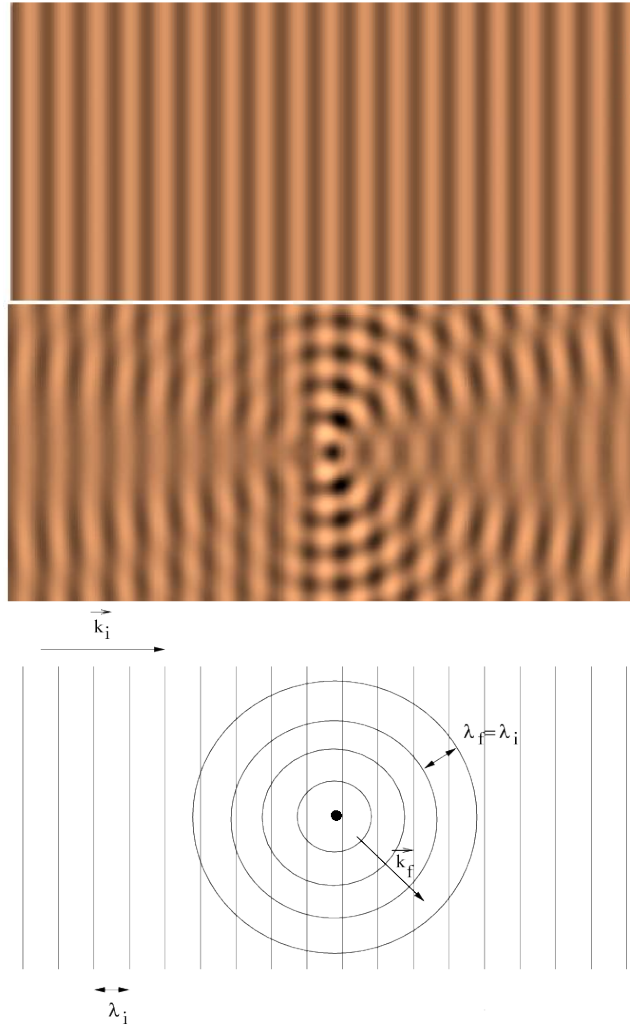


Figure 3.3: Illustration of the scattering of an incoming plane wave (top plot) by a localized repulsive centrifugal potential. The outgoing wave function (middle plot) beyond the range of the potential has the form given by Eq. (3.18).

$$f(E, \theta) = \frac{1}{k} \sum_c (2l + 1) C_c(E) P_l(\cos(\theta)), \quad (3.22)$$

where $C_c(E)$ represents the forward scattering amplitude ($\theta = 0$) of the outgoing wave in the channel c that accounts for the phase shift ϕ_c originating from the potential:

$$C_c(E) = e^{2i\phi_c(E)} \sin(2\phi_c(E)). \quad (3.23)$$

The amplitude $C_c(E)$ can be conveniently rewritten as follows:

$$C_c(E) = \frac{1}{2i} (S_c(E) - 1), \quad (3.24)$$

with

$$S_c(E) = e^{2i\phi_c(E)}. \quad (3.25)$$

The latter expression of the S-matrix elements shows that all what scattering did is to shift the phase of the emerging wave by $2\phi_c$. Eq. (3.25) is valid in the case where there is no absorption of the incident particle, otherwise S_c must be redefined by:

$$S_c(E) = |S_c(E)|e^{2i\phi_c(E)}. \quad (3.26)$$

In the "L-S" coupling scheme (section 3.1.2), the S-matrix elements are:

$$S_c(E) = S_{lJ}(E), \quad (3.27)$$

and for the "j-j" coupling scheme (section 3.1.3):

$$S_c(E) = S_{l_j}^J(E). \quad (3.28)$$

In the ground-state channels ($n = 0$), Eqs. (3.27) and (3.28) become formally identical when the ground-state spin of the target nucleus is zero ($I = 0$):

$$S_{l_j=J}^J(E) = S_{lJ}(E) \quad (3.29)$$

3.3.2 The total and shape-elastic cross sections

According to Eq. (3.24), the forward scattering amplitude $C_c(E)$ is related to the S-matrix elements by the expression [42]:

$$S_c(E) = 1 + 2iC_c(E). \quad (3.30)$$

The S-matrix elements may be used as an alternative to the phase shift to parameterize the angle-integrated cross section. Convenient expressions for the total and shape-elastic cross sections have been reported in major papers as a function of the diagonal component ($c = c'$) of the S-matrix [32, 37]:

$$\sigma_t(E) = \frac{2\pi}{k^2} \sum_c g_{lJ}(2l+1)\{1 - \text{Re}[S_c(E)]\}, \quad (3.31)$$

and

$$\sigma_e(E) = \frac{\pi}{k^2} \sum_c g_{lJ}(2l+1)|1 - S_c(E)|^2. \quad (3.32)$$

The statistical spin factor g_{lJ} may be defined as the ratio of the favorable spin cases to all possible spin cases. It gives out the probability of getting the allowed total angular momentum J from the intrinsic spins of the target nucleus and of the incident particle:

$$g_{lJ} = \frac{2J + 1}{(2i + 1)(2I + 1)(2l + 1)}. \quad (3.33)$$

By introducing expression (3.30) into Eqs. (3.31) and (3.32), the total cross section in the channel c becomes proportional to the imaginary part of the forward scattering amplitude $C_c(E)$:

$$\sigma_{t_c}(E) = \frac{4\pi}{k^2} \text{Im}[C_c(E)], \quad (3.34)$$

and the shape-elastic cross section is given by the squared of the absolute value of $C_c(E)$:

$$\sigma_{e_c}(E) = \frac{4\pi}{k^2} |C_c(E)|^2. \quad (3.35)$$

The connection between the imaginary part of C_c and σ_{t_c} is known as the "optical theorem". The physical origin of this theorem can be illustrated via the picture given by Hodgson [48] in which the incident particle is represented by a flux. After scattering, the flux loss along the incident direction ($\theta = 0$) is proportional to the total cross section or equivalently to the imaginary part of the forward scattering amplitude.

3.3.3 The compound-nucleus cross section

A simple expression of the neutron transmission coefficient can be established in the particular case corresponding to the ground state channel of the target nucleus. According to Eq. (3.13), the cross section for formation of the compound nucleus can be obtained as the following difference:

$$\sigma_C(E) = \sigma_t(E) - \sigma_e(E) - \sigma_D(E). \quad (3.36)$$

By introducing Eqs. (3.31) and (3.32) in Eq. (3.36), σ_C appears to be the product of the maximum possible cross section times the neutron transmission coefficient T_c :

$$\sigma_C(E) = \frac{\pi}{k^2} \sum_c g_{lJ}(2l + 1)T_c(E), \quad (3.37)$$

in which T_c is defined as:

$$T_c(E) = \mathcal{T}_c(E) - T_{D_c}(E). \quad (3.38)$$

The coefficient T_{D_c} represents the contribution of the direct reactions and \mathcal{T}_c has the form reported by Blatt and Weisskopf [32]:

$$\mathcal{T}_c(E) = 1 - |S_c(E)|^2. \quad (3.39)$$

By introducing expression (3.30) into Eq. (3.39), the neutron transmission coefficient can be written as follow:

$$T_c(E) = 4\text{Im}[C_c(E)] - 4|C_c(E)|^2 - T_{D_c}(E). \quad (3.40)$$

In the case of spherical nucleus, the contribution T_{D_c} of the direct reactions are negligible. The transmission coefficients become:

$$T_c(E) = 4\text{Im}[C_c(E)] - 4|C_c(E)|^2 \quad (3.41)$$

A simple physical meaning of T_c is given by Hodgson [48]. He suggests imagining that a certain amount of flux (representing the incident projectile) "enters" the target nucleus (in order to form the compound nucleus) and it subsequently escapes through the open reaction channels. For each of these channels, a transmission coefficient T_c can be defined for representing the "readiness" of the channel to transmit a certain amount of flux. In the case where there is no flux loss (no absorption of the incident particle), we find the condition $|S_c(E)| = 1$ as given by Eq. (3.25).

The neutron transmission coefficient is also called penetrability of the incident particles by Hauser and Feshbach in the paper that lays the basis of the eponymous statistical model [49]. These quantities are different from the so-called penetration factor P_c . The relationship between T_c and P_c is given in section 4.1.4.

3.4 Connections between the matching and channel radius

The purpose of this section is to accommodate the wave description of the nuclear scattering, presented up-above, within the R-Matrix framework. Several works address this issue [39, 43, 50]. Here, we focus on the role of the channel radius a_c . This parameter is one of the boundary condition introduced in the R-matrix theory assuming an abrupt division of the configuration space. Therefore, the resonance theory has some undesirable features of the square-well potential for which the nuclear radius R and the channel radii a_c are the same quantities chosen more or less arbitrarily. In the following sections, the definition of a_c is clarified thanks to the review of the R-Matrix theory proposed by Vogt in Ref. [51].

3.4.1 Diffuse-edge potential

In the optical model, the incident nucleon interacts with a complex mean-field potential of the generic form:

$$V(r) = \text{Re}[V(r)] + i \text{Im}[V(r)], \quad (3.42)$$

in which the real part of the potential refracts the incoming waves and the imaginary part absorbs them. The real and imaginary part of the optical potential may be expressed as a sum of the volume (v), surface (s) and spin-orbit (so) components:

$$V(r) = V_v(r) + V_s(r) + V_{so}(r), \quad (3.43)$$

The difficulty of this model is to find the appropriate potential $V(r)$, which will reproduce the experimental data when it is introduced in the Schrodinger equation. In this work, we use a phenomenological description of the volume, surface and spin-orbit contributions to the nuclear-nucleon interaction $v(r)$. If the matter density distribution $\rho_m(r)$ is defined as the sum of the neutron and proton distributions:

$$\rho_m(r) = \rho_n(r) + \rho_p(r), \quad (3.44)$$

the volume component of the potential $V(r)$ can be written as [48]:

$$V_v(r) \propto \int \rho_m(r') v(r - r') dr'. \quad (3.45)$$

Such a potential follows the nuclear density. The shape of $\rho_m(r)$ is assumed "flat" almost up to the nuclear radius R and falls off in a distance a . As shown in Fig. 3.4 (top plot), a Wood-Saxon form factor can be used to represent these features:

$$f(r, R, a) = \frac{1}{1 + e^{\frac{r-R}{a}}}. \quad (3.46)$$

The fall-off parameter of the nuclear density is called the diffuseness. Its value is lower than 1 fm. In optical model calculations, the natural choice for the nuclear radius is $R = r_0 A^{1/3}$. The meaning of the reduced radius r_0 is close to that of the constant called the "effective range" of the nuclear forces in Ref. [52]. In using this terminology, it should be pointed out that r_0 depends on the depth of the potential. The value of r_0 is subject to variations from element to element with some evidence that r_0 is smaller for high values of A . Numerical calculations with global spherical optical models show that the reduced radius for the real part of the volume component lies in general between 1.23 fm and 1.3 fm [53, 54]. Among the optical model parameters reported in the Reference Input Parameter Library RIPL-3 [40], Morillon and Romain proposed simple expressions for nuclei heavier than iron:

$$r_0 = 1.295 - 2.7 \times 10^{-4} A \quad (\text{in fm}), \quad (3.47)$$

$$a = 0.566 + 5 \times 10^{-9} A^3 \quad (\text{in fm}). \quad (3.48)$$

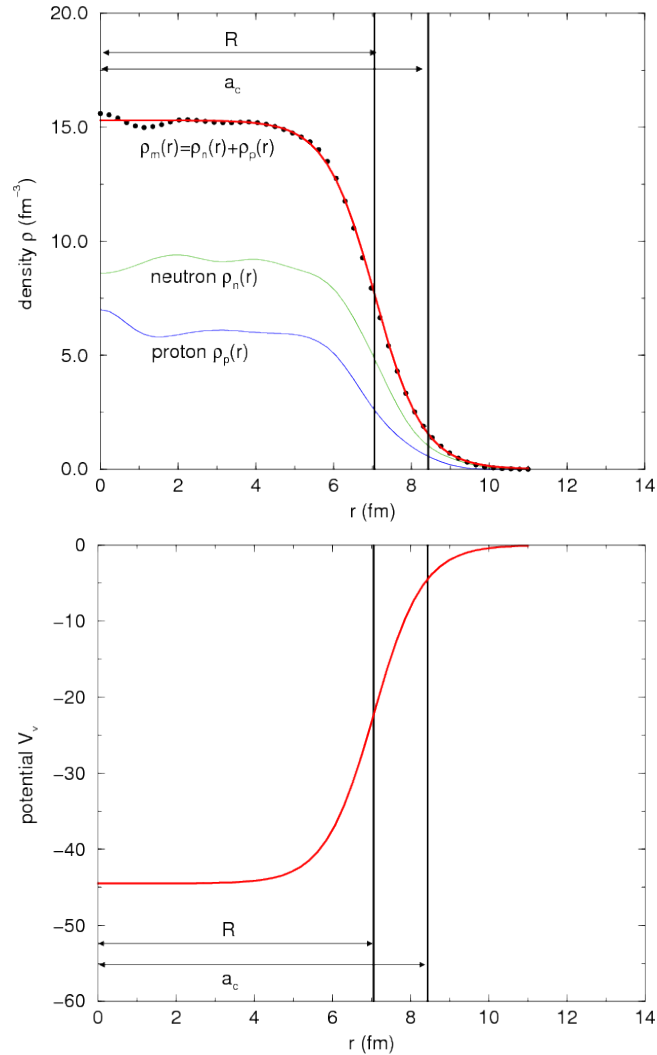


Figure 3.4: Matter density distribution (top plot) and real part of the volume potential (bottom plot) for the nuclear system $^{241}\text{Am}+n$. The densities ρ_n and ρ_p are taken from the AMEDE data base [56]. The channel radius a_c is calculated with the ENDF convention (3.16).

In optical model calculations, it is common to treat the radius and the diffuseness of the nuclear matter distribution as an adjustable parameter. These parameters can be determined by comparison with experimental data [48]. As a consequence, the channel radius (called matching radius) can be evaluated directly from the analysis of the neutron cross sections via phenomenological relationships. In the spherical optical model of the CONRAD code, the matching radius is calculated with the convention used in the SCAT code [55]:

$$r_m = a_c = 1.5(R + 7.0 a) \quad \text{with} \quad R = r_0 A^{1/3}. \quad (3.49)$$

3.4.2 Square-well potential approximation

At low energy, the conventional treatment of nuclear reactions in the resonance theories is essentially a square-well treatment. One of the motivations for using square-well potentials into the analysis is the explicit form of the resulting expressions for small values of kR [35]. Below 3 MeV, Feshbach shows that a square well potential of the simple form

$$V(r) = \begin{cases} V_0 (1 + i \alpha) & \text{for } r < R \\ 0 & \text{for } r > R \end{cases} \quad (3.50)$$

is good enough to represent the variations with the mass number A of the total cross sections and of the angular distributions of the elastically-scattered neutrons [37]. The real part represents the average potential in the nucleus ($\text{Re}[V(r)] = V_0$) and the imaginary part is a constant fraction of the real part ($\text{Im}[V(r)] \propto V_0$). The spin-orbit contribution is omitted.

The pioneer work of Feshbach is clearly unphysical. However, in the late 60s, interesting conclusions were reported in Ref. [39] about the connections between real and square-well potentials. Thanks to the study of the wave properties of the optical model, it was found that for each diffuse-edge optical potential an equivalent square well can be defined uniquely. An additional result was reported by Vogt in the 90s about the unique "natural" choice of a_c for each reaction channel [43]. The dominant conclusion is that the R-Matrix yields the correct results for a square well if and only if the channel radius a_c is chosen to be the square well radius R .

These earlier studies indicate how the physics of the nuclear mean field could be accommodated in the resonance theory. The potential $V(r)$ (Eq. 3.43) does not have to be a square-well shape. However, we have to assume that it vanishes in the external region, and thus we have to find the channel radius a_c for which the following conditions are satisfied:

$$\begin{cases} V(r) = \text{Re}[V(r)] + i \text{Im}[V(r)] & \text{for } r < a_c \\ V(r) \simeq 0 & \text{for } r > a_c \end{cases} \quad (3.51)$$

For typical nuclear reactions, the choice of a_c is not obvious because the square-well model has more reflection than a real nucleus and gives absorption cross sections that are too small [48]. This attenuation of absorption can be compensated by an appropriate increase of the channel radius [39]. Therefore, we would choose a_c not too close to the usual nuclear radius R and large enough so that most of the mean field is in the internal region. Vogt suggests to chose a radius greater than R by an amount roughly equal to the diffuseness [51]:

$$a_c \simeq R + a \quad \text{with} \quad R = r_0 A^{1/3}. \quad (3.52)$$

An estimation of a_c can be obtained by using the geometrical parameters (r_0 and a) of the real volume potentials reported in the Reference Input Parameter Library [40] or given by Eqs. (3.47) and (3.48). Figure 3.5 shows that the combination of the empirical formula (3.52) with the expressions (3.47) and (3.48) provides values of a_c close to those obtained with the expression (3.16) routinely used in the Evaluated Nuclear Data Files, in which $r_0 \simeq 1.23$ fm

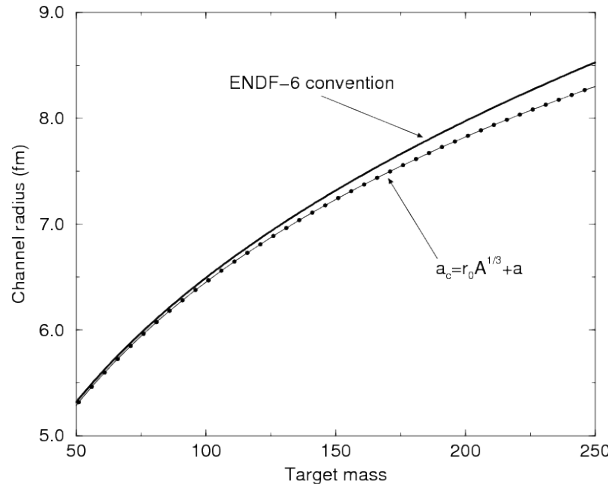


Figure 3.5: Comparison of the channel radius calculated with the expressions (3.16) and (3.52). The reduced radius r_0 and the surface diffuseness a of the real part of the volume potential are calculated with Eqs (3.47) and (3.48).

and $a = 0.8$ fm. However, the lower plot of Fig. 3.4 indicates that Eq. (3.51) is not satisfied for the system $^{241}\text{Am}+n$ if the ENDF convention is used to calculate a_c ($V(a_c) \neq 0$).

The impact on the choice of the channel radius on the optical model calculations was investigated with the reaction $^{208}\text{Pb}+n$. The total, shape and reaction cross sections obtained with the two extreme cases (Eqs. (3.49) and (3.52)) are reported in Fig. 3.6. Comparison with different combinations between R and a seems to indicate that R should be increased by three (or four) times the diffuseness. The present results suggest replacing the ENDF convention for ^{208}Pb by the expression:

$$a_c \geq R + 3a. \quad (3.53)$$

3.4.3 Equivalent hard-sphere scattering

As indicated by Eqs (3.51), the abrupt change of $V(r)$ at the channel radius introduces square-well phase shifts. Therefore, instead of using the empiric formulas (3.52) and (3.53), we can choose a_c such that the optical model and its equivalent square-well provide the same phase shifts at the common channel radii.

Beyond the range of the potential, the asymptotic expression (3.18) of the partial-wave solution to the Schrodinger equation with zero potential is a linear combination of spherical Bessel functions. As a consequence, the phase shift of Eq. (3.25) becomes a simple function of $\rho = ka_c$:

$$\phi_c(E) = \phi_l(\rho) = \tan^{-1} \left(\frac{j_l(\rho)}{\eta_l(\rho)} \right), \quad (3.54)$$

where $j_l(\rho)$ and $\eta_l(\rho)$ stand for the spherical Bessel and Neumann functions of the 1st and 2nd

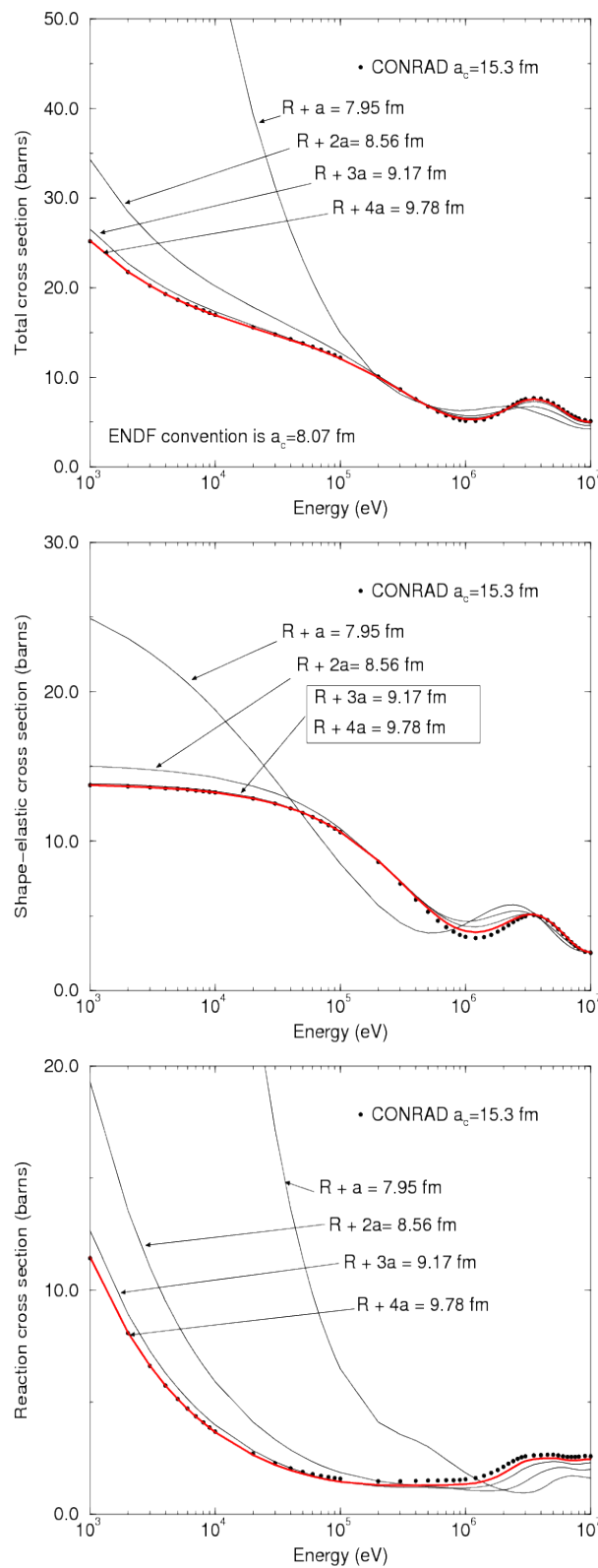


Figure 3.6: Total, shape and reaction cross sections for $^{208}\text{Pb}+n$ calculated with the spherical optical model of CONRAD with parameters of Ref. [54] for different values of channel radius.

kind respectively. All the j_l and η_l functions can be generated from the Rayleigh's recurrence formulas:

$$j_l(\rho) = (-1)^l \rho^l \left(\frac{1}{\rho} \frac{d}{d\rho} \right)^l j_0(\rho), \quad (3.55)$$

$$\eta_l(\rho) = (-1)^l \rho^l \left(\frac{1}{\rho} \frac{d}{d\rho} \right)^l \eta_0(\rho). \quad (3.56)$$

For $l = 0, 1, 2$, the solutions are:

$$j_0(\rho) = \frac{\sin(\rho)}{\rho}, \quad (3.57)$$

$$j_1(\rho) = \frac{\sin(\rho)}{\rho^2} - \frac{\cos(\rho)}{\rho}, \quad (3.58)$$

$$j_2(\rho) = \left(\frac{3}{\rho^3} - \frac{1}{\rho} \right) \sin(\rho) - \frac{3 \cos(\rho)}{\rho^2}, \quad (3.59)$$

$$\eta_0(\rho) = -\frac{\cos(\rho)}{\rho}, \quad (3.60)$$

$$\eta_1(\rho) = -\frac{\cos(\rho)}{\rho^2} - \frac{\sin(\rho)}{\rho}, \quad (3.61)$$

$$\eta_2(\rho) = -\left(\frac{3}{\rho^3} - \frac{1}{\rho} \right) \cos(\rho) - \frac{3 \sin(\rho)}{\rho^2}. \quad (3.62)$$

Simple analytical expressions of the phase shift for small angular momentum l are not immediately evident from the usual presentation of the Bessel functions written as a mix of powers and trigonometric functions. After few simplifications, the Eqs (3.57) to (3.62) lead to the following expressions:

$$\begin{cases} \phi_0(\rho) &= \rho, \\ \phi_1(\rho) &= \rho - \tan^{-1}(\rho), \\ \phi_2(\rho) &= \rho - \tan^{-1}\left(\frac{3\rho}{3-\rho^2}\right). \end{cases} \quad (3.63)$$

Fig. 3.7 shows the behavior of the phase shift $\phi_c(E)$ for s, p, and d-waves. They were calculated with the optical model code ECIS for the nuclear system $^{241}\text{Am}+n$. We used the optical model parameters recommended in the Japanese library JENDL-4.

Equivalent hard-sphere radii can be obtained from the least squares fit of $\phi_c(E)$ with Eqs. (3.63). Values for the channels $c = \{l, J\}$ are reported in Table 3.1. Radii for s-waves ($l = 0$) are summarized in Table 3.2. The ENDF convention (3.16) underestimates by 1 fm the equivalent hard-sphere radius. The latter is correctly predicted by the empirical formula (3.53) established for the nuclear system $^{208}\text{Pb}+n$.

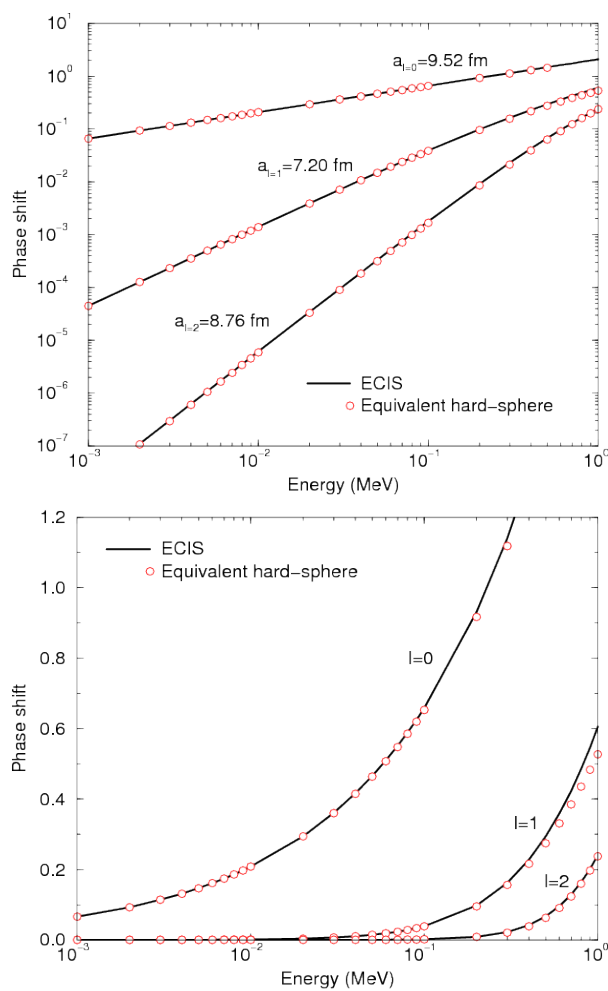


Figure 3.7: Energy dependence of the phase shift ($l = 0, 1, 2$) calculated with the optical model code ECIS for the nuclear system $^{241}\text{Am}+n$ in log-log and log-lin scales. The open circles represent the equivalent hard-sphere phase shift calculated with Eq. (3.63).

Table 3.1: Equivalent hard-sphere channel radii obtained from the least squares fit of the phase shift calculated by ECIS for the nuclear system $^{241}\text{Am}+n$.

Channel radius	Orbital momentum		
	$l = 0$	$l = 1$	$l = 2$
$a_{l,J=0}$			9.26 fm
$a_{l,J=1}$		5.51 fm	9.41 fm
$a_{l,J=2}$	9.51 fm	7.66 fm	8.79 fm
$a_{l,J=3}$	9.52 fm	7.81 fm	8.22 fm
$a_{l,J=4}$		6.07 fm	8.83 fm
$a_{l,J=5}$			8.88 fm
a_l	9.52 fm	7.20 fm	8.76 fm

Table 3.2: Comparison of the equivalent hard-sphere radius for the nuclear system $^{241}\text{Am}+n$ with results obtained from Eqs. (3.16), (3.52) and (3.53).

Channel radius		Ref.	Value
Vogt's prescription	(Eq. (3.52))	[51]	8.28 fm
ENDF convention	(Eq. (3.16))	[3]	8.43 fm
Empirical formula	(Eq. (3.53))		≥ 9.56 fm
Equivalent hard-sphere	$(l = 0)$		9.52 fm

These results show how the ideas of the optical model can be incorporated in the resonance theory. Indeed, in the early 60s, Vogt suggested that a better approximation than Eq. (3.63) could be obtained by replacing all the phase shifts by those of the diffuse-edge potential in order that the elements of the scattering matrix (Eq. (3.30)) no longer has an artificial dependence on the channel radii [50]. This conclusion has a significant impact on the determination of the neutron strength functions involved in the theory of average cross section. The latter is described in chapter 4.

Chapter 4

Theory of average cross section within the Reich-Moore approximation

Experimentally we can observe that there is a continuous transition from the extreme situation of well-isolated resonances to complete overlap. This transition can be described within the R-Matrix theory [1] by using appropriate approximations. One of the first description of the theory of average cross section was proposed in 1954 by Feshbach et al. [37]. This work indicates how the R-Matrix and optical models coexist between the "resonance region" and the "continuum region". The main ingredients of the theory of average cross section and links with the S-matrix formalism are exemplified in this chapter.

4.1 Average R-Matrix approximation

For the sake of clarity, we define U_c , \bar{U}_c and S_c the elements of the scattering matrix respectively used in the Resolved Resonance Range, in the Unresolved Resonance Range and in the "continuum" for $c = c'$. Historically, \bar{U}_c is called the average collision function by analogy with the collision matrix U_c involved in the R-Matrix theory.

4.1.1 Average collision function in the Bethe's assumptions

In the resonance region, the elements of the collision matrix U_c exhibit rapid fluctuations coming from the numerous close-spaced resonances of the compound nucleus. An average value of U_c can be defined over an interval ΔE containing many overlapping levels. This condition can be written as follow:

$$\Delta E \gg D_c, \tag{4.1}$$

where D_c stands for the average spacing of the compound levels. However, ΔE must be small enough so that the elements of the scattering matrix can be regarded as energy independent.

In that case, the average value of the total and shape elastic cross sections can be evaluated with Eqs. (3.31) and (3.32) (or alternatively with Eqs. (3.34) and (3.35)):

$$\bar{\sigma}_{t_e} \simeq \frac{2\pi}{k^2}(1 - \text{Re}[\bar{U}_c]), \quad (4.2)$$

$$\bar{\sigma}_{e_e} \simeq \frac{\pi}{k^2}|1 - \bar{U}_c|^2, \quad (4.3)$$

and the neutron transmission coefficients are obtained from Eq. (3.39):

$$\mathcal{T}_c = 1 - |\bar{U}_c|^2, \quad (4.4)$$

in which S_c is replaced by the average collision function:

$$\bar{U}_c = \frac{1}{\Delta E} \int_{\Delta E} U_c(E) \, dE. \quad (4.5)$$

Soon after the publication of Feshbach [37], Thomas [57] discussed two opposite approximations of the collision matrix for the compound nucleus due to Newton [58] and Bethe [59]. The former approximation is characterized by very strong correlations between the matrix elements, while for the second approximation they vanish.

The main parameters involved in these assumptions are the reduced width amplitudes $\gamma_{\lambda c}$ and $\gamma_{\lambda c'}$ of the resonance λ . By definition, $\gamma_{\lambda c}$ is the probability amplitude for the formation of compound state λ via the entrance channel c , and $\gamma_{\lambda c'}$ is the probability amplitude for the decay of compound state via the exit channel c' . Cross sections formulae are usually written in terms of partial widths $\Gamma_{\lambda c}$ rather than decay amplitudes. The square of the reduced width amplitude is related to the partial width via the penetration factor P_c of the centrifugal barrier for the compound system at the channel radius a_c [41]:

$$\gamma_{\lambda c}^2 = \frac{\Gamma_{\lambda c}}{2P_c}. \quad (4.6)$$

According to Thomas, the work of Newton leads to strange prediction while Bethe provides the fundamental assumptions of the statistical model: $\gamma_{\lambda c}$ and $\gamma_{\lambda c'}$ are independent, uncorrelated and have random signs. These assumptions are consistent with the complicated wave function of the nuclear states. They imply that the statistical properties of the exit channel c' contain no memory of the entrance channel, which is the essential feature of the Bohr compound nucleus mechanism.

One of the consequence of the Bethe's assumptions is that the average contribution of the reduced width amplitudes tends to cancel for $c \neq c'$:

$$\langle \gamma_{\lambda c} \gamma_{\lambda c'} \rangle_{\Delta E} \simeq 0. \quad (4.7)$$

In the absence of correlations among channel width amplitudes, Moldauer [60] concludes that the formula relating elements of the average collision matrix with the average reduced width amplitudes should be the same as for the single-channel case, which is given by:

$$U_c(E) = e^{2i\phi_c(E)} \frac{1 + iP_c(E)R_c(E)}{1 - iP_c(E)R_c(E)}. \quad (4.8)$$

If the interval ΔE is small enough to assume constant the phase shift ϕ_c , the penetration factor P_c and the reduced R-function R_c , it follows that the average collision function is simply given by:

$$\bar{U}_c \simeq e^{2i\phi_c} \frac{1 + iP_c\bar{R}_c}{1 - iP_c\bar{R}_c} \quad \text{for } c = c'. \quad (4.9)$$

An identical relationship was found by Thomas in the case where the competing channels have small transmission factors [57]. The work of Moldauer seems to provide a more general validity of the relations given above. We can just keep in mind that the R-function rather than the full R-Matrix can be used for the calculations of the average total and shape elastic cross sections when all the partial widths, except the entrance-channel width, are small compared with the level spacing D_c .

4.1.2 Average R-function in the uniform level approximation

In this work, we introduce in Eq. (4.8) the reduced R-function given by the Reich-Moore approximation of the R-Matrix theory [61]:

$$R_c(E) = \sum_{\lambda} \frac{\gamma_{\lambda n_c}^2}{E_{\lambda} - E - i\Gamma_{\lambda\gamma_c}/2} + \mathcal{R}_c(E), \quad (4.10)$$

in which E_{λ} is the resonance energy, $\gamma_{\lambda n_c}$ is the reduced neutron width amplitude and $\Gamma_{\lambda\gamma_c}$ is the partial radiation width of the compound state λ . The background term $\mathcal{R}_c(E)$ was introduced in the R-Matrix theory by Wigner and Eisenbud [35] as an arbitrary real-symmetric matrix independent of the energy. In the idealized situation, the continuity requirement at a_c between the internal and external regions should leads to $\mathcal{R}_c = 0$.

Additional works were performed by Lynn in order to provide explicit expressions for the background term $\mathcal{R}_c(E)$. He derived an expression for the cross sections in which \mathcal{R}_c is complex [62]:

$$R_c(E) = \sum_{\lambda} \frac{\gamma_{\lambda n_c}^2}{E_{\lambda} - E - i\Gamma_{\lambda\gamma_c}/2} + R_c^{\infty}(E) + R_c^{\text{loc}}(E) + i\pi s_c^{\text{loc}}(E). \quad (4.11)$$

The real part of \mathcal{R}_c can be split into the contributions of neighboring (R_c^{loc}) and far-off levels (R_c^{∞}). Feshbach [37] assumes that only the immediate-neighbor resonances R_c^{loc} contribute appreciably. He suggests that such a contribution may formally be replaced by sums over an

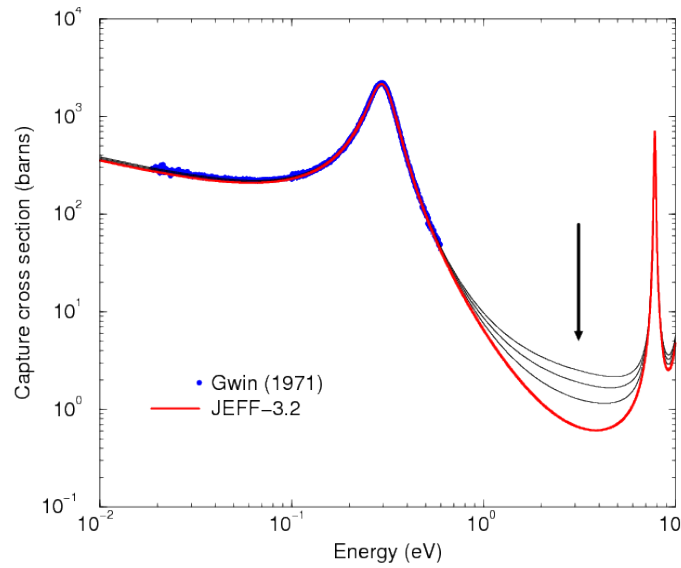


Figure 4.1: Modelisation of the ^{239}Pu capture cross section with non zero background s_c^{loc} .

infinite number of external levels, having negative or positive energies, which may provide a finite contribution:

$$R_c^{\text{loc}}(E) \simeq \sum_{\mu} \frac{\gamma_{\mu n_c}^2}{|E_{\mu}| - E - i\Gamma_{\mu\gamma_c}/2}. \quad (4.12)$$

As the consequence, the contribution of these "fictitious" resonances can be easily included in the sum over levels λ of the reduced R-matrix (Eq. (4.10)):

$$R_c \simeq \sum_{\eta=\lambda,\mu} \frac{\gamma_{\eta n_c}^2}{|E_{\eta}| - E - i\Gamma_{\eta\gamma_c}/2} + R_c^{\infty}(E) + i\pi s_c^{\text{loc}}(E). \quad (4.13)$$

Throughout the R-matrix theory, R_c^{∞} is called the distant level parameter. Its value is lower than unity [50]. Lynn [63] indicates that the far away contribution R_c^{∞} modifies the hard-sphere potential scattering length a_c to give the true potential scattering length R' . By analogy, the imaginary part $\text{Im}[R_c] = \pi s_c^{\text{loc}}$ will modify the absorption cross section. Figure 4.1 displays the impact of non zero background s_c^{loc} between the first and second resonances of ^{239}Pu .

In the uniform level approximation, where the amplitude $\gamma_{\eta n_c}^2$ are all equal and the levels η are uniformly spaced by an amount D_c , the average value of the reduced R-function R_c is:

$$\overline{R}_c \simeq \int_a^b \frac{s_c}{E' - z} dE' + \frac{1}{\Delta E} \int_a^b R_c^{\infty}(E') dE' + \frac{i\pi}{\Delta E} \int_a^b s_c^{\text{loc}}(E') dE', \quad (4.14)$$

with

$$z = E + i\frac{\Gamma_\gamma}{2}, \quad (4.15)$$

in which Γ_γ represents the average radiation width. The lower and upper bounds of the integral are defined by the midpoint of the interval ΔE :

$$a = \epsilon - \frac{\Delta E}{2}, \quad (4.16)$$

$$b = \epsilon + \frac{\Delta E}{2}. \quad (4.17)$$

The first integral of the expression (4.14) is called the Stieltjes transform of the pole strength function s_c , where s_c is a probability density function defined as the ratio of the average reduced width to level spacings:

$$s_c = \frac{\langle \gamma_{n_c}^2 \rangle}{D_c}. \quad (4.18)$$

The method used by Thomas [57] for assigning a value to the Stieltjes transform of the pole strength function relies on the Sokhotsky's formula (see Sokhotsky-Weierstrass theorem). The latter state that:

$$\lim_{x \rightarrow 0} \frac{1}{x \mp i\varepsilon} = \mathcal{P} \left(\frac{1}{x} \right) \pm i\pi\delta(x), \quad (4.19)$$

where $\delta(x)$ is the delta function and \mathcal{P} is the Cauchy principal value of the inverse function $1/x$. According to the expression (4.14), we have $\varepsilon = \Gamma_\gamma/2$ and $x = E' - E$. The Sokhotsky-Weierstrass theorem can be applied if Γ_γ is small. This criteria is satisfied in the unresolved resonance range of many isotopes, such as actinides, for which the order of magnitude of the average radiation widths is close to 50 meV. As a consequence, the well established identity (4.19) can be introduced in Eq. (4.14) to give:

$$\bar{R}_c \simeq i\pi s_c + \underbrace{\mathcal{P} \int_a^b \frac{s_c}{E' - E} dE' + \frac{1}{\Delta E} \int_a^b R_c^\infty(E') dE'}_{\bar{R}_c^\infty} + i\pi \underbrace{\frac{1}{\Delta E} \int_a^b s_c^{\text{loc}}(E') dE'}_{\bar{s}_c^{\text{loc}}}. \quad (4.20)$$

This mathematical trick allows to distinguish, without much complication, the "statistical R-function" $i\pi s_c$ and the background contribution \bar{R}_c^∞ . By using this notation, the Stieltjes transform of the pole strength function becomes:

$$\bar{R}_c \simeq \bar{R}_c^\infty + i\pi (s_c + \bar{s}_c^{\text{loc}}). \quad (4.21)$$

4.1.3 Average cross sections

According to Eq. (4.21), the average collision function (4.9) can be rearranged into the form:

$$\bar{U}_c \simeq e^{2i\phi_c} \frac{1 - \pi P_c(s_c + \bar{s}_c^{\text{loc}}) + iP_c \bar{R}_c^\infty}{1 + \pi P_c(s_c + \bar{s}_c^{\text{loc}}) - iP_c \bar{R}_c^\infty}. \quad (4.22)$$

By introducing Eq. (4.22) in Eqs. (4.2) and (4.3), the total and shape-elastic cross sections can be written as:

$$\bar{\sigma}_{t_c} = \frac{2\pi}{k^2} \left\{ 1 - \frac{[P_c^2(\bar{R}_c^{\infty 2} + \pi^2 s^2) - 1] \cos(2\phi_c) - 2P_c \bar{R}_c^\infty \sin(2\phi_c)}{(1 + \pi P_c s)^2 + P_l^2 \bar{R}_c^{\infty 2}} \right\}, \quad (4.23)$$

and

$$\bar{\sigma}_{e_c} = \frac{2\pi}{k^2} \left\{ 1 - \frac{[P_c^2(\bar{R}_c^{\infty 2} + \pi^2 s^2) - 1] \cos(2\phi_c) - 2P_c \bar{R}_c^\infty \sin(2\phi_c) - 2\pi P_l s}{(1 + \pi P_c s)^2 + P_l^2 \bar{R}_c^{\infty 2}} \right\}, \quad (4.24)$$

where

$$s = s_c + \bar{s}_c^{\text{loc}}. \quad (4.25)$$

Equivalent expressions relying on the Bethe's assumption and uniform level approximation can be found in many papers. If $\bar{s}_c^{\text{loc}} = 0$, Eq. (4.22) corresponds to the formulation of the average R-Matrix approximation reported by Moldauer in Ref. [60]. This approximation was implemented in the nuclear data codes SAMMY and CONRAD. These implementations use a modified form provided by Frohner in his code FITACS [13] in which the pole strength function s_c and the background term \bar{R}_c^∞ are free parameters.

Fig. 4.2 compares the total cross sections for the hafnium isotopes obtained by using the average R-Matrix formalism introduced in the CONRAD code with the results provided by the optical model code ECIS. A good agreement between CONRAD and ECIS is observed up to few hundred of keV. Detailed explanations are given in Ref. [20] (see Appendix).

4.1.4 Neutron transmission coefficients

In the average R-Matrix approximation, the neutron transmission coefficients are obtained by introducing Eq. (4.22) in Eq. (4.4):

$$\mathcal{T}_c = \frac{4\pi P_c(s_c + \bar{s}_c^{\text{loc}})}{[1 + \pi P_c(s_c + \bar{s}_c^{\text{loc}})]^2 + P_c^2 \bar{R}_c^{\infty 2}}. \quad (4.26)$$

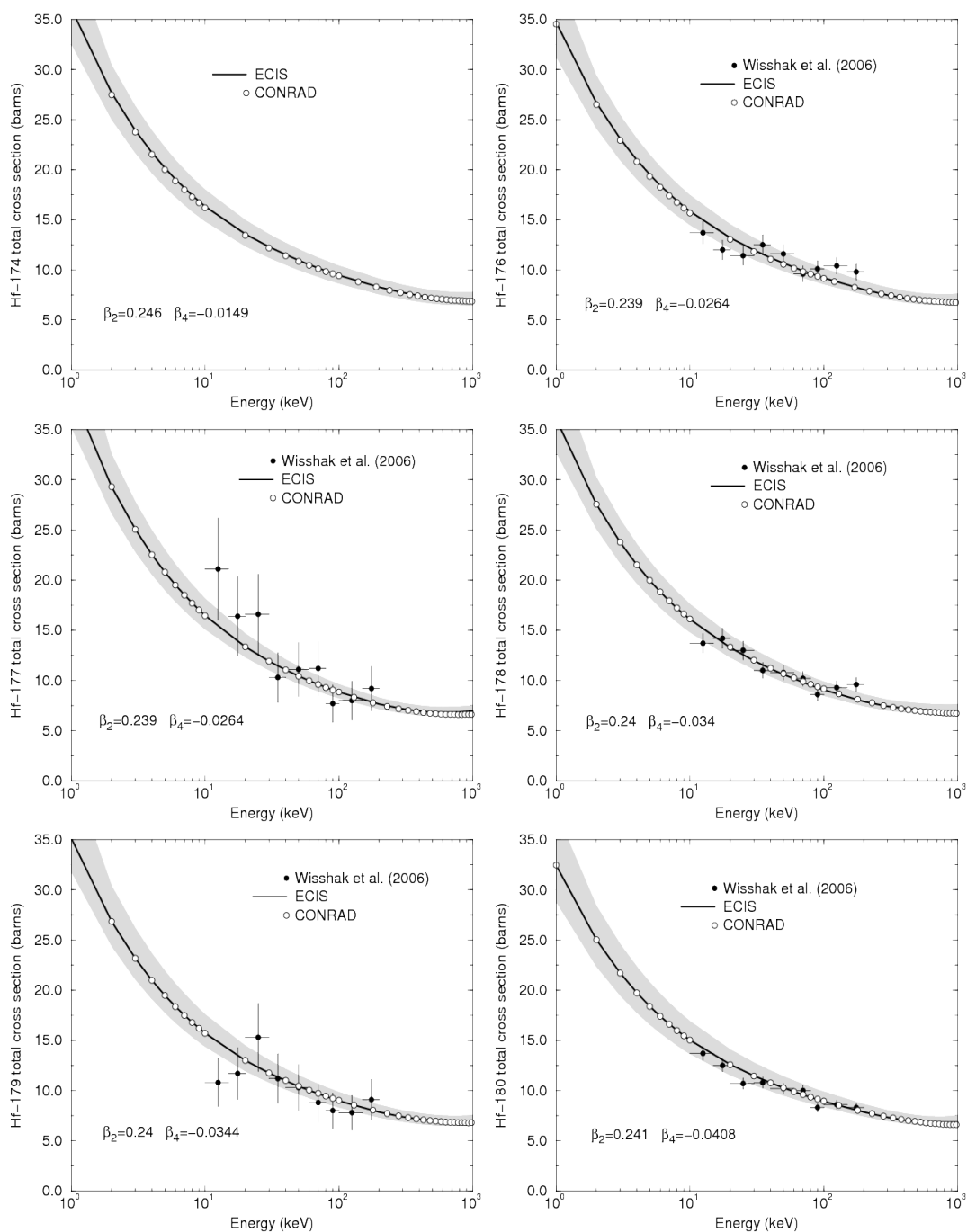


Figure 4.2: Total cross sections for the hafnium isotopes obtained with the average R-Matrix formalism of the CONRAD code. The optical model calculations, performed with the ECIS code, are based on the parameters given in Ref [20]. Parameters β_2 and β_4 define the dipole and quadrupole deformation parameters. The data for the total cross section were retrieved from EXFOR.

The latter expression can be split in two contributions:

$$\mathcal{T}_c = \underbrace{\frac{4\pi P_c s_c}{[1 + \pi P_c (s_c + \bar{s}_c^{\text{loc}})]^2 + P_c^2 \bar{R}_c^{\infty 2}}}_{T_c} + \underbrace{\frac{4\pi P_c \bar{s}_c^{\text{loc}}}{[1 + \pi P_c (s_c + \bar{s}_c^{\text{loc}})]^2 + P_c^2 \bar{R}_c^{\infty 2}}}_{T_{D_c}}. \quad (4.27)$$

For spherical or weakly deformed nuclei, the contribution of the direct reactions T_{D_c} disappears ($\bar{s}_c^{\text{loc}} = 0$), and the expression of the neutron transmission coefficient becomes:

$$\mathcal{T}_c = T_c = \frac{4\pi P_c s_c}{(1 + \pi P_c s_c)^2 + P_c^2 \bar{R}_c^{\infty 2}} \quad (4.28)$$

By using the notation

$$f = \frac{1}{(1 + \pi P_c s_c)^2 + P_c^2 \bar{R}_c^{\infty 2}}, \quad (4.29)$$

the expression (4.28) can be rewritten as:

$$T_c = 4\pi P_c s_c f. \quad (4.30)$$

The latter result indicates that the neutron transmission coefficient and the penetration factor differ by a factor equal to $4\pi s_c f$. In Ref. [39], f was also introduced to account for the difference in reflexion between a diffuse-edge optical potential and its equivalent square-well. If we consider the external wave function for channel c as a combination of Bessel j_l and Neumann η_l functions (see section 3.4.3), the "square-well" penetration factor at a_c was found to have a l -dependent function of $\rho = ka_c$ [57]:

$$P_c = P_l(\rho) = \frac{\rho}{\rho^2 j_l^2(\rho) + \rho^2 \eta_l^2(\rho)}. \quad (4.31)$$

Eqs. (3.57) to (3.62) give the following expressions for $l = 0, 1, 2$:

$$\begin{cases} P_0(\rho) &= \rho, \\ P_1(\rho) &= \frac{\rho^3}{1+\rho^2}, \\ P_2(\rho) &= \frac{\rho^5}{9+3\rho^2+\rho^4}. \end{cases} \quad (4.32)$$

4.2 Average R-Matrix parameters

In the frame of the average R-Matrix approximation, the parameter \bar{R}_c^{∞} , the pole strength function s_c and the background term \bar{s}_c^{loc} involved in Eq. (4.22) are free parameters. Prior

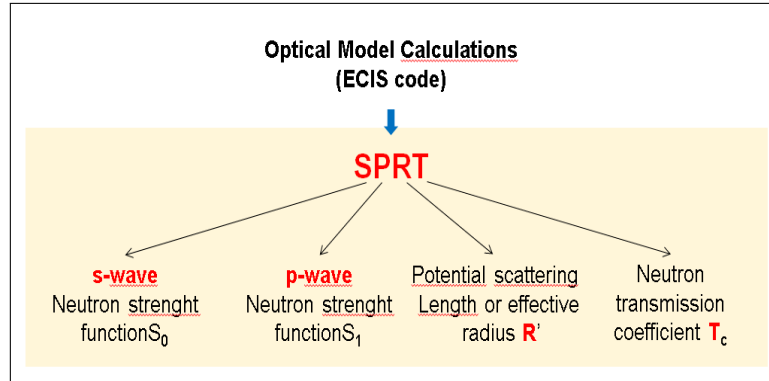


Figure 4.3: Schematic description of the SPRT method established by Delaroche et al. [64]. The standard SPRT method provides an estimate of the neutron strength functions (S_0 and S_1) and potential scattering length R' via the neutron transmission coefficients and the shape-elastic cross section calculated by Optical Model.

values can be estimated from the statistical analysis of the resolved resonance parameters or deduced from optical model parameters. Links with results provided by optical model calculations are discussed below.

4.2.1 Generalization of the SPRT method

The SPRT method is used to study the consistency between the average R-Matrix parameters adjusted on experimental data and those given by optical model calculations. The standard SPRT method [64] was developed for s- and p-wave parameters ($l = 0, 1$). Figure 4.3 presents a schematic description of the standard SPRT method. The method was generalized in order to provide pole strength functions and parameter \bar{R}_c^∞ for higher order partial wave ($l \geq 1$) [19]. A detailed description of the SPRT method is reported in Appendix A. The work consists of determining s_c and R_c^∞ as:

$$\bar{\sigma}_{t_c}(\bar{U}_c) = \frac{4\pi}{k^2} \text{Im}[C_c], \quad (4.33)$$

$$\bar{\sigma}_{e_c}(\bar{U}_c) = \frac{4\pi}{k^2} |C_c|^2. \quad (4.34)$$

By using Eqs. (4.23) and (4.24), the system of equations (4.33) and (4.34) lead directly to the following solution:

$$P_c \bar{R}_c^\infty = \frac{2\alpha_c \cos[2\phi_c] + (1 - 2\beta_c) \sin[2\phi_c]}{1 + 2\gamma_c^2 - 2\beta_c + (1 - 2\beta_c) \cos[2\phi_c] - 2\alpha_c \sin[2\phi_c]}, \quad (4.35)$$

$$\pi P_c (s_c + \bar{s}_c^{\text{loc}}) = \frac{2(\beta_c - \gamma_c^2)}{1 + 2\gamma_c^2 - 2\beta_c + (1 - 2\beta_c) \cos[2\phi_c] - 2\alpha_c \sin[2\phi_c]}. \quad (4.36)$$

in which α_c , β_c and γ_c are free parameters. General expressions for these parameters are given in Ref. [19]. In the ground state channel, for target nucleus with $I = 0$, they represent

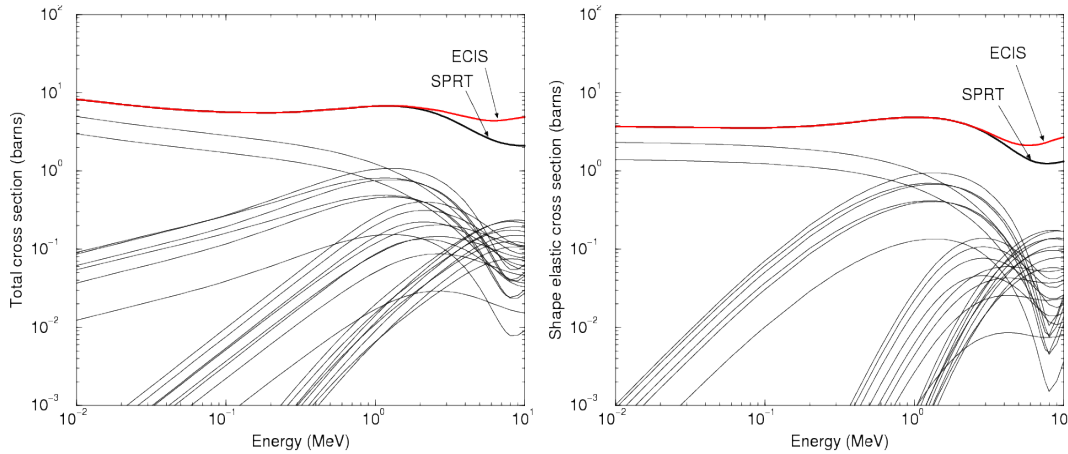


Figure 4.4: Partial wave breakdown calculations performed with the generalization of the SPRT method on $^{131}\text{Xe}+n$ up to $l = 4$.

the real part, the imaginary part and the absolute value of the forward scattering amplitude C_c :

$$\begin{cases} \alpha_c = \text{Re}[C_c] \\ \beta_c = \text{Im}[C_c] \\ \gamma_c = |C_c| \end{cases} \quad (4.37)$$

Fig. 4.4 illustrates the partial wave breakdown calculations performed with the generalization of the SPRT method on the nuclear system $^{131}\text{Xe}+n$. Due to the proximity of the magic number $N = 82$ and $Z = 50$, xenon isotopes should be weakly deformed. In this work, we have adopted parameters of the spherical potential established in Ref. [22].

4.2.2 Neutron strength function

The neutron widths $\Gamma_{\lambda n_c}$ with the same total angular momentum and parity strongly fluctuate among resonances. According to Eq. (4.6), the fluctuations must be attributed to the reduced neutron width amplitude $\gamma_{\lambda n_c}$ because of the smooth energy dependence of the penetration factor P_c . On the basis of the Bethe's assumptions, $\gamma_{\lambda n_c}$ have random signs which nearly cancel positive and negative contributions. Thus, the most objective probability distribution for $\gamma_{\lambda n_c}$ is a Gaussian with zero mean. This argument accounts for the fact that the reduced neutron width amplitudes are chosen as real. This assumption leads to the one-channel reduced neutron width distribution hypothesized by Hughes and Harvey [65], which was found to be a chi-squared function with one degree of freedom by Porter and Thomas [66]:

$$P(x)dx = \frac{e^{-\frac{x}{2}}}{\sqrt{2\pi x}} dx, \quad (4.38)$$

with

$$x = \frac{\Gamma_{\lambda n_c}^l}{\langle \Gamma_{\lambda n_c}^l \rangle}, \quad (4.39)$$

in which the reduced neutron widths at the resonance energy E_λ is defined as follow:

$$\Gamma_{\lambda n_J}^l = \Gamma_{\lambda n_{lJ}} \frac{P_0}{P_l} \sqrt{\frac{1 \text{ eV}}{E_\lambda}}. \quad (4.40)$$

As indicated by Porter and Thomas, the definition of the dimensionless variable x relies on the existence over a given energy interval ΔE with a reasonably well-defined average reduced neutron width $\langle \Gamma_{\lambda n_c}^l \rangle$. The existence of such an average was suggested by the work of Feshbach [37] and Lane [67] relying on the pole strength function (Eq. (4.18)). By introducing the reduced neutron width amplitude $\gamma_{\lambda n_c}$, we obtain:

$$\Gamma_{\lambda n_c}^l = 2\gamma_{\lambda n_c}^2 P_0 \sqrt{\frac{1 \text{ eV}}{E_\lambda}}. \quad (4.41)$$

If the interval ΔE is small enough so that the penetration factor may be considered as constant, the average value of the reduced neutron width divided by the mean level spacing, defined as the neutron strength function S_c , is given by:

$$S_c = \frac{\langle \Gamma_{n_c}^l \rangle}{D_c} = 2 \frac{\langle \gamma_{n_c}^2 \rangle}{D_c} P_0 \sqrt{\frac{1 \text{ eV}}{E}}. \quad (4.42)$$

From Eq. (4.18), the relationship between the neutron strength function S_c and the pole strength function s_c is:

$$S_c = 2s_c P_0 \sqrt{\frac{1 \text{ eV}}{E}}. \quad (4.43)$$

The systematic trends of the s- and p-wave neutron strength functions with respect to the mass number of the compound nucleus are shown in Fig. 4.5. Results reported for Iodine [68], Xenon [22], Hafnium [20], Neptunium [21] and Americium [69] are compared with values recommended in the Reference Input Parameter Library RIPL-3. For s-waves, the neutron strength functions were deduced from the statistical analysis of the resolved resonance parameters by using the ESTIMA method [70, 71]. The p-wave values were calculated with the generalized SPRT method. Examples for fissile (Neptunium) and non-fissile (Hafnium) isotopes are reported in Appendix B and C, respectively.

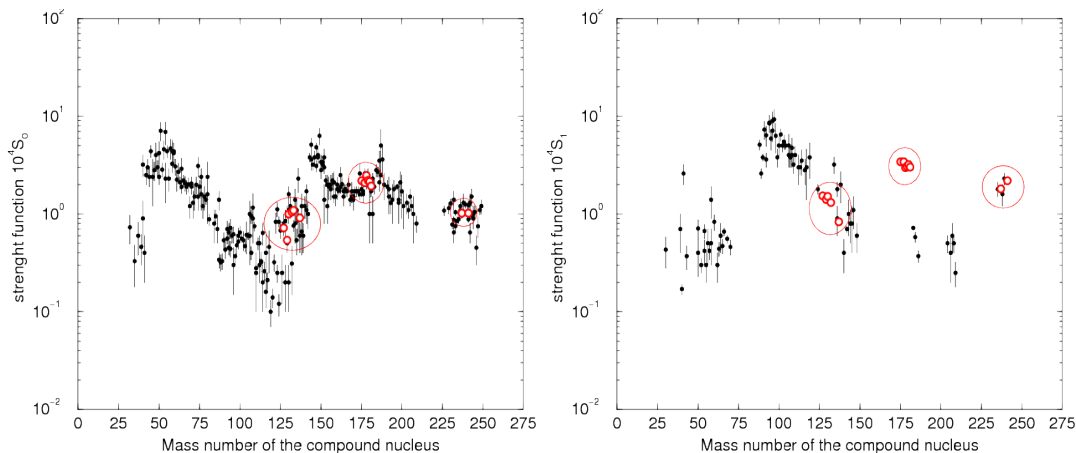


Figure 4.5: Systematic behavior of the s- and p-wave neutron strength functions with the mass number of the compound nucleus. Values for Iodine, Xenon, Hafnium, Neptunium and Americium are compared with data compiled in the RIPL library.

4.2.3 Low neutron energy approximations

This latest section aims to show how the SPRT method in association with the equivalent hard-sphere radius makes it possible the coexistence of the direct and compound nucleus reactions at low energy in in the frame of the R-Matrix theory. Simple expressions valid for slow neutrons are given for the neutron transmission coefficient and for the shape elastic cross section.

When the neutron transmission coefficients are much smaller than unity, Eq. (4.30) can be approximated by the "low-energy" expression ($f \simeq 1$):

$$T_l \simeq 4\pi P_l S_l. \quad (4.44)$$

The l -dependent neutron transmission coefficient can be rearranged by introducing the expression (4.43) of the neutron strength function and the s-wave penetration factor $P_0 = ka_c$:

$$T_l \simeq 2\pi \frac{P_l}{P_0} S_l \sqrt{E}. \quad (4.45)$$

The product $P_l S_l / P_0$ can be calculated with the SPRT method (Eq. 4.36). Figure. 4.6 shows the neutron strength function S_l and the distant level parameter \overline{R}_l^∞ obtained for the nuclear system $^{241}\text{Am}+n$ by using the optical model parameters proposed in the evaluated nuclear data file of the Japanese library JENDL-4. The (l, J) dependent distance level parameters $\overline{R}_{l,J}^\infty$ are shown in Fig 4.7. The ^{241}Am neutron strength functions were deduced from the SPRT results by introducing the equivalent hard sphere radii listed in Table 3.1 and the channel radius of the ENDF convention reported in Table 3.2. A Lagrange polynomial interpolation was used to extrapolate the low energy behavior of S_l and \overline{R}_l^∞ . Results reported in Table 4.1 are given at the binding energy. As expected, non negligible differences is obtained for p- and d-wave neutron strength functions. However, when the equivalent hard sphere radii are

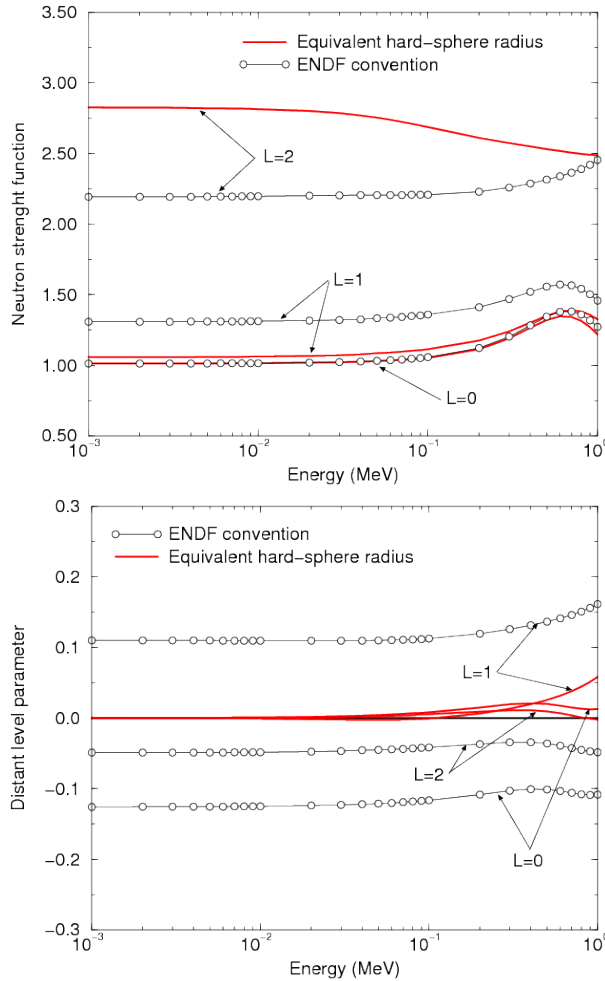


Figure 4.6: Neutron strength functions (top plot) and distant level parameters (bottom plot) obtained with the SPRT method (Eqs. (4.35) and (4.36)) for the nuclear system $^{241}\text{Am}+n$. Channel radii calculated in the equivalent hard-sphere approximation and in the ENDF convention are reported in Tables 3.1 and 3.2. The coupled channel calculations were performed with ECIS by using the parameters reported in the Japanese library JENDL-4.

used, the distant level parameter vanishes ($\overline{R}_l^\infty \simeq 0$) which allows to remove the artificial dependence on the channel radius.

The neutron transmission coefficients calculated in the equivalent hard sphere approximation are compared in Fig. 4.8 with those provided by the ECIS code. Below 10 keV, the discrepancies between the low energy approximation (4.45) and the optical model calculations remains below 1%. The present results confirm that the penetration factor P_l used in the Resolved Resonance Range can be deduced from the expression (4.45) by introducing neutron transmission coefficients given by optical model calculations.

For the shape elastic cross section, the low energy expression becomes similar to the potential scattering cross section for which the s-wave channels dominates:

$$\sigma_{pot} = \sum_J g_{l=0,J} \lim_{E \rightarrow 0} \sigma_{e_{l=0,J}}(E). \quad (4.46)$$

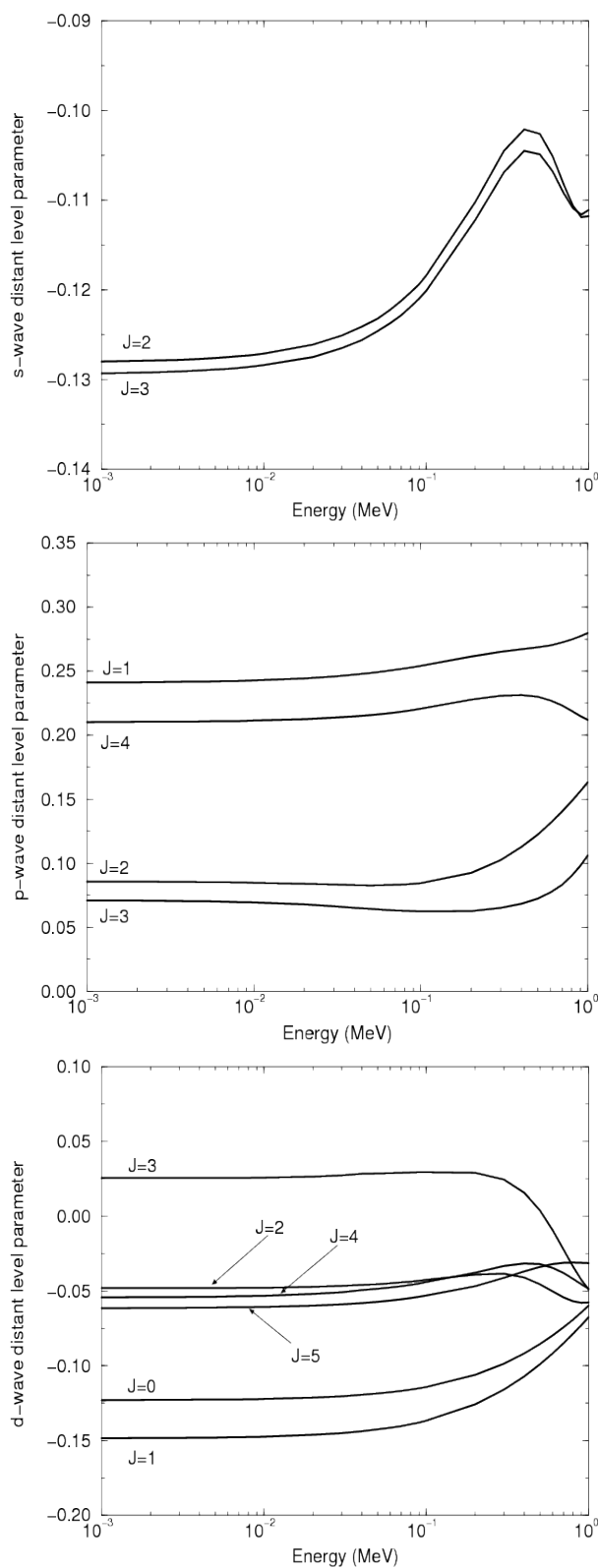


Figure 4.7: Distant level parameters obtained with the SPRT method (Eq. (4.35)) for the nuclear system $^{241}\text{Am}+n$ by using the channel radius of the ENDF convention (3.2). The coupled channel calculations were performed with ECIS by using the parameters reported in the Japanese library JENDL-4.

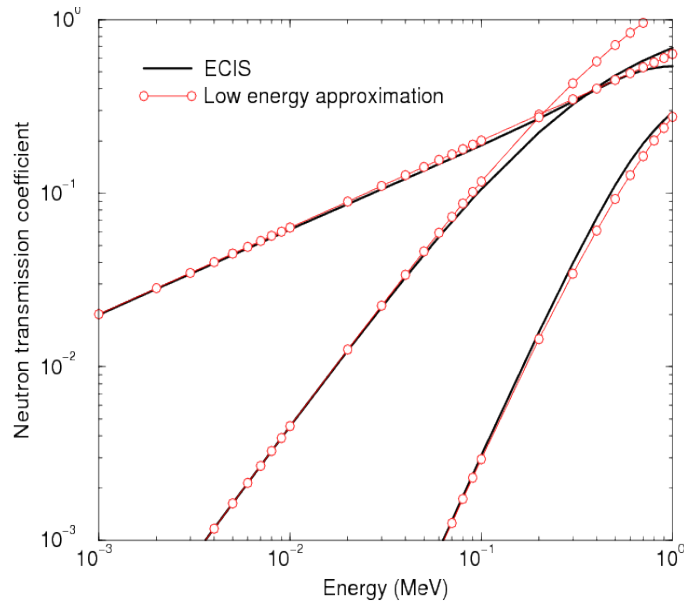


Figure 4.8: Comparison of the neutron transmission coefficients provided by the ECIS code and calculated with Eqs. (4.45) for the nuclear system $^{241}\text{Am}+n$. The equivalent hard sphere radii of Table 3.1 are used. The coupled channel calculations were performed with ECIS by using the parameters reported in the Japanese library JENDL-4.

By introducing the average collision function (4.22), σ_{pot} turns into a simple function of \bar{R}_{lJ}^∞ , s_{lJ} and $\bar{s}_{lJ}^{\text{loc}}$:

$$\sigma_{pot} \simeq 4\pi \sum_J g_{l=0,J} a_{l=0,J}^2 \left[(1 - \bar{R}_{l=0,J}^\infty)^2 + \pi^2 (s_{l=0,J} + \bar{s}_{l=0,J}^{\text{loc}})^2 \right]. \quad (4.47)$$

The definition of the potential scattering cross section (Eq. (3.17)):

$$\sigma_{pot} = 4\pi R'^2, \quad (4.48)$$

leads to the radius R' whose value can be calculated via the SPRT results:

$$R' \simeq \sqrt{\sum_J g_{l=0,J} a_{l=0,J}^2 \left[(1 - \bar{R}_{l=0,J}^\infty)^2 + \pi^2 (s_{l=0,J} + \bar{s}_{l=0,J}^{\text{loc}})^2 \right]}. \quad (4.49)$$

The latest term of this expression is negligible because the order of magnitude of the pole strength function is close to 10^{-2} :

$$R' \simeq \sqrt{\sum_J g_{l=0,J} a_{l=0,J}^2 (1 - \bar{R}_{l=0,J}^\infty)^2}. \quad (4.50)$$

Table 4.1: Neutron strength functions S_l and distant level parameters \overline{R}_l^∞ obtained with the SPRT method (Eqs. (4.35) and (4.36)) for the nuclear system $^{241}\text{Am}+n$. The channel radii a_c are taken from Tables 3.1 and 3.2. The coupled channel calculations were performed with ECIS by using the parameters reported in the Japanese library JENDL-4. Results are compared with those reported in Refs. [28, 69].

Parameters	ENDF	Equivalent	Mughabghab [28]	Lampoudis [69]
	convention Eq. (3.16)	hard sphere Eq. (3.63)		
$10^4 S_0$	1.01	1.01	0.90 ± 0.09	0.98 ± 0.10
$10^4 S_1$	2.19	2.82		
$10^4 S_2$	1.31	1.06		
\overline{R}_0^∞	-0.13	0		
\overline{R}_1^∞	0.11	0		
\overline{R}_2^∞	-0.05	0		
$a_c (l = 0)$	8.43	9.52		
$a_c (l = 1)$	8.43	7.20		
$a_c (l = 2)$	8.43	8.76		

According to the results reported in Table 4.1, the equivalent hard-sphere approximation also allows to remove the parameter \overline{R}_{lJ}^∞ from the expression of the effective radius:

$$R' \simeq \sqrt{\sum_J g_{l=0,J} a_{l=0,J}^2}. \quad (4.51)$$

In the case of a target nucleus of spin zero, the potential scattering length R' becomes strictly equivalent to the channel radius for s-waves. It represents the "effective" radius of the target at zero energy. This result confirms that the concept of "effective" radius is applicable only in the low-energy limit and only for $l = 0$ [72]. The potential scattering lengths obtained for the xenon, hafnium, neptunium and americium isotopes are reported in Table 4.2.

Table 4.2: Effective radius R' calculated with optical models described in Refs. [20–22] and reported in the Atlas of Neutron Resonances [28]. For $^{241}\text{Am}+n$, the given radius is a preliminary result.

Nuclear system	Optical Model	Mughaghab [28]
$^{124}\text{Xe}+n$	5.9 ± 0.2 fm	
$^{126}\text{Xe}+n$	5.8 ± 0.3 fm	
$^{128}\text{Xe}+n$	5.7 ± 0.3 fm	
$^{129}\text{Xe}+n$	5.6 ± 0.3 fm	
$^{130}\text{Xe}+n$	5.6 ± 0.3 fm	
$^{131}\text{Xe}+n$	5.5 ± 0.3 fm	
$^{132}\text{Xe}+n$	5.5 ± 0.3 fm	
$^{134}\text{Xe}+n$	5.3 ± 0.4 fm	
$^{136}\text{Xe}+n$	5.2 ± 0.4 fm	
$^{174}\text{Hf}+n$	7.9 ± 0.1 fm	7.5 ± 0.6 fm
$^{176}\text{Hf}+n$	7.8 ± 0.1 fm	7.6 ± 0.7 fm
$^{177}\text{Hf}+n$	7.4 ± 0.1 fm	
$^{178}\text{Hf}+n$	7.7 ± 0.1 fm	7.5 ± 0.7 fm
$^{179}\text{Hf}+n$	7.6 ± 0.1 fm	
$^{180}\text{Hf}+n$	7.8 ± 0.1 fm	8.0 ± 0.7 fm
$^{237}\text{Np}+n$	9.8 ± 0.1 fm	
$^{241}\text{Am}+n$	9.5 ± 0.6 fm	

Chapter 5

Conclusions

The present document gives an overview of the link between the R-Matrix and the S-Matrix formalisms. We focus the discussion on the role of the neutron strength function S_c , distant level parameter \overline{R}_c^∞ , channel radius a_c and potential scattering length (or "effective" radius) R' . The mathematical relationships between these parameters are explicated by using "standard" boundary conditions.

The theory of average cross sections was established in the 1950s. The mathematical treatment relies on the statistical nature of the neutron resonances. Average resonance parameters for s-waves (mean level spacings, neutron strength functions and average partial widths) can be determined from the statistical analysis of the resonance parameters extracted from the Resolved Resonance Range (RRR). For higher order partial waves ($l \geq 1$), we show that channel radii and neutron strength functions can be obtained by using the S-Matrix average cross section theory in conjunction with optical model calculations.

The main difficulty is the treatment of the distant level parameters \overline{R}_c^∞ . In applications of the R-Matrix theory, the latter mimic the contribution of the shape elastic reaction. Other direct reactions such as those involved in the inelastic process do not easily emerge from the R-matrix framework. The present work indicates how this problem can be solved according to the parameterization of the reduced R-function established by Lynn [62, 63]. We found that the final average expressions of the reduced R-function (Eq. (4.21)) and collision function (Eq. (4.22)) depend not only on the pole strength function s_c and distant level parameter \overline{R}_c^∞ , but also of a third parameter $\overline{s}_c^{\text{loc}}$ which accounts for the direct mechanisms. The generalized expressions of the SPRT method (Eqs. (4.35) and (4.36)) and the neutron transmission coefficient (Eq. (4.27)) were rearranged accordingly. In a second step, their artificial dependence on the channel radius can be removed by calculating the phase shift (Eq. (3.63)) and penetration factor (Eq. (4.32)) with equivalent hard-sphere radii deduced from optical model calculations. For the nuclear system $^{241}\text{Am}+n$, we found that this condition is satisfied if $\overline{R}_c^\infty = 0$.

In summary, the work presented here provides a description of the existing theory for treating the unresolved resonance range of the neutron induced reactions. New developments and methodologies are also presented. Parts of this work were implemented in existing nuclear data codes (CONRAD, TALYS) and applied to non-fissile (Hf, Xe) and fertile (Am, Np) isotopes. Results obtained for the nuclear system $^{241}\text{Am}+n$ were included in the version JEFF-3.2 of the Joint Evaluated Fission and Fusion File library.

Chapter 6

Perspectives

This document aims at presenting the knowledge acquired on the theory of average cross sections via the generalization of the SPRT method. This methodology is described in Appendix A. It was successfully used to analyse the unresolved resonance range of fissile and non-fissile nuclear systems. Examples for the Neptunium and Hafnium isotopes are reported in Appendices B and C. From these earlier studies, three main perspectives can be identified for improving the modeling of the neutron cross sections in the Resolved and Unresolved Resonance Ranges. The first perspective deals with the statistical nature of the neutron resonances in the low energy range. The second perspective consists in studying the limit of the theory of average cross section in order to extend the resolved resonance range. Such issues rely on the systematic behavior of the average parameters with the target mass.

6.1 Statistical nature of the neutron resonances

The new URR methodology, shortly presented in this document, has been implemented in the nuclear data code TALYS. This model relies on the conversion of the transmission coefficients calculated by the TALYS code in average resonance parameters. Furthermore, processing codes, such as the NJOY and CALENDF codes, can use these average parameters to calculate self-shielding factors or to generate ladders of statistical resonances. The latter treatment is illustrated in Fig. 6.1. The URR model of TALYS was applied to split the JEFF-311 pointwise representation of the ^{135}Xe capture cross section in three distinct energy ranges, namely Resolved Resonance Range, Unresolved Resonance Range and continuum. Some unknown or poorly known cross sections of intermediate-mass and heavy nuclei could take advantage of a similar modeling of the Resolved and Unresolved Resonance Ranges. In the TENDL library, the resolved resonance parameters and the average resonance parameters are generated via the URR model of TALYS [73]. With this new approach, all resonances are unique, following only statistical rules.

6.2 Extension of the Resolved Resonance Range

The statistical nature of the neutron resonances are of great interest to produce ladders of pseudo resonances able to reproduce the average behavior of the neutron cross sections. Figure 6.2 illustrates such a result for the nuclear system $^{241}\text{Am}+n$. A deeper investigation

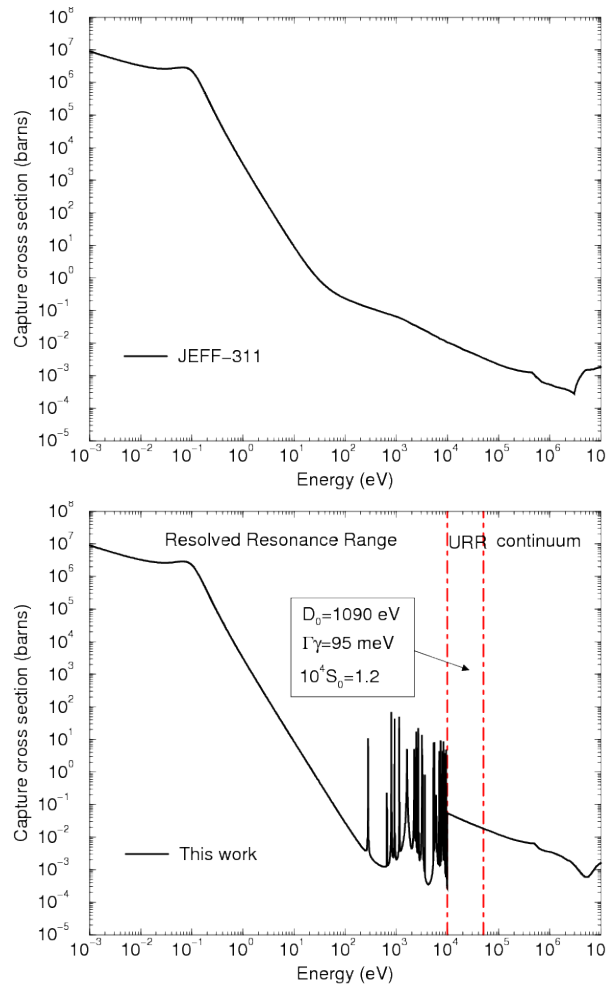


Figure 6.1: ^{135}Xe capture cross section from JEFF-311 (top plot) and reconstructed via average R-Matrix parameters calculated with the SPRT method under the Equivalent hard-sphere approximation (bottom plot). The optical model used for the SPRT calculations is described in Ref. [22].

of this result is needed in order to quantify the agreement between the R-Matrix and S-Matrix treatments over broad energy groups. Conclusions of this study will help to verify if the link between the low and high energy model calculations is correctly described by the generalization of the SPRT method.

6.3 Systematic behavior of the average parameters

Preliminary results presented in sections 6.1 and 6.2 rely on the statistical nature of the neutron resonances. The increasing amount of time-of-flight data, taken in last decade, will allow further analysis of the systematic behavior of the average parameters with the compound nucleus mass number. For non-fissile nuclei, evidence for non-statistical effects in both s- and p- wave radiative neutron capture could be useful to identify mass regions compatible with the "extreme" statistical model. For fissile nuclei, the link between the phenomenological fission widths of the Reich-Moore approximation and the transmission

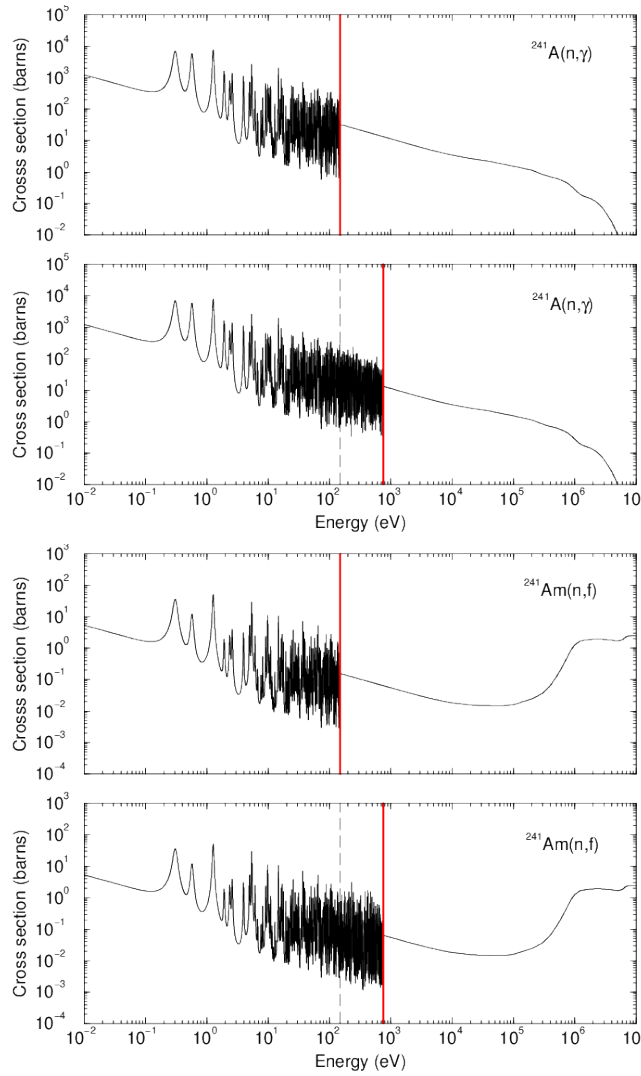


Figure 6.2: Extension of the Resolved Resonance Range of ^{241}Am with ladders of resonances whose partial widths were calculated via the SPRT method and the equivalent hard-sphere radius formalism.

coefficients through the fission barrier could be clarified. And finally, a reliable order of magnitude for the correlations between the reduced neutron widths and the radiative widths could be established for a correct processing of the Probability Tables.

Bibliography

- [1] A.M. Lane and R.G. Thomas, *Rev. Mod. Phys.* 30, 257 (1958).
- [2] F.C. Barker, *Aust. J. Phys.* 25, 341 (1972).
- [3] M. Herman, Data format and procedures for the evaluated nuclear data file, Report BNL-NCS-44945-05-Rev, Brookhaven National Laboratory, 2005.
- [4] T. Kawano et al., *Phys. Rev. C* 80, 024611 (2009).
- [5] P. Ribon and J-M. Maillard, Probability Tables Application to Cross Section Processing for Neutronic, NEACRP-L-294, 1986.
- [6] R.D. Mosteller and R.C. Little, Impact of MCNP Unresolved Resonance Probability-Table Treatment on Uranium and Plutonium Benchmarks, Los Alamos report LA-UR-98-2943, 1998.
- [7] J-C. Sublet et al., Unresolved resonance range cross section probability and self shielding factors, CEA Report CEA-R-6227, 2009.
- [8] G. Noguere et al., Contribution of the URR analysis for JEFF, OECD/NEA JEFDOC-1409, 2011.
- [9] J. Tommasi, E. Dupont and P. Marimbeau, *Nucl. Sci. Eng.* 154, 119 (2006).
- [10] J. Tommasi and G. Noguere, *Nucl. Sci. Eng.* 160, 232 (2008).
- [11] L. Leal et al., Assessment of the unresolved resonance treatment for cross-section and covariance representation, Report NEA/NSC/WPEC/DOC(2011)430.
- [12] C. Vaglio-Gaudard et al., *Nucl. Sci. Eng.* 166, 89 (2006).
- [13] F.H. Frohner, *Nucl. Sci. Eng.* 103, 119 (1989).
- [14] A. Courcelle et al., *Nucl. Sci. Eng.* 156, 391 (2007).
- [15] C. De Saint Jean et al., *Nucl. Sci. Eng.* 161, 363 (2009).
- [16] N.T. Koyumdjieva, N.B. Janeva and K.N. Volev, *Nucl. Sci. Eng.* 137, 194 (2001).
- [17] L.C. Leal, H. Derrien, and N.M. Larson, in: *Proceedings of PHYSOR 2004 - The Physics of Fuel Cycles and Advanced Nuclear Systems: Global Developments*, Chicago, USA, 2004.
- [18] I. Sirakov, in : *Proceedings of the WONDER Workshop on Nuclear Data Evaluation for Reactor Applications*, Cadarache, France, 2006.
- [19] E. Rich et al., *Nucl. Sci. Eng.* 162, 76 (2009).
- [20] G. Noguere et al., *Nucl. Phys. A* 831, 106 (2009).

-
- [21] G. Noguere, *Phys. Rev. C* 81, 044607 (2010).
- [22] G. Noguere et al., *Nucl. Phys. A* 870, 131 (2011).
- [23] E. Rich et al., *Nucl. Sci. Eng.* 162, 178 (2009).
- [24] P. Archier, Contribution à l'amélioration des données nucléaires neutroniques du sodium pour le calcul des réacteurs de génération IV, PhD Thesis, Grenoble University, 2011.
- [25] G. Noguere et al., *J. Korean Phys. Soc.* 59, 1343 (2011).
- [26] C. Lampoudis et al. submitted to *Eur. Phys. J.*
- [27] M.C. Moxon and J.B. Brisland, REFIT a Least Squares Fitting Program for Resonance Analysis of Neutron Transmission and Capture Data Computer Code, AEA-INTEC-0630, AEA Technology, 1991.
- [28] S.F. Mughabghab, *Atlas of Neutron Resonances* (Elsevier, Amsterdam, 2006).
- [29] S.I.Sukhoruchkin and Z.N.Soroko, *Atomic Mass and Nuclear Binding Energy*, Springer-Materials - The Landolt-Brnstein Database, 2009.
- [30] P. Romain, H. Duarte and B. Morillon, *Phys. Rev. C* 85, 044603 (2012).
- [31] G. Kessedjian, *Phys. Lett. B* 692, 297 (2010).
- [32] J.M. Blatt and V.F. Weisskopf, *Theoretical Nuclear Physics* (John Wiley and Sons, New York, 1952).
- [33] G. Breit, *Phys. Rev.* 58, 506, 1068 (1940).
- [34] A. Foderaro, *The Elements of Neutron Interaction Theory* (The MIT Press, Massachusetts, 1971)
- [35] E.P. Wigner and L. Eisenbud, *Phys. Rev.* 72, 29 (1947).
- [36] P.L. Kapur and R. Peierls, *Proc. Roy. Soc. (Lond.) A* 166, 277 (1938).
- [37] H. Feshbach, C.E. Porter and V.F. Weisskopf, *Phys. Rev.* 96, 448 (1954).
- [38] J. Raynal, Coupled Channel, Statistical Model, Schroedinger and Dirac Equation, Dispersion Relation, NEA-0850 ECIS-06.
- [39] G. Michaud, L. Scherk and E. Vogt, *Phys. Rev. C* 1, 864 (1970).
- [40] R. Capote et al., *Nuclear Data Sheets* 110, 3107 (2009).
- [41] T. Teichmann and E.P. Wigner, *Phys. Rev.* 87, 123 (1952).
- [42] T. Tamura, *Rev. Mod. Phys.* 37, 679 (1965).
- [43] E. Vogt, *Phys. Lett. B* 389, 637 (1996).
- [44] S.D. Drell, *Phys. Rev.* 100, 97 (1955).
- [45] W.D. Myers, *Nucl. Phys. A* 145, 387 (1970).
- [46] M. Bolsterli, E.O. Fiset, J.R. Nix and J.L. Norton, *Phys. Rev. C* 5, 1050 (1972).
- [47] H.A. Bethe and G. Placzek, *Phys. Rev.* 51, 450 (1937).
- [48] P.E. Hodgson, *Rep. Prog. Phys.* 34, 765 (1971).

-
- [49] W. Hauser and H. Feshbach, *Phys. Rev.* 87, 366 (1952).
- [50] E. Vogt, *Rev. Mod. Phys.* 34, 723 (1962).
- [51] E. Vogt, R-Matrix theory, R-Matrix School of the Joint Institute for Nuclear Astrophysics, Notre Dame University, Indiana, USA, 2004.
- [52] H.A. Bethe, *Phys. Rev.* 76, 38 (1949).
- [53] A.J. Koning and J.P. Delaroche, *Nucl. Phys. A* 713, 231 (2003).
- [54] B. Morillon and P. Romain, *Phys. Rev. C* 70, 014601 (2004).
- [55] O. Bersillon, Cross Sections and Angular Distributions for Spherical Nuclei by Optical Model, NEA-0829 SCAT-2, SCAT-2B.
- [56] S. Hilaire and M. Girod, *Eur. Phys. J. A* 33, 237 (2007).
- [57] R.G. Thomas, *Phys. Rev.* 97, 224 (1955).
- [58] T.D. Newton, *Can. J. Phys.* 30, 53 (1952).
- [59] H.A. Bethe, *Rev. Mod. Phys.* 9, 69 (1937).
- [60] P.A. Moldauer, *Phys. Rev.* 129, 754 (1963).
- [61] C.W. Reich and M.S. Moore, *Phys. Rev.* 111, 929 (1958).
- [62] J.E. Lynn, *The Theory of Neutron Resonance Reactions* (Clarendon Press, Oxford, 1968).
- [63] J.E. Lynn, *Proc. Phys. Soc.* 82, 903 (1963).
- [64] J-P. Delariche, Ch. Lagrange and J. Salvy, in: *Proceedings of a Consultants Meeting on the Use of Nuclear Theory in Neutron Nuclear Data Evaluation*, Trieste, Italy, 1975; See also IAEA-190, *International Atomic Energy Agency Nuclear Data Services* (1976).
- [65] D.J. Hughes and J.A. Harvey, *Phys. Rev.* 99, 1032 (1955).
- [66] C.E. Porter and R.G. Thomas, *Phys. Rev.* 104, 483 (1956).
- [67] A.M. Lane, R.G. Thomas and E.P. Wigner, *Phys. Rev.* 98, 693 (1955).
- [68] G. Noguere et al., *Phys. Rev. C* 74, 055802 (2006).
- [69] C. Lampoudis et al., *Eur. Phys. J. Plus* 128, 86 (2013).
- [70] E. Fort and J.P. Doat, *Neutron Width Level Spacing, Neutron Strength Function of S-Wave, P-Wave Resonances*, NEA-0892 ESTIMA.
- [71] O. Litaize et al., in: *Proceedings of the International Conference on Nuclear Data for Science and Technology*, Jeju Island, Korea, 2010.
- [72] F. Frohner, *Evaluation and analysis of nuclear resonance data*, JEFF Report 18, OECD/NEA, 2000.
- [73] A.J. Koning and D. Rochman, *Nucl. Data Sheets* 113, 2841 (2012).

Appendices

Appendix A

SPRT method

Generalization of the SPRT Method for the Modeling of the Neutron Cross Sections in the Unresolved Resonance Range

E. Rich, G. Noguère,* and C. De Saint Jean

Commissariat à l’Energie Atomique, DEN Cadarache, F-13108 Saint-Paul-Lez-Durance, France

and

A. Tudora

Bucarest University, Bucarest-Măgurele POB MG-11 R-76900, Romania

Received April 7, 2008

Accepted September 6, 2008

Abstract—*For the modeling of the neutron cross sections, three energy ranges can be distinguished. The resolved resonance range can be interpreted in terms of single-level, multilevel, Reich-Moore, or R-matrix parameters. The unresolved resonance range (URR) is described with the average R-matrix and Hauser-Feshbach formalisms. For the high energies (“continuum”), optical model parameters are used in association with statistical and preequilibrium models. One of the main challenges of such a work is to study the consistency of the average parameters obtained by these different calculations. With the ESTIMA and SPRT methods, we provide a set of parameters for partial s-waves and p-waves (strength functions S_l and effective potential scattering radius R'). However, accurate analysis of the URR domain needs more information than parameters R' and S_l associated with orbital moments $l = 0$ and $l = 1$. Using links between the average R-matrix formalism and the optical model calculations, we propose a generalization of the SPRT method for $l > 1$ and a new description of the URR domain in terms of S_l and R_{lj}^∞ .*

I. INTRODUCTION

The neutron cross sections of a given isotope are generally divided into three parts, each one being treated with a different formalism. At low energy, the resolved resonance range (RRR) can be analyzed by using appropriate approximations of the R-matrix formalism. The unresolved resonance range (URR) is commonly analyzed with the average R-matrix formalism. At higher energy (“continuum”), optical model calculations (direct interaction) are used in association with statistical and preequilibrium models.

One systematic challenge for this kind of work is the consistent description of the overlapping energy ranges. The link between the resolved and unresolved energy ranges is treated with statistical tests based on the distributions of the resonance parameters (see ESTIMA method described in Ref. 1). Concerning the relationships between the unresolved and continuum energy ranges, we

use the SPRT approach.² The latter consists of comparing the strength function (S_0, S_1) and the scattering radius R' by using mathematical models valid at low energy.

The link between the average R-matrix formalism and the optical model proposed in this paper is inspired from the work of Lane and Thomas.³ Relationships between these two models will be used to generalize the SPRT method to higher-order l values ($l > 1$). Moreover, as the parameterization in terms of l -dependent scattering radius R' is equivalent to a parameterization in terms of distant level parameter R^∞ (Ref. 4), we decided to propose a new description of the URR in terms of R_{lj}^∞ .

In Secs. II and III, basic features of the R-matrix formalism and optical model are given. Section IV focuses on the SPRT method and its generalization. Average parameters obtained for the compound systems $^{232}\text{Th} + n$, $^{238}\text{U} + n$, $^{240}\text{Pu} + n$, and $^{242}\text{Pu} + n$ are presented in Sec. V. Our results are then compared with those reported in the literature before concluding on the impact of such a work for the nuclear data evaluation activities.

*E-mail: gilles.noguere@cea.fr

II. AVERAGE R-MATRIX FORMALISM

The scattering theory, also called the R -matrix theory, is a phenomenological description of measured cross sections. It does not constitute a nucleon-nucleus model because it does not rely on physical phenomena of the interaction. It is a parameterization of the cross sections in terms of resonance parameters. From the theoretical point of view, the R -matrix formalism rests on the description of binary reactions between a projectile and a target nucleus in terms of wave functions of the entrance and exit channels. This presentation guesses the definition of what we call a channel c , corresponding to the identification of a pair of particles (in the entrance and exit channels) characterized by a given channel spin s , angular momentum J , and parity π . Considering the spin I of the target, the spin i of the projectile and its orbital momentum l , the total angular momentum J of the compound system satisfies the quantum-mechanical triangle relations as follows:

$$\vec{J} = \vec{l} + \vec{s} ,$$

where

$$\vec{s} = \vec{I} + \vec{i} . \quad (1)$$

Their vectorial combination leads to the following expressions:

$$|l - s| \leq J \leq l + s$$

and

$$|I - i| \leq s \leq I + i . \quad (2)$$

If π_I and π_i stand, respectively, for the parity of the target nucleus and of the projectile, the parity of the nuclear system is given by

$$\pi = (-1)^l \pi_I \pi_i . \quad (3)$$

The nuclear forces being short-range interactions, the system can be divided into two parts: one inside a sphere of radius a_c , where the compound nucleus process takes place, and one outside the sphere where direct interactions take place. According to the rules used in the Evaluated Nuclear Data Files,⁵ a reasonable choice for the channel radius a_c in the actinide region is

$$a_c \cong 1.35A^{1/3} \text{ fm} . \quad (4)$$

The internal range (where nuclear forces dominate) will be treated in terms of the collision matrix because the complexity of the interactions inside the compound nucleus does not allow the ab initio knowledge of the nuclear system wave function. This theory uses the non-relativistic quantum mechanics because the nucleon velocity is supposed to be very low compared to the light speed. However, it is possible to use this theory for rel-

ativistic neutron energies and to correct the result for relativistic effects.

In the R -matrix formalism, the collision matrix is generally called U . The matrix element $U_{cc'}(E)$ represents the amplitude of the exit wave c' induced by the interaction between the target and the projectile in the entrance channel c . The probability for this interaction to take place is given as

$$P_{c \rightarrow c'} = |U_{cc'}(E)|^2 . \quad (5)$$

In the frame of the collision matrix formalism, the total cross section $\sigma_t(E)$ and the shape elastic cross section $\sigma_e(E)$ are described as follows:

$$\sigma_t(E) = \frac{2\pi}{k^2} \sum_l (2l+1) \sum_J g_{lJ} \{1 - \text{Re}[U_{lJ}(E)]\} \quad (6)$$

and

$$\sigma_e(E) = \frac{\pi}{k^2} \sum_l (2l+1) \sum_J g_{lJ} |1 - U_{lJ}(E)|^2 , \quad (7)$$

where g_{lJ} stands for the statistical spin factor:

$$g_{lJ} = \frac{2J+1}{(2i+1)(2I+1)(2l+1)} . \quad (8)$$

In the URR, the experimental resolution is not sufficient to distinguish the individual resonances. However, these resonances exist and may have a significant impact on the self-shielding calculations. As cross sections cannot be analyzed with Eqs. (6) and (7), average expressions are used to characterize the physics in this energy range. In practice, the average formulation of the R -matrix theory is used to describe the total and shape elastic cross sections.

In the frame of the average R -matrix formalism, the total cross section, the shape elastic cross section, and the neutron transmission coefficients are modeled in terms of neutron strength function S_{lJ} and distant level parameter R_{lJ}^∞ . By using the standard boundary conditions as defined in Ref. 6, the average collision matrix averaged over resonances is given by Ref. 7:

$$\bar{U}_{lJ}(E) = \frac{e^{-2i\phi_l(E)}(1 + iP_l(E)R_{lJ}^\infty - s_{lJ}P_l(E)\pi)}{1 - iP_l(E)R_{lJ}^\infty + s_{lJ}P_l(E)\pi} . \quad (9)$$

Parameter s_{lJ} is called the pole strength. It can be written in terms of the dimensionless neutron strength function S_{lJ} as follows:

$$S_{lJ} = \frac{S_{lJ}\sqrt{E}}{2ka_c} . \quad (10)$$

If the neutron incident energy is given in electron volts, with the neutron wave number k is defined as

$$k = \frac{1}{\lambda} = \frac{\sqrt{2m_n E_{cm}}}{\hbar} = 2.1968 \times 10^{-4} \left(\frac{A}{A+1} \right) \sqrt{E} . \quad (11)$$

In Eq. (9), $P_l(E)$ and $\phi_l(E)$ are, respectively, the penetration factor of the centrifugal barrier and the phase shift of the incident wave scattered by a sphere. In the case of a neutral incident particle, $P_l(E)$ and $\phi_l(E)$ are given by

$$P_l(E) = \frac{\rho^2(E)P_{l-1}(E)}{(l - F_{l-1}(E))^2 + P_{l-1}^2(E)}$$

with

$$P_0(E) = \rho(E) \quad (12)$$

and

$$\phi_l(E) = \phi_{l-1}(E) - \tan^{-1} \left(\frac{P_{l-1}(E)}{l - F_{l-1}(E)} \right)$$

$$\phi_0(E) = \rho(E) . \quad (13)$$

The $F_l(E)$ factor represents the phase shift factor. Its standard expression is

$$F_l(E) = \frac{\rho^2(E)(l - F_{l-1}(E))}{(l - F_{l-1}(E))^2 + P_{l-1}^2(E)} - l$$

with

$$F_0(E) = 0 . \quad (14)$$

In Eqs. (12), (13), and (14), $\rho(E)$ is the product of the wave number by the channel radius:

$$\rho(E) = ka_c . \quad (15)$$

Equation (9) permits obtaining a simple expression of the transmission coefficient in terms of s_{lJ} and R_{lJ}^∞ . For a given orbital momentum l and a given J^π , we have

$$T_{lJ}(E) = 1 - |\bar{U}_{lJ}(E)|^2 = \frac{4\pi P_l(E)s_{lJ}}{(1 + \pi P_l(E)s_{lJ})^2 + P_l(E)^2 R_{lJ}^{\infty 2}} . \quad (16)$$

By the same way, introducing the average collision matrix expression given by Eq. (9) in Eq. (6), the average total cross section for a given l and a given J^π can be written as

$$\sigma_t^{lJ}(E) = \frac{2\pi}{k^2} \left\{ 1 - \frac{[P_l(E)^2(R_{lJ}^{\infty 2} + \pi^2 s_{lJ}^2) - 1] \cos(2\phi_l(E)) - 2P_l(E)R_{lJ}^\infty \sin(2\phi_l(E))}{(1 + \pi P_l(E)s_{lJ})^2 + P_l(E)^2 R_{lJ}^{\infty 2}} \right\} . \quad (17)$$

The shape elastic cross section for a given l and J^π can be easily deduced from Eq. (7) by combining Eqs. (16) and (17) as follows:

$$\sigma_e^{lJ}(E) = \sigma_t^{lJ}(E) - \frac{\pi}{k^2} T_{lJ}(E) . \quad (18)$$

We obtain

$$\sigma_e^{lJ}(E) = \frac{2\pi}{k^2} \left\{ 1 - \frac{[P_l(E)^2(R_{lJ}^{\infty 2} + \pi^2 s_{lJ}^2) - 1] \cos(2\phi_l(E)) - 2P_l(E)R_{lJ}^\infty \sin(2\phi_l(E)) - 2\pi P_l(E)s_{lJ}}{(1 + \pi P_l(E)s_{lJ})^2 + P_l(E)^2 R_{lJ}^{\infty 2}} \right\} . \quad (19)$$

After that, the potential cross section σ_{pot} is defined as the limit value of $\sigma_e(E)$ as follows:

$$\sigma_{pot} = \sum_J g_{l=0,J} \lim_{E \rightarrow 0} \sigma_e^{l=0,J}(E) . \quad (20)$$

At low energy, only s -waves contribute:

$$\sigma_{pot} = 4\pi a_c^2 \sum_J g_{l=0,J} \{ (1 - R_{l=0,J}^\infty)^2 + \pi^2 s_{l=0,J}^2 \} . \quad (21)$$

As $s_{l=0,J}$ is lower than unity, Eq. (21) becomes

$$\sigma_{pot} = 4\pi R'^2, \quad (22)$$

where R' stands for the effective scattering radius. For s -waves, it is defined as

$$R' = R'_{l=0} = a_c \sqrt{\sum_J g_{l=0,J} (1 - R_{l=0,J}^\infty)^2}. \quad (23)$$

For a ground-state spin $I = 0$, only one value is possible for J ($J = \frac{1}{2}$). In this case, R' becomes a simple function of the distant level parameter:

$$R' = a_c (1 - R_0^\infty). \quad (24)$$

This expression is used to take into account the link between the scattering radius and the entrance channel radius a_c . The variation of the effective radius R' with the entrance channel can be approximated as follows⁸:

$$R'_l \approx a_c [1 - (2l + 1)R_l^\infty]^{1/(2l+1)}. \quad (25)$$

III. OPTICAL MODEL CALCULATIONS

In the optical model, we consider that the incident nucleon interacts with a complex mean-field potential. These calculations consist of solving the Schrödinger equation by separating the space of the system states into two orthogonal spaces: The first one is relative to the case of the separated nucleon and the target nucleus, when the second one concerns the compound nucleus. The difficulty of this model is to find the appropriate potential, which will reproduce the experimental data when it is introduced in the Schrödinger equation. Two types of approaches can be used to build an optical potential as follows:

1. the semimicroscopic approach, which tries to evaluate the potential based on fundamental elements (as the nucleon-nucleon interaction, for example)
2. the phenomenological approach, which consists in parameterizing a potential and adjusting its parameters to be consistent with the experimental data.

In this work, we have used a phenomenological description of the potential whose volume, surface, and spin-orbit components are described with Wood-Saxon form factors. Parameters of the model (well depths, radius, diffuseness, etc.) are compiled in the Reference Input Parameter Library⁹ (RIPL). Many papers address the parameterization of local or global potentials above the kilo-electron-volt neutron energy range. An example of parameterization for nonspherical nuclei and a specific discussion on the effect of the nuclear deformation on the scattering properties at low neutron energies (below a few mega-electron-volts) can be found in Ref. 10.

In practice, the total cross section, the shape elastic cross section, and the transmission coefficients are obtained by using the real and imaginary parts of the collision matrix. In optical model calculations, the collision matrix is generally noted C . The matrix elements are related to the elements of the scattering matrix S by the expression

$$S_{cc'}(E) = 1 + 2iC_{cc'}(E). \quad (26)$$

In this representation, the reaction channel definition is slightly different from the one used in the R -matrix formalism. In the case of elastic or inelastic neutron scattering reactions where spin-orbit interactions are large, it is convenient to define the neutron with angular momenta l and j . The latter quantum number can take two different values as follows:

$$\begin{cases} j = l - \frac{1}{2} \\ j = l + \frac{1}{2} \end{cases}, \quad (27)$$

so that the total angular momentum J of the target and the neutron is given by

$$|j - I_n| \leq J \leq j + I_n. \quad (28)$$

I_n represents the spin of the fundamental levels of rotational bands ("head bands") used to model the collective excitation modes by a vibrational coupling. The level $n = 1$ is the fundamental level of the target nucleus having a ground-state spin I .

By using the definitions proposed in Eqs. (6), (7), and (8), the total cross section $\sigma_t(E)$ and the shape elastic cross section $\sigma_e(E)$ can be written as

$$\sigma_t(E) = \frac{2\pi}{k^2} \sum_l (2l + 1) \sum_j g_{lj} \{1 - \text{Re}[S_{lj}^J(E)]\} \quad (29)$$

and

$$\sigma_e(E) = \frac{\pi}{k^2} \sum_l (2l + 1) \sum_j g_{lj} |1 - S_{lj}^J(E)|^2. \quad (30)$$

By introducing expression (26) into Eqs. (29) and (30), we obtain a more compact formulation for the total and shape elastic cross sections. For a given couple (l, j) , $\sigma_t^{lj}(E)$ and $\sigma_e^{lj}(E)$ are written as

$$\sigma_t^{lj}(E) = \frac{4\pi}{k^2} \text{Im}[C_{lj}^J(E)] \quad (31)$$

and

$$\sigma_e^{lj}(E) = \frac{4\pi}{k^2} |C_{lj}^J(E)|^2. \quad (32)$$

The neutron transmission coefficients are related to the total reaction cross section. They can be obtained by combining the expression of the total cross section and those of shape elastic and direct inelastic cross sections. We obtain

$$T_{lj}(E) = 4 \operatorname{Im}[C_{lj}^J(E)] - 4 |C_{lj}^J(E)|^2 - 4 \sum_{l' \neq l} \sum_{j' \neq j} |C_{l'j'}^J(E)|^2 . \quad (33)$$

In the case of optical model calculations using a spherical potential (no coupling), the last term of Eq. (33) disappears, and the expression of the $T_{lj}(E)$ becomes

$$T_{lj}(E) = 4 \operatorname{Im}[C_{lj}^J(E)] - 4 |C_{lj}^J(E)|^2 . \quad (34)$$

The aim of the work presented in this paper consists of linking Eqs. (31) and (32) to Eqs. (17) and (19).

IV. SPRT METHOD

IV.A. Presentation of the Standard Method

The SPRT method is used to study the consistency between the average R -matrix parameters adjusted on experimental data and those given by optical model calculations. The standard method proposed in Ref. 2 is applied to strength functions (S_0 and S_1) and effective scattering radius R' . In the case of the "low-energy" approximation of the average R -matrix formalism, transmission coefficients involved in Eq. (16) become

$$T_l(E) \approx 4\pi P_l(E) s_l . \quad (35)$$

In the frame of the optical model calculations, the l -dependent transmission coefficients can be calculated as follows:

$$T_l(E) = \sum_j \sum_J g_{lJ} T_{lj}(E) . \quad (36)$$

By replacing the pole strength s_l in Eq. (35) with the following expression:

$$s_l = \frac{S_l \sqrt{E}}{2ka_c} , \quad (37)$$

and by using Eq. (36), the neutron strength function is then given by

$$S_l \approx \frac{1}{2\pi} \frac{ka_c \sqrt{E}}{P_l(E)} \sum_j \sum_J g_{lJ} T_{lj}(E) . \quad (38)$$

Another parameter involved in the SPRT method is the scattering radius R' . At low energy, it could be simply deduced from the shape elastic cross section as follows:

$$R' \approx \sqrt{\frac{1}{4\pi} \sigma_e(E)} . \quad (39)$$

This relationship allows a direct comparison of the potential scattering obtained from optical model calculations with values reported in the literature. Its domain of application is rather limited because Eq. (39) supposes a weak variation of the shape elastic cross section with the incident neutron energy.

The TALYS code¹¹ uses this standard SPRT method to provide values of S_0 , S_1 , and R' below 100 keV. The interest of such a process is to obtain the energy dependence of each parameter and to extrapolate if necessary their value at B_n (i.e., $E = 0$). However, this method is limited because it is restricted to $l \leq 1$ and gives an R' value that is not directly present in the R -matrix formalism. The use of the average collision matrix elements will be the starting point to generalize the SPRT method in order to deduce average parameters useful for the modeling of the URR.

IV.B. Generalization of the Method

The generalization of the SPRT method could not be only supported by neutron transmission coefficients. Actually, R -matrix formalism does not reproduce the direct contribution of inelastic reactions, which is, on the other hand, correctly taken into account by coupled-channel calculations. Then, in order to generalize the SPRT approach, we decided to use the expressions of the total and shape elastic cross sections. In the URR domain, the exercise consists of determining the parameters s_{lJ} and R_{lJ}^∞ as

$$\begin{cases} \sigma_t(s_{lJ}, R_{lJ}^\infty, E) = \sigma_t(\operatorname{Im}[C_{lj}^J(E)]) \\ \sigma_e(s_{lJ}, R_{lJ}^\infty, E) = \sigma_e(|C_{lj}^J(E)|) . \end{cases} \quad (40)$$

Expressions of the total cross section σ_t and of the shape elastic cross section σ_e used in the R -matrix formalism and the optical model calculations are very similar. Equations (29) and (30) become identical to expressions (6) and (7) when the ground-state spin of the target nucleus is zero ($I = 0$). In this case, the scattering matrix elements and the average collision matrix become formally identical:

$$S_{ij=J}^J(E) = \bar{U}_{lJ}(E) . \quad (41)$$

Consequently, Eq. (41) leads directly to the following analytical expressions. For a couple (l, J) , we obtain

$$R_{IJ}^{\infty} = \frac{2a_{IJ}(E)\cos[2\phi_l(E)] + (1 - 2b_{IJ}(E))\sin[2\phi_l(E)]}{P_l(E)(1 + 2c_{IJ}^2(E) - 2b_{IJ}(E) + (1 - 2b_{IJ}(E))\cos[2\phi_l(E)] - 2a_{IJ}(E)\sin[2\phi_l(E)])} \quad (42)$$

and

$$s_{IJ} = \frac{2(b_{IJ}(E) - c_{IJ}^2(E))}{\pi P_l(E)(1 + 2c_{IJ}^2(E) - 2b_{IJ}(E) + (1 - 2b_{IJ}(E))\cos[2\phi_l(E)] - 2a_{IJ}\sin[2\phi_l(E)]} . \quad (43)$$

For a ground-state spin $I = 0$, parameters $a_{IJ}(E)$, $b_{IJ}(E)$, and $c_{IJ}(E)$ are defined as

$$\begin{cases} a_{IJ}(E) = \text{Re}[C_{ij=J}^J(E)] \\ b_{IJ}(E) = \text{Im}[C_{ij=J}^J(E)] \\ c_{IJ}(E) = |C_{ij=J}^J(E)| . \end{cases} \quad (44)$$

The expressions above are very close to those coming from Ref. 12. The generalization of these relationships to the target nucleus having a ground-state spin different from zero consists of combining the real and imaginary parts of the collision matrix elements and of calculating the average value of the following quantities:

$$a_{IJ}^2(E) = c_{IJ}^2(E) - b_{IJ}^2(E) , \quad (45)$$

$$b_{IJ}(E) = \langle \text{Im}[C_{ij}^J(E)] \rangle_j , \quad (46)$$

and

$$c_{IJ}^2(E) = \langle |C_{ij}^J(E)|^2 \rangle_j . \quad (47)$$

Equations (42) through (47) constitute a system of expressions that will be used to generalize the SPRT method. Equations (42) through (47) permit obtaining the strength function and the distant level parameter for a given couple (l, J) .

In the frame of the low-energy approximation, the phase shift ϕ_l of the incident wave scattered on a sphere can be considered as lower than unity and leads to these following asymptotic expressions:

$$R_{ij}^{\infty} \approx \frac{a_{IJ}(E) + \phi_l(E)}{P_l(E)} \quad (48)$$

and

$$s_{IJ} \approx \frac{b_{IJ}(E) - c_{IJ}^2(E)}{\pi P_l(E)} . \quad (49)$$

In practice, the treatment of the URR domain with the average R -matrix formalism implies the knowledge of the average parameters for a given orbital momentum l . The system to be solved is now

$$\begin{cases} \sigma_t^l(s_l, R_l^{\infty}, E) = \sum_J \sum_j g_{lJ} \sigma_t^{lj}(\text{Im}[C_{ij}^J(E)]) \\ \sigma_e^l(s_l, R_l^{\infty}, E) = \sum_J \sum_j g_{lJ} \sigma_e^{lj}(|C_{ij}^J(E)|) . \end{cases} \quad (50)$$

Expressions of parameters s_l and R_l^{∞} satisfying the conditions given above are formally identical to Eqs. (42) and (43). Parameters $a_{IJ}(E)$, $b_{IJ}(E)$, and $c_{IJ}(E)$ are replaced by $a_l(E)$, $b_l(E)$, and $c_l(E)$, which are defined as

$$a_l^2(E) = c_l^2(E) - b_l^2(E) , \quad (51)$$

$$b_l(E) = \sum_J \sum_j g_{lJ} \text{Im}[C_{ij}^J(E)] , \quad (52)$$

and

$$c_l^2(E) = \sum_J \sum_j g_{lJ} |C_{ij}^J(E)|^2 . \quad (53)$$

This formalism is very powerful because the total and shape elastic cross sections are defined by a restricted set of parameters. Two parameters are sufficient to calculate the contribution of each partial wave. However, as we want to build a consistent modeling of the neutron-induced reaction cross sections from the thermal to mega-electron-volt energy ranges, combining s_l and R_{ij}^{∞} parameters is a priority. In the R -matrix frame, the distant level parameter for a given (l, J) couple has a more physical sense than the scattering radius, and we want to maintain it over the URR. For the strength function, parameterization in terms of l is sufficient as it is generally difficult to extract realistic average reduced neutron width for a given J . Then, the generalization of the SPRT method consists of determining the R_{ij}^{∞} parameters with Eq. (42). The s_l parameter is determined by minimization of the following conditions:

$$\begin{cases} \sigma_t^l(s_l, R_{ij}^{\infty}, E) = \sigma_t^l(s_{lJ}, R_{ij}^{\infty}, E) \\ \sigma_e^l(s_l, R_{ij}^{\infty}, E) = \sigma_e^l(s_{lJ}, R_{ij}^{\infty}, E) . \end{cases} \quad (54)$$

For analyzing the RRR, the REFIT shape analysis code¹³ allowed the parameterization in terms of R_{ij}^{∞} . To satisfy the coherence criteria, this choice was also included in the CONRAD code,¹⁴ dedicated to the neutron cross-section analysis in the RRR and URR.

V. APPLICATION OF THE GENERALIZED SPRT METHOD TO ACTINIDES

V.A. Comparison of the Results Obtained with the ECIS and OPTMAN Codes

The generalized SPRT method was applied to several actinides, ^{232}Th , ^{238}U , ^{240}Pu , and ^{242}Pu . For the optical model calculations, the coupled-channel codes ECIS (Ref. 15) and OPTMAN (Refs. 16 and 17) were used with the optical model parameters reported in RIPL (Ref. 9). The final SPRT values reported in this work are based on the results of these coupled-channel codes.

For this study, coupled-channel calculations were performed by using the optical model parameters established by Capote et al.¹⁸ This dispersive and relativistic potential is one of the most recent proposed in RIPL, which is dedicated to the modeling of the neutron-induced reactions in the actinide region for incident energies ranging from 1 keV to 200 MeV. Results obtained by Capote et al. prove that its coupled-channel optical potential with dispersive relations can be used for prediction of optical data for nucleon-induced reactions on experimentally uninvestigated minor actinide nuclei. For proof, results obtained with this potential are in excellent agreement with the experimental data for the $^{238}\text{U} + n$ and $^{232}\text{Th} + n$ reactions.

As we chose the optical model parameters determined by Capote et al., the OPTMAN code must be preferred to ECIS because the geometry is different for the Hartree-Fock real potential V_{hf} and the imaginary potential W_v . However, as OPTMAN provides only l -dependent results and ECIS gives collision matrix elements for a given couple (l, j) , we decided to apply our generalized SPRT method by running the ECIS code with the optical model parameters of Capote et al. Average parameters for $^{232}\text{Th} + n$ and $^{238}\text{U} + n$ obtained with ECIS and OPTMAN are reported in Table I. The comparison of the SPRT results in both cases shows that the

TABLE I

Strength Functions (S_0), Distant Level Parameters (R_0^∞), and Scattering Radius R' for $^{232}\text{Th} + n$ and $^{238}\text{U} + n$ Obtained with the Generalized SPRT Method by Using the OPTMAN and ECIS Codes with the Optical Model Parameters Determined by Capote et al.*

SPRT Parameters	OPTMAN		ECIS	
	$^{232}\text{Th} + n$	$^{238}\text{U} + n$	$^{232}\text{Th} + n$	$^{238}\text{U} + n$
$10^4 S_0$	0.86	0.93	0.86	0.93
R_0^∞	-0.17	-0.15	-0.17	-0.15
R'	9.71 fm	9.66 fm	9.70 fm	9.67 fm

*Reference 18.

discrepancy between these two different codes can be disregarded.

V.B. Comparison of the Results Obtained with the Standard and Generalized SPRT Methods

The most important contribution of the generalization of the SPRT method is the better consideration of the energy dependence of the average parameters, like strength functions and distant level parameters. This is done by extending the calculation to any orbital momentum, using the energy-dependent S -matrix elements.

As ^{232}Th and ^{238}U have a ground-state spin $I = 0$, the solid curves of Fig. 1 represent the generalized SPRT results calculated with Eqs. (42), (43), and (44). The dashed curves stand for the results obtained with the standard SPRT method. They have been obtained with Eq. (49), i.e., in the frame of the low-energy approximation. These results are consistent with those coming from the TALYS calculations. At low energy, Eq. (38) used in TALYS is equivalent to Eq. (49).

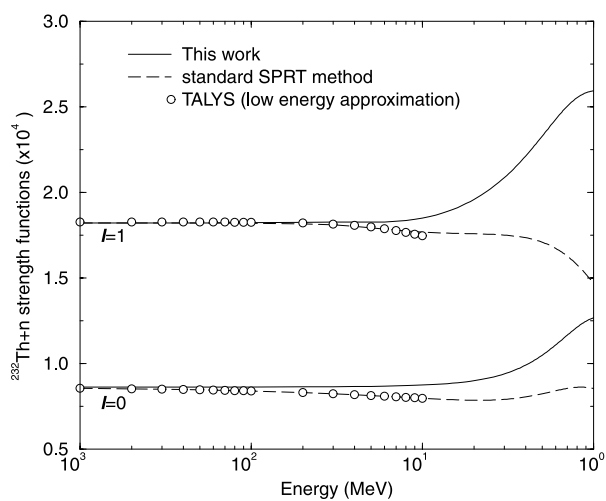
Below 10 keV, all the investigated methods give consistent results. Above this arbitrary energy limit, the formalism based on the low-energy approximation becomes rapidly inappropriate to describe the energy independence of the average parameters. At 100 keV, the discrepancy between the two formalisms is $\sim 10\%$.

V.C. Results on Actinides

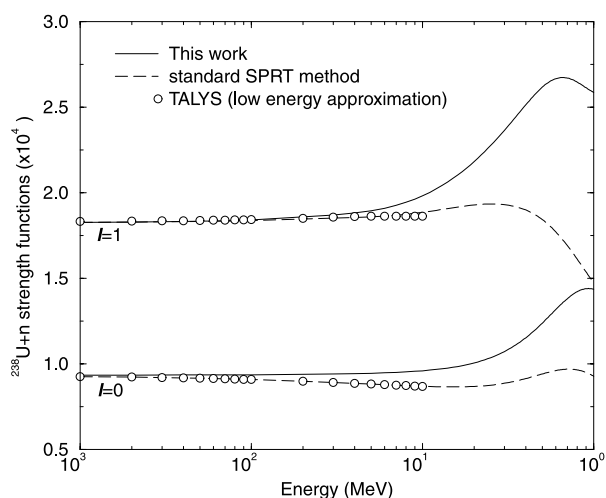
The ^{232}Th and ^{238}U strength functions S_l and distant level parameters R_l^∞ (for s -, p -, d -, and f -waves) obtained with the generalized SPRT method as a function of the incident neutron energy are presented in Figs. 2 and 3. The energy dependence of each parameter is described with an interpolating polynomial in the Lagrange form.

The values of the distant level parameters and scattering radii obtained with the generalized SPRT method and extrapolated to the binding energy B_n are given in Table II for $^{232}\text{Th} + n$, $^{238}\text{U} + n$, $^{240}\text{Pu} + n$, and $^{242}\text{Pu} + n$. The scattering radius R' is calculated using Eq. (24). Concerning this last parameter, the results provided by the generalized SPRT method are in good agreement with those reported in the last edition of the *Atlas of Neutron Resonances*¹⁹ and remain within the limits of the recommended uncertainties.

The strength functions obtained with the generalized SPRT method and extrapolated to the binding energy B_n are given in Table III for the same nuclear systems. Our s -wave strength functions are in good agreement with those reported in RIPL. They are either within the limits of the associated uncertainties (for ^{232}Th and ^{240}Pu) or at the lower limits of them (for ^{238}U and ^{242}Pu). However, the comparison of our results with the values reported in the *Atlas of Neutron Resonances* highlights significant discrepancies for $^{232}\text{Th} + n$ and $^{238}\text{U} + n$. The agreement could be improved by tuning slightly the



(a)



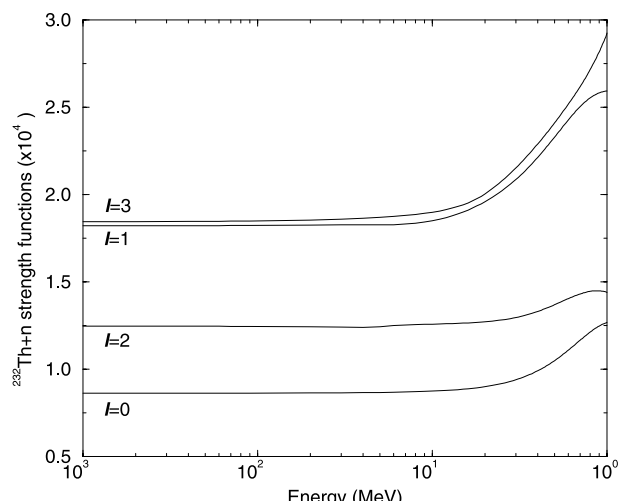
(b)

Fig. 1. The ^{232}Th and ^{238}U strength functions obtained with the generalized SPRT method by using the ECIS code with the optical model parameters established by Capote et al.¹⁸ Our results are compared with those given by the standard SPRT method² and the TALYS code.¹¹

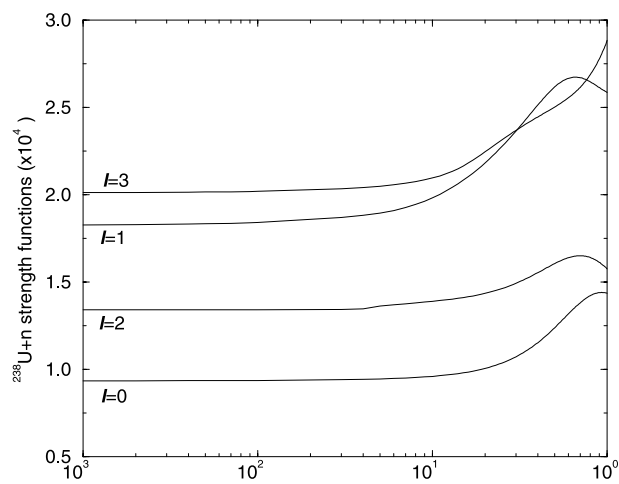
quadrupole deformation β_2 within the accepted limits of the Möller and Nix systematic.²⁰

V.D. The Generalized SPRT Method and CONRAD

The average parameters reported in this work have been determined to be used as input parameters of the FITACS option of the SAMMY and CONRAD codes.^{6,14} The latter codes were designed to adjust l -dependent strength functions, distant level parameters, and average partial widths on experimental total and partial cross sections. The total cross section is calculated with the



(a)



(b)

Fig. 2. The s -, p -, d -, f -wave strength functions for (a) $^{232}\text{Th} + n$ and (b) $^{238}\text{U} + n$ obtained with the generalized SPRT method by running the ECIS code with the optical model parameters established by Capote et al.¹⁸

average R -matrix formalism, using strength functions and distant level parameters at B_n . For the partial cross sections, these codes use the Hauser-Feshbach formulas with the Moldauer prescriptions for the width fluctuations. The energy dependence of the average radiation width is described by a Giant Dipole Resonance formalism. In CONRAD and SAMMY, values of the l -dependent mean level spacing are calculated with the Gilbert-Cameron formulas, and the fission barrier transmission coefficients are based on the Hill-Wheeler treatment.

As our results obtained on ^{242}Pu are consistent with those reported in RIPL and in the *Atlas of Neutron Resonances*, we decided to compare the theoretical ^{242}Pu

TABLE II

Distant Level Parameters (R_{ij}^∞) and Scattering Radii (R') Obtained with the Generalized SPRT Method, Using the ECIS Code with the Optical Model Parameters Established by Capote et al.*

Nuclear Systems	This Work			Mughabghab ¹⁹
$^{232}\text{Th} + n$				
$l = 0$	$R_0^\infty = -0.170$	$R_{0,1/2}^\infty = -0.170$		
$l = 1$	$R_1^\infty = 0.101$	$R_{1,1/2}^\infty = 0.044$	$R_{1,3/2}^\infty = 0.137$	
$l = 2$	$R_2^\infty = -0.097$	$R_{2,3/2}^\infty = -0.151$	$R_{2,5/2}^\infty = -0.053$	
$l = 3$	$R_3^\infty = 0.217$	$R_{3,5/2}^\infty = 0.198$	$R_{3,7/2}^\infty = 0.228$	
	$R' = 9.7 \text{ fm}$			$R' = 9.65 \pm 0.08 \text{ fm}$
$^{238}\text{U} + n$				
$l = 0$	$R_0^\infty = -0.155$	$R_{0,1/2}^\infty = -0.155$		
$l = 1$	$R_1^\infty = 0.119$	$R_{1,1/2}^\infty = 0.066$	$R_{1,3/2}^\infty = 0.159$	
$l = 2$	$R_2^\infty = -0.074$	$R_{2,3/2}^\infty = -0.127$	$R_{2,5/2}^\infty = -0.028$	
$l = 3$	$R_3^\infty = 0.219$	$R_{3,5/2}^\infty = 0.227$	$R_{3,7/2}^\infty = 0.211$	
	$R' = 9.67 \text{ fm}$			$R' = 9.6 \pm 0.1 \text{ fm}$
$^{240}\text{Pu} + n$				
$l = 0$	$R_0^\infty = -0.138$	$R_{0,1/2}^\infty = -0.138$		
$l = 1$	$R_1^\infty = 0.127$	$R_{1,1/2}^\infty = 0.083$	$R_{1,3/2}^\infty = 0.160$	
$l = 2$	$R_2^\infty = -0.053$	$R_{2,3/2}^\infty = -0.100$	$R_{2,5/2}^\infty = -0.014$	
$l = 3$	$R_3^\infty = 0.219$	$R_{3,5/2}^\infty = 0.218$	$R_{3,7/2}^\infty = 0.218$	
	$R' = 9.55 \text{ fm}$			$R' = 9.6 \pm 0.2 \text{ fm}$
$^{242}\text{Pu} + n$				
$l = 0$	$R_0^\infty = -0.137$	$R_{0,1/2}^\infty = -0.137$		
$l = 1$	$R_1^\infty = 0.130$	$R_{1,1/2}^\infty = 0.082$	$R_{1,3/2}^\infty = 0.167$	
$l = 2$	$R_2^\infty = -0.055$	$R_{2,3/2}^\infty = -0.104$	$R_{2,5/2}^\infty = -0.014$	
$l = 3$	$R_3^\infty = 0.229$	$R_{3,5/2}^\infty = 0.231$	$R_{3,7/2}^\infty = 0.226$	
	$R' = 9.56 \text{ fm}$			$R' = 9.8 \pm 0.2 \text{ fm}$

*Reference 18.

total cross section obtained with ECIS and CONRAD with two experimental data sets retrieved from the EXFOR database. Results are shown in Fig. 4. The older experiment was carried out at the Material Testing Reactor fast chopper of Idaho.²¹ The second data set was measured at the pulsed neutron facility of Los Alamos National Laboratory²² (LANL). Both experiments used the time-of-flight method. The first one was designed to investigate the low-energy range (i.e., from 1.3 meV to 7.7 keV), and the LANL experiment was dedicated to the high-energy range (from 676 keV to 175 MeV).

The ECIS calculations were done with the optical model parameters established by Capote et al. The CONRAD code uses the average parameters provided by the generalized SPRT method (Tables II and III). At low energy, experimental and theoretical results are in good agreement. Between 100 keV and 1 MeV, the discrepancy remains lower than 4%. The agreement could be significantly improved by introducing energy-dependent neutron strength function and distant level parameters

in the CONRAD code. This functionality is under development.

VI. CONCLUSIONS

Comparison between the average parameters extracted from high-energy calculations and those adjusted on experimental data with the average R -matrix formalism is crucial for the accurate modeling of the URR. In the present work, the generalized SPRT method, used in association with the optical model parameters established by Capote et al., leads to a consistent description of the total cross section up to 1 MeV. This study can be easily repeated with other spherical or deformed optical potentials. For the modeling of neutron-induced reactions on a large number of nonfissile isotopes, the consistency of the l -dependent average parameters reported in the literature is under investigation with phenomenological optical model potential containing dispersive terms and based on refined microscopical calculations.^{23,24}

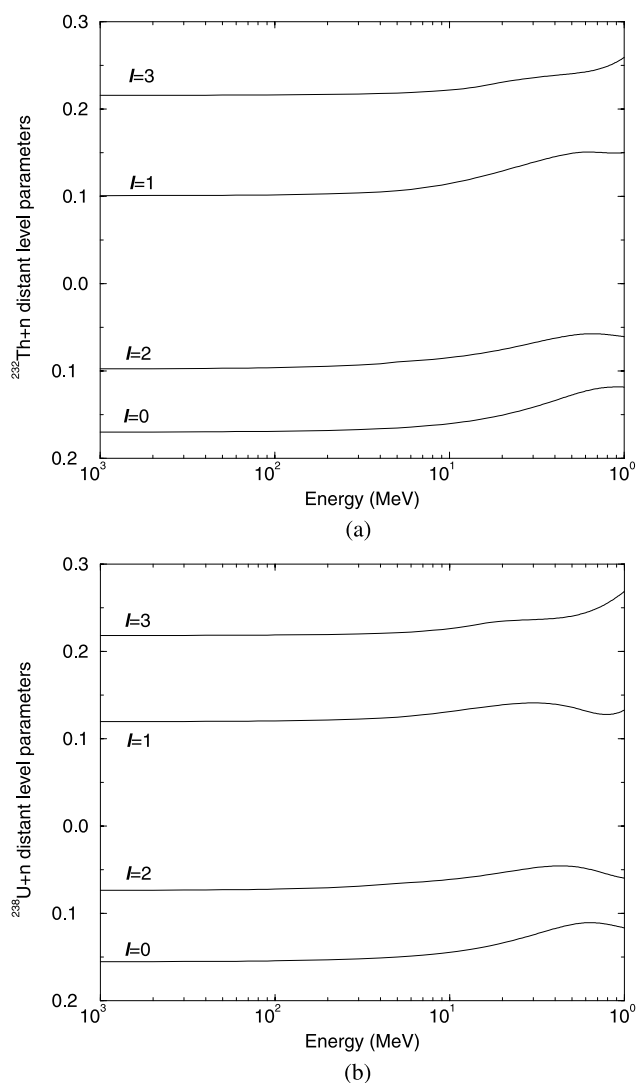


Fig. 3. The s -, p -, d -, f -wave distant level parameters for (a) $^{232}\text{Th} + n$ and (b) $^{238}\text{U} + n$ obtained with the generalized SPRT method by running the ECIS code with the optical model parameters established by Capote et al.¹⁸

ACKNOWLEDGMENT

The authors wish to express their appreciation to P. Romain for the fruitful discussions about optical model calculations with ECIS.

REFERENCES

1. E. FORT and J. P. DOAT, "ESTIMA Computer Code," NEANDC-161U, Nuclear Energy Agency Nuclear Data Committee (1983).
2. J-P. DELAROCHE, CH. LAGRANGE, and J. SALVY, in *Proc. Consultants' Mtg. Use of Nuclear Theory in Neutron*

TABLE III
Neutron Strength Functions (S_l) Obtained with the Generalized SPRT Method by Using the ECIS Code with the Optical Model Parameters Established by Capote et al.*

	$^{232}\text{Th} + n$	$^{238}\text{U} + n$	$^{240}\text{Pu} + n$	$^{242}\text{Pu} + n$
This work				
$10^4 S_0$	0.86	0.93	1.05	0.89
$10^4 S_1$	1.82	1.83	1.88	2.07
$10^4 S_2$	1.25	1.34	1.51	1.22
$10^4 S_3$	1.85	2.03	2.02	2.15
RIPL (Ref. 9)				
$10^4 S_0$	0.87 ± 0.07	1.03 ± 0.08	1.05 ± 0.1	0.98 ± 0.08
$10^4 S_1$		1.60 ± 0.40		
Mughabghab ¹⁹				
$10^4 S_0$	0.71 ± 0.04	1.29 ± 0.13	1.11 ± 0.08	0.92 ± 0.10
$10^4 S_1$	1.35 ± 0.04	2.17 ± 0.19	2.80 ± 0.80	
$10^4 S_2$	1.12 ± 0.06			

*Reference 18, Capote et al. Our results are compared with those reported in RIPL (Ref. 9) and in the *Atlas of Neutron Resonances*.¹⁹

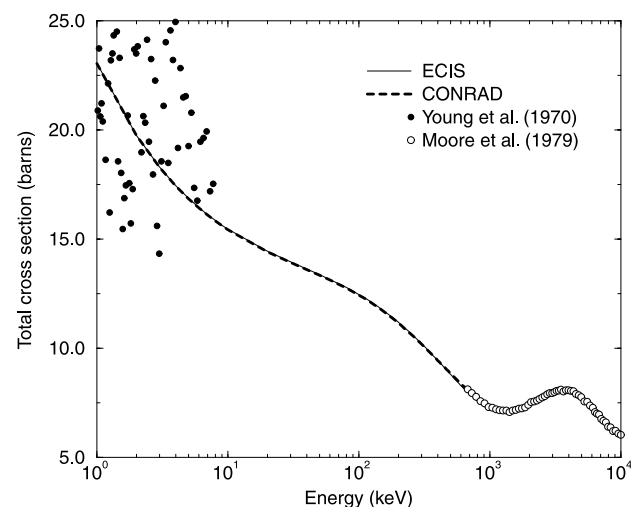


Fig. 4. The ^{242}Pu total cross section calculated with the CONRAD (Ref. 14) and ECIS (Ref. 15) codes. The theoretical curves are compared with experimental data reported by Young and Reeder²¹ and Moore et al.²²

Nuclear Data Evaluation, Trieste, Italy, December 8–12, 1975; see also IAEA-190, International Atomic Energy Agency Nuclear Data Services (1976).

3. A. M. LANE and R. G. THOMAS, *Rev. Mod. Phys.*, **30**, 2 (1958).
4. I. SIRAKOV, in *Proc. Workshop Nuclear Data and Evaluation for Reactor Applications*, Chateau de Cadarache, France, October 9–11, 2006, Nuclear Energy Agency (2007).

5. "ENDF-102 Data Formats and Procedures for the Evaluated Nuclear Data File ENDF-6," BNL-NCS-44945-05-Rev, M. HERMAN, Ed., Brookhaven National Laboratory (2005).
6. N. M. LARSON, "Updated User's Guide for SAMMY," ORNL/TM-9179/R7, Oak Ridge National Laboratory (2006).
7. F. H. FRÖHNER, "Evaluation of the Unresolved Resonance Range of ^{238}U ," *Nucl. Sci. Eng.*, **103**, 119 (1989).
8. F. H. FRÖHNER, in *Proc. Int. Conf. Computation and Analysis of Nuclear Data Relevant to Nuclear Energy and Safety*, Trieste, Italy, February 10–March 13, 1992; see also KFK-5073, Kernforschungszentrum Karlsruhe (1992).
9. T. BELGYA et al., "Handbook for Calculations of Nuclear Reaction Data RIPL-2," IAEA-TECDOC-1506, International Atomic Energy Nuclear Data Services (2005).
10. C. L. DUNFORD, H. FENECH, and J. T. REYNOLDS, *Phys. Rev.*, **177**, 1395 (1969).
11. A. J. KONING, S. HILAIRE, and M. C. DUIJVESTIJN, in *Proc. Int. Conf. Nuclear Data for Science and Technology*, Santa Fe, New Mexico, September 26–October 1, 2004, R. C. HAIGHT et al., Eds., American Institute of Physics (2005).
12. A. COURCELLE, Private Communication (2004).
13. M. C. MOXON and J. B. BRISLAND, "REFIT Computer Code," CBNM/ST/90-131/1, Harwell Laboratory (1990).
14. C. DE SAINT JEAN, G. NOGUERE, and B. IOSS, in *Proc. PHYSOR-2006 Topl. Mtg. Reactor Physics*, Vancouver, Canada, September 10–14, 2006, American Nuclear Society (2006) (CD-ROM).
15. J. RAYNAL, in *Proc. Specialists' Mtg. Nucleon Nucleus Optical Model up to 200 MeV*, Bruyères-le-Chatel, France, November 13–15, 1996, Nuclear Energy Agency (1997).
16. E. SOUKHOVITSKII et al., JAERI-DATA/CODE 2005-002, Japan Atomic Energy Institute (2005).
17. E. SOUKHOVITSKII et al., *Phys. Rev. C*, **72**, 024604 (2005).
18. R. CAPOTE et al., in *Proc. Int. Conf. Perspectives of Nuclear Data for the Next Decade*, Bruyères-le-Chatel, France, September 26–28, 2005, Nuclear Energy Agency (2006).
19. S. F. MUGHABGHAB, *Atlas of Neutron Resonances*, 5th ed., Elsevier, Amsterdam (2006).
20. P. MOLLER, J. R. NIX, W. D. MYERS, and W. J. SWIATECKI, *At. Data Nucl. Data Tables*, **59**, 185 (1995).
21. T. E. YOUNG and S.D. REEDER, "Total Neutron Cross Section of ^{242}Pu ," *Nucl. Sci. Eng.*, **40**, 389 (1970).
22. M. S. MOORE et al., in *Proc. Int. Conf. Nuclear Cross Sections for Technology*, Knoxville, Tennessee, October 22–26, 1979; see also NBS-SP-594, National Bureau of Standards (1980).
23. B. MORILLON and P. ROMAIN, *Phys. Rev. C*, **70**, 014601 (2004).
24. B. MORILLON and P. ROMAIN, *Phys. Rev. C*, **74**, 014601 (2006).

Appendix B

Average cross section of Neptunium

Neutron average cross sections of ^{237}Np

G. Noguere*

Atomic Energy Commission (CEA), DEN Cadarache, F-13108 Saint Paul Les Durance, France

(Received 8 December 2009; published 16 April 2010)

This work reports ^{237}Np neutron resonance parameters obtained from the simultaneous analysis of time-of-flight data measured at the GELINA, ORELA, KURRI, and LANSCE facilities. A statistical analysis of these resonances relying on average R -matrix and optical model calculations was used to establish consistent l -dependent average resonance parameters involved in the description of the unresolved resonance range of the ^{237}Np neutron cross sections. For neutron orbital angular momentum $l = 0$, we obtained an average radiation width $\langle\Gamma_\gamma\rangle = 39.3 \pm 1.0$ meV, a neutron strength function $10^4 S_0 = 1.02 \pm 0.14$, a mean level spacing $D_0 = 0.60 \pm 0.03$ eV, and a potential scattering length $R' = 9.8 \pm 0.1$ fm.

DOI: 10.1103/PhysRevC.81.044607

PACS number(s): 24.60.Dr, 25.40.Ny, 25.40.Lw, 25.60.Dz

I. INTRODUCTION

Neutron-induced reactions important for transmutation studies have been widely investigated within the frame of a collaboration between the Institute for Reference Materials and Measurements (IRMM) and the French Atomic Energy Commission (CEA). Previous neutron resonance spectroscopy of ^{237}Np , ^{99}Tc , ^{127}I , and ^{129}I are reported in Refs. [1–4]. These works provide consistent sets of s -wave mean level spacing D_0 and neutron strength function S_0 . However, statistical analysis of the resolved resonances of the iodine isotopes points out the difficulties in establishing unambiguous average values for higher-order partial waves ($l > 0$).

The focus of the present work is a statistical analysis of the ^{237}Np resonance parameters with methodologies relying on optical model and average R -matrix calculations. The average R -matrix cross sections are parameterized in terms of neutron strength functions S_l and distant level parameters R_l^∞ [5]. At low energy, $R_{l=0}^\infty$ is related to the potential scattering length R' . Optical model calculations were used to establish simple relationships between the s -wave parameters (S_0 and D_0) and the average R -matrix parameters (S_l and R_l^∞).

The R -matrix code CONRAD [6], the optical model code ECIS [7], and the statistical model code TALYS [8] were used to reconstruct ^{237}Np neutron cross sections. Nuclear models implemented in CONRAD are parameterized in terms of neutron strength function S_l , distant level parameter R_l^∞ , mean level spacing D_l , and average radiation width $\langle\Gamma_\gamma\rangle$. Comparison of the theoretical cross section with data reported in the literature confirmed the model parameters established in this work.

II. RESONANCE SHAPE ANALYSIS

Neutron resonances of the $n + ^{237}\text{Np}$ nuclear system have been studied with data measured at the GELINA facility [1] and with capture cross sections retrieved from EXFOR [9]. Neutron resonances λ were parametrized in terms of resonance energy E_λ , neutron width $\Gamma_{\lambda,n}$, and radiation width $\Gamma_{\lambda,\gamma}$ by using the Reich-Moore approximation of the R -matrix theory

[10]. Fission widths were taken from the European library JEFF-3.1 [11].

Measurements carried out at the GELINA facility were performed with the neutron transmission technique. Li-glass detectors (NE912) located 30 and 50 m from the neutron source were used to collect a wide number of experimental data. Detailed descriptions of the experimental setup are given elsewhere [1]. The resolved and unresolved resonance ranges were investigated from 0.3 eV to 2.0 keV by using four NpO_2 samples of different thicknesses. The (n, γ) reaction was analyzed with experimental values measured at the ORELA [12], KURRI [13,14], and LANSCE [15] facilities. The KURRI and LANSCE data sets were used below 10 eV. ORELA data were analyzed up to 100 eV. Tables I and II summarize briefly the main characteristics of the transmission and capture data adopted in our resonance shape analysis.

The least-squares fitting code REFIT [16] was used to adjust the resonance parameters for the data. For transmission data, REFIT simulates the attenuation of the incident neutron beam as follows:

$$T(E) = \int_0^\infty R_E^T(E') \exp\left(-\sum_i n_i \sigma_{t,i}(E')\right) dE', \quad (1)$$

where i labels the isotopes contained in the sample, n_i stands for the atomic surface density as atoms per barn, $\sigma_{t,i}(E)$ represents the Doppler broadened total cross section, and R_E^T is the experimental resolution of the GELINA spectrometer.

For modeling of the experimental capture cross section, neutron scattering corrections in thin neptunium samples were assumed to be negligible. The following expression of the capture yield was used in our REFIT calculations:

$$Y(E) = N \int_0^\infty R_E^Y(E') (1 - T(E')) \frac{\sigma_\gamma(E')}{\sigma_t(E')} dE', \quad (2)$$

where σ_γ (σ_t) stands for the ^{237}Np Doppler broadened capture (total) cross section, N represents the normalization factor, and R_E^Y is the experimental resolution for the capture measurements.

A preliminary analysis of the low-energy resonances (<10 eV) was reported in Ref. [17]. The latter demonstrates that Monte Carlo techniques can be used to propagate the

* gilles.noguere@cea.fr

TABLE I. Experimental characteristics of the capture data used in this work.

Author(s)	Ref. no.	Facility	Flight length (mm)	Sample diameter (mm)	Sample thickness (at/b)
Weston and Todd	[12]	ORELA	20	50.8	0.25×10^{-3}
Kobayashi <i>et al.</i>	[13]	KURRI	12	30	0.35×10^{-3}
Shcherbakov <i>et al.</i>	[14]	KURRI	24.2	30	0.35×10^{-3}
Esch <i>et al.</i>	[15]	LANSCE	20	6.4	0.0035×10^{-3}

experimental uncertainties during the least-squares fitting procedure. Monte Carlo algorithms and uncertainty propagation techniques are presented in Refs. [18] and [19]. In the present analysis, similar stochastic techniques were used to determine the ^{237}Np resonance parameters up to 500 eV.

Examples of least-squares fits are shown in Fig. 1. Parameters <100 eV are reported in Table III. The given uncertainties take into account the experimental information summarized in Table IV. Comparison of our results with the parameters recommended in the European library JEFF-3.1 points out discrepancies of $<2\%$ on average. However, as shown in Fig. 2, significant discrepancies, $>10\%$, can be observed for the neutron widths. The increasing contribution of the experimental resolution makes unambiguous identification of complex overlapping structures above a few tens of electron volts difficult.

Negative resonances (“external levels”) reported in Sec. III were adjusted to accurately reproduce the thermal capture cross section of 180 ± 5 b measured at the ILL facility [20] and the contribution of the shape-elastic cross section observed between the resonances in the transmission data. This analysis yielded a potential scattering length of

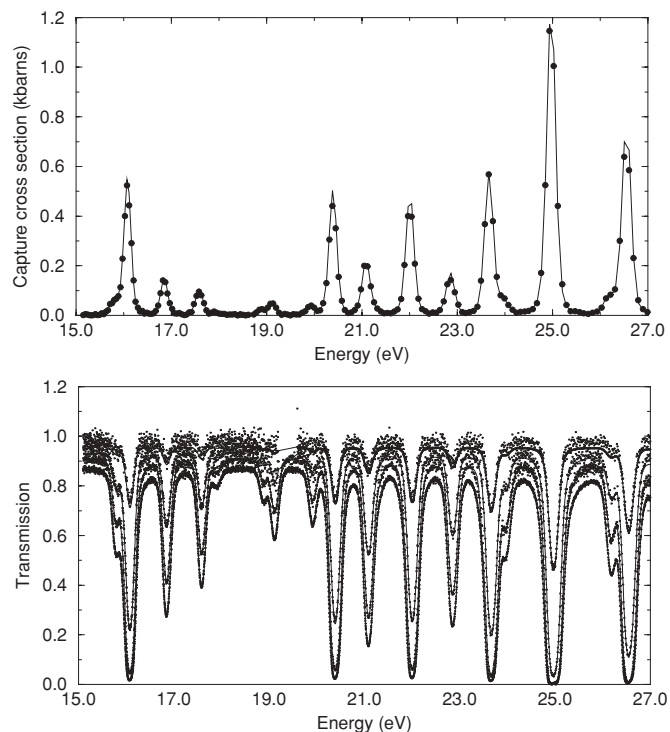
$$R' = 9.8 \pm 0.1 \text{ fm.}$$

In the frame of the R -matrix theory, contributions of the direct interaction can be simulated with the so-called distant level parameter R_0^∞ . For an s wave, the relationship between R' and R_0^∞ is given by

$$R' = a_c(1 - R_0^\infty). \quad (3)$$

TABLE II. Main characteristics of the transmission measurements performed by Gressier [1] at the GELINA facility.

Date	Flight length (m)	Frequency (Hz)	Sample temperature (K)	“Antioverlap” filter	Sample thickness (at/b)
Feb. 1997	26.453	100	290	Cd	2.49 ± 0.02
Feb. 1997	26.453	100	290	Cd	0.497 ± 0.003
Oct. 1997	49.332	800	300	^{10}B	5.03 ± 0.03
Jan. 1998	26.453	800	300	Cd	7.52 ± 0.04
Feb. 1998	49.332	100	300	Cd	5.03 ± 0.03
June 1998	49.332	800	300	^{10}B	5.03 ± 0.03

FIG. 1. Examples of $n + ^{237}\text{Np}$ resonance peaks observed in the experimental capture cross section measured by Weston and Todd [12] and in the transmission spectra measured by Gressier [1]. Solid lines represent the theoretical curves adjusted by the REFIT code [16].

According to conventions used in the Evaluated Nuclear Data Files [21], the channel radius a_c is defined as follows:

$$a_c = 1.23 \left(\frac{A}{m_n} \right)^{1/3} + 0.8 \text{ (fm)}, \quad (4)$$

where $(A/m_n) = 235.012$ is defined as the ratio of the target mass to the neutron mass. By using $a_c = 8.39$ fm and $R' = 9.8$ fm, the s -wave distant level parameter for the $n + ^{237}\text{Np}$ nuclear system is

$$R_0^\infty = -0.168 \pm 0.012.$$

The average radiation width was determined from the individual $\Gamma_{\lambda,\gamma}$ values of 19 resonances observed below 23 eV. If they are assumed to be independent, the weighted mean value is close to 39.2 ± 0.2 meV. By taking into account correlation coefficients between the resonance parameters, the mean value

TABLE III. ^{237}Np resonance parameters below 100 eV.

E_λ (eV)	J	This work (meV)		JEFF-3.1 (meV)	
		$\Gamma_{\lambda,\gamma}$	$\Gamma_{\lambda,n}$	$\Gamma_{\lambda,\gamma}$	$\Gamma_{\lambda,n}$
-2.8 ± 0.03	2.0	40.0 ± 0.4	2.794 ± 0.050	40.0	2.176
-0.91 ± 0.02	3.0	40.0 ± 0.4	1.182 ± 0.098	40.0	0.450
0.49 ± 0.01	2.0	39.4 ± 0.7	0.047 ± 0.001	40.5	0.047
1.32 ± 0.01	3.0	37.9 ± 0.4	0.031 ± 0.001	40.3	0.032
1.48 ± 0.01	2.0	41.6 ± 0.9	0.184 ± 0.004	40.5	0.184
1.97 ± 0.01	3.0	37.2 ± 0.6	0.014 ± 0.001	39.5	0.014
3.05	[3.0]			40.8	<0.001
3.86 ± 0.01	3.0	40.4 ± 0.6	0.211 ± 0.002	39.7	0.212
4.26 ± 0.01	2.0	40.0 ± 0.9	0.033 ± 0.001	40.4	0.033
4.86 ± 0.01	2.0	40.1 ± 1.2	0.043 ± 0.001	40.0	0.042
5.78 ± 0.01	3.0	42.1 ± 0.8	0.533 ± 0.009	41.9	0.528
6.38 ± 0.01	3.0	38.8 ± 1.2	0.079 ± 0.001	39.6	0.079
6.68 ± 0.01	2.0	39.3	0.014 ± 0.001	40.1	0.013
7.19 ± 0.00	2.0	39.3	0.010 ± 0.001	40.0	0.009
7.42 ± 0.01	3.0	39.0 ± 1.5	0.124 ± 0.001	38.4	0.122
7.67 ± 0.01	2.0	39.3	0.003 ± 0.001	40.0	0.002
8.30 ± 0.01	3.0	39.7 ± 1.4	0.093 ± 0.001	37.6	0.090
8.98 ± 0.01	3.0	37.2 ± 1.3	0.104 ± 0.001	37.0	0.102
9.30 ± 0.01	2.0	41.8 ± 0.9	0.611 ± 0.006	41.4	0.602
10.23 ± 0.01	2.0	39.3	0.030 ± 0.001	40.0	0.028
10.68 ± 0.01	3.0	39.3	0.439 ± 0.005	40.0	0.432
10.84 ± 0.01	3.0	39.3	0.701 ± 0.011	40.0	0.689
11.10 ± 0.01	2.0	42.2 ± 1.1	1.032 ± 0.013	43.8	1.010
12.20 ± 0.01	3.0	39.3	0.048 ± 0.001	40.0	0.049
12.62 ± 0.01	2.0	38.9 ± 1.2	0.925 ± 0.010	40.2	0.911
13.13 ± 0.01	3.0	39.3	0.017 ± 0.001	40.0	0.017
14.39 ± 0.01	2.0	39.3	0.002 ± 0.001	40.0	0.002
15.79 ± 0.01	3.0	39.3	0.069 ± 0.001	40.0	0.069
15.94 ± 0.01	3.0	39.3	0.038 ± 0.001	40.0	0.038
16.08 ± 0.01	2.0	38.1 ± 1.8	1.069 ± 0.012	40.0	1.052
16.86 ± 0.01	2.0	39.3	0.304 ± 0.002	37.8	0.299
17.59 ± 0.01	3.0	39.3	0.159 ± 0.001	39.1	0.156
17.90 ± 0.01	2.0	39.3	0.018 ± 0.001	40.0	0.018
17.94 ± 0.01	3.0	39.3	0.003 ± 0.001	40.0	0.003
18.89 ± 0.02	2.0	39.3	0.048 ± 0.001	40.0	0.048
19.13 ± 0.02	3.0	39.3	0.089 ± 0.001	40.0	0.088
19.92 ± 0.01	3.0	39.3	0.069 ± 0.001	40.0	0.070
20.40 ± 0.01	2.0	37.1 ± 1.9	1.395 ± 0.015	39.4	1.368
21.09 ± 0.02	3.0	39.3	0.450 ± 0.003	40.0	0.446
21.31 ± 0.02	2.0	39.3	0.032 ± 0.001	40.0	0.028
22.01 ± 0.02	2.0	36.5 ± 1.8	1.521 ± 0.018	39.5	1.498
22.86 ± 0.02	3.0	38.2 ± 2.4	0.386 ± 0.003	38.5	0.380
23.67 ± 0.02	3.0	39.3	1.436 ± 0.018	38.0	1.420
23.99 ± 0.02	2.0	39.3	0.182 ± 0.002	40.0	0.191
24.85 ± 0.02	3.0	39.3	0.034 ± 0.006	40.0	0.026
24.98 ± 0.02	3.0	39.3	3.661 ± 0.059	40.0	3.665
26.19 ± 0.02	3.0	39.3	0.196 ± 0.002	40.0	0.199
26.56 ± 0.02	3.0	39.3	2.389 ± 0.039	40.7	2.336
27.09 ± 0.02	2.0	39.3	0.039 ± 0.001	40.0	0.038
28.46 ± 0.02	2.0	39.3	0.093 ± 0.006	40.0	0.094
28.61 ± 0.02	3.0	39.3	0.031 ± 0.007	40.0	0.031
28.93 ± 0.02	2.0	39.3	0.138 ± 0.002	40.0	0.137
29.48 ± 0.02	2.0	39.3	0.083 ± 0.002	40.0	0.084
30.42 ± 0.02	3.0	39.3	3.135 ± 0.055	38.2	3.145
30.74 ± 0.02	2.0	39.3	0.358 ± 0.007	40.0	0.371

TABLE III. (Continued.)

E_λ (eV)	J	This work (meV)		JEFF-3.1 (meV)	
		$\Gamma_{\lambda,\gamma}$	$\Gamma_{\lambda,n}$	$\Gamma_{\lambda,\gamma}$	$\Gamma_{\lambda,n}$
31.30 ± 0.02	3.0	39.3	0.245 ± 0.003	40.0	0.245
31.66 ± 0.03	3.0	39.3	0.042 ± 0.001	40.0	0.043
32.48 ± 0.03	2.0	39.3	0.011 ± 0.002	40.0	0.011
33.42 ± 0.02	3.0	39.3	0.395 ± 0.005	40.0	0.395
33.90 ± 0.03	2.0	39.3	0.487 ± 0.006	40.0	0.487
34.08 ± 0.03	3.0	39.3	0.039 ± 0.006	40.0	0.035
34.69 ± 0.03	3.0	39.3	0.163 ± 0.002	40.0	0.170
35.20 ± 0.03	2.0	39.3	0.413 ± 0.004	40.0	0.409
36.38 ± 0.03	3.0	39.3	0.121 ± 0.002	40.0	0.126
36.82 ± 0.03	2.0	39.3	0.085 ± 0.003	40.0	0.087
37.15 ± 0.03	3.0	39.3	1.152 ± 0.011	37.4	1.138
37.83 ± 0.03	2.0	39.3	0.042 ± 0.004	40.0	0.042
38.05 ± 0.03	2.0	39.3	0.208 ± 0.007	40.0	0.208
38.19 ± 0.03	3.0	39.3	1.199 ± 0.013	40.0	1.193
38.91 ± 0.03	3.0	39.3	0.820 ± 0.013	40.0	0.816
39.01 ± 0.03	2.0	39.3	0.410 ± 0.014	40.0	0.410
39.24 ± 0.03	3.0	39.3	0.532 ± 0.007	40.0	0.529
39.80 ± 0.03	2.0	39.3	0.088 ± 0.004	40.0	0.088
39.93 ± 0.03	3.0	39.3	0.453 ± 0.005	40.0	0.450
41.36 ± 0.03	3.0	39.3	1.963 ± 0.027	38.9	1.947
42.38 ± 0.03	3.0	39.3	0.084 ± 0.017	40.0	0.084
42.84 ± 0.03	3.0	39.3	0.083 ± 0.004	40.0	0.083
43.19	3.0			40.6	0.004
43.65 ± 0.03	2.0	39.3	0.345 ± 0.007	40.0	0.339
44.28 ± 0.04	2.0	39.3	0.026 ± 0.012	40.0	0.026
44.92 ± 0.04	2.0	39.3	0.012 ± 0.002	40.0	0.012
45.71 ± 0.04	2.0	39.3	0.516 ± 0.009	40.0	0.511
46.03 ± 0.04	3.0	39.3	0.584 ± 0.010	40.0	0.570
46.36 ± 0.04	3.0	39.3	2.604 ± 0.023	45.3	2.629
47.33 ± 0.04	2.0	39.3	2.900 ± 0.025	38.2	2.863
48.44 ± 0.04	2.0	39.3	0.105 ± 0.006	40.0	0.104
48.77 ± 0.04	3.0	39.3	0.347 ± 0.007	40.0	0.349
48.89 ± 0.04	2.0	39.3	0.172 ± 0.008	40.0	0.172
49.27	2.0			40.0	0.007
49.82 ± 0.04	3.0	39.3	4.194 ± 0.061	36.5	4.169
50.34	2.0			31.3	2.101
50.40 ± 0.04	3.0	39.3	7.399 ± 0.157	46.8	7.396
51.69 ± 0.04	3.0	39.3	0.096 ± 0.005	40.0	0.112
52.21 ± 0.04	2.0	39.3	0.399 ± 0.006	40.0	0.401
52.65 ± 0.04	2.0	39.3	0.886 ± 0.010	40.0	0.880
53.05 ± 0.04	3.0	39.3	0.061 ± 0.005	40.0	0.058
53.89 ± 0.04	2.0	39.3	0.491 ± 0.006	40.0	0.490
54.27 ± 0.04	2.0	39.3	0.167 ± 0.005	40.0	0.157
55.04 ± 0.04	3.0	39.3	0.261 ± 0.004	40.0	0.259
56.02 ± 0.04	2.0	39.3	1.351 ± 0.035	40.0	1.213
56.16 ± 0.05	3.0	39.3	0.613 ± 0.020	40.0	0.718
56.57 ± 0.05	2.0	39.3	0.036 ± 0.007	40.0	0.036
56.86	3.0			40.0	0.013
57.40	2.0			56.0	0.006
58.40 ± 0.04	3.0	39.3	0.397 ± 0.010	40.0	0.372
58.63 ± 0.05	3.0	39.3	0.218 ± 0.007	40.0	0.245
59.51 ± 0.04	2.0	39.3	2.339 ± 0.021	40.0	2.337
60.06 ± 0.04	3.0	39.3	2.325 ± 0.030	40.0	2.274
60.96 ± 0.04	3.0	39.3	1.595 ± 0.018	40.0	1.562
61.37	3.0			40.0	0.015

TABLE III. (Continued.)

E_λ (eV)	J	This work (meV)		JEFF-3.1 (meV)	
		$\Gamma_{\lambda,\gamma}$	$\Gamma_{\lambda,n}$	$\Gamma_{\lambda,\gamma}$	$\Gamma_{\lambda,n}$
61.62	3.0			40.2	0.122
61.65 ± 0.04	3.0	39.3	0.451 ± 0.005	40.0	0.452
62.39 ± 0.05	2.0	39.3	0.421 ± 0.035	40.0	0.382
62.50 ± 0.05	3.0	39.3	1.403 ± 0.027	40.0	1.415
62.92 ± 0.05	3.0	39.3	1.529 ± 0.019	40.0	1.485
63.45 ± 0.05	2.0	39.3	0.083 ± 0.005	40.0	0.083
63.95 ± 0.05	3.0	39.3	0.230 ± 0.004	40.0	0.247
64.97 ± 0.05	3.0	39.3	0.867 ± 0.009	40.0	0.855
65.71 ± 0.05	3.0	39.3	4.003 ± 0.069	47.4	3.787
66.36	2.0			40.0	0.028
66.80	2.0			40.8	0.017
67.48 ± 0.05	3.0	39.3	5.070 ± 0.077	42.8	4.866
67.98 ± 0.05	2.0	39.3	2.932 ± 0.034	40.0	2.824
68.78 ± 0.06	3.0	39.3	0.326 ± 0.015	40.0	0.308
69.28	2.0			40.0	0.013
70.26 ± 0.05	3.0	39.3	1.683 ± 0.023	40.0	1.663
70.68 ± 0.06	2.0	39.3	0.598 ± 0.060	40.0	0.624
71.22 ± 0.06	3.0	39.3	2.008 ± 0.200	40.0	1.824
71.48 ± 0.06	2.0	39.3	3.063 ± 0.224	40.0	2.407
71.55	3.0			40.0	0.584
72.30	2.0			40.8	0.005
72.97	2.0			40.0	0.010
73.87 ± 0.06	3.0	39.3	0.278 ± 0.016	40.0	0.276
74.29 ± 0.06	2.0	39.3	1.770 ± 0.044	40.0	1.694
74.59 ± 0.06	3.0	39.3	0.462 ± 0.051	40.0	0.455
75.14 ± 0.06	2.0	39.3	0.170 ± 0.020	40.0	0.146
75.65	3.0			40.0	0.010
76.22 ± 0.06	3.0	39.3	0.029 ± 0.010	40.0	0.029
76.59 ± 0.06	2.0	39.3	0.206 ± 0.017	40.0	0.175
77.00 ± 0.06	3.0	39.3	0.305 ± 0.008	40.0	0.281
77.57 ± 0.06	2.0	39.3	0.033 ± 0.019	40.0	0.033
77.83	3.0			40.8	0.017
78.33 ± 0.06	3.0	39.3	1.383 ± 0.135	40.0	1.470
78.44 ± 0.06	2.0	39.3	0.896 ± 0.200	40.0	0.693
79.28 ± 0.06	2.0	39.3	3.041 ± 0.041	40.0	2.933
79.90	3.0			40.8	0.010
80.39 ± 0.06	2.0	39.3	0.237 ± 0.030	40.0	0.214
80.65 ± 0.06	3.0	39.3	0.460 ± 0.018	40.0	0.428
81.63 ± 0.07	2.0	39.3	0.504 ± 0.015	40.0	0.478
82.13 ± 0.07	3.0	39.3	0.740 ± 0.014	40.0	0.688
82.40	2.0			40.0	0.063
83.43 ± 0.07	2.0	39.3	3.894 ± 0.200	40.0	3.271
83.74 ± 0.06	2.0	39.3	6.526 ± 0.207	40.0	3.152
83.82	2.0			40.0	2.507
85.22 ± 0.07	3.0	39.3	0.935 ± 0.020	40.0	0.933
86.09 ± 0.07	2.0	39.3	0.994 ± 0.060	40.0	1.022
86.53 ± 0.06	3.0	39.3	4.810 ± 0.064	40.0	4.789
87.60 ± 0.06	2.0	39.3	1.950 ± 0.199	40.0	1.626
87.77 ± 0.07	3.0	39.3	1.639 ± 0.150	40.0	1.835
88.18 ± 0.07	3.0	39.3	0.899 ± 0.043	40.0	0.922
88.96 ± 0.07	3.0	39.3	1.561 ± 0.029	40.0	1.602
89.47 ± 0.07	3.0	39.3	3.393 ± 0.058	40.0	3.568
89.94	2.0			40.8	0.068
90.88 ± 0.07	3.0	39.3	4.357 ± 0.064	40.0	4.291
91.01	2.0			40.8	0.362

TABLE III. (Continued.)

E_λ (eV)	J	This work (meV)		JEFF-3.1 (meV)	
		$\Gamma_{\lambda,\gamma}$	$\Gamma_{\lambda,n}$	$\Gamma_{\lambda,\gamma}$	$\Gamma_{\lambda,n}$
91.37 ± 0.07	2.0	39.3	0.176 ± 0.036	40.0	0.187
91.99 ± 0.07	3.0	39.3	0.493 ± 0.009	40.0	0.482
92.78 ± 0.07	3.0	39.3	0.178 ± 0.007	40.0	0.160
93.41 ± 0.07	2.0	39.3	2.228 ± 0.031	40.0	2.180
94.25 ± 0.08	3.0	39.3	0.332 ± 0.011	40.0	0.309
94.52 ± 0.08	2.0	39.3	0.100 ± 0.016	40.0	0.098
94.98 ± 0.08	3.0	39.3	0.066 ± 0.006	40.0	0.072
95.43 ± 0.08	2.0	39.3	0.444 ± 0.015	40.0	0.424
96.18 ± 0.08	3.0	39.3	0.071 ± 0.011	40.0	0.076
96.64 ± 0.08	2.0	39.3	0.528 ± 0.016	40.0	0.467
97.39	2.0			40.8	0.018
97.77 ± 0.07	2.0	39.3	4.080 ± 0.054	40.0	3.967
98.51 ± 0.08	2.0	39.3	2.740 ± 0.037	40.0	2.596
99.12 ± 0.08	3.0	39.3	0.080 ± 0.010	40.0	0.098
99.54 ± 0.08	3.0	39.3	1.578 ± 0.040	40.0	1.593
100.23 ± 0.08	3.0	39.3	4.496 ± 0.072	40.0	4.327
101.08 ± 0.08	2.0	39.3	6.437 ± 0.098	40.0	6.218
101.68 ± 0.08	2.0	39.3	1.632 ± 0.128	40.0	1.681
102.02 ± 0.08	2.0	39.3	2.134 ± 0.141	40.0	2.087

and its uncertainty become

$$\langle \Gamma_\gamma \rangle = 39.3 \pm 1.0 \text{ meV.}$$

Table V compares the average radiation width obtained in this work with those reported in the literature. Although our work suggests a slight decrease in $\langle \Gamma_\gamma \rangle$, agreement between the different values remains within the limit of the given uncertainties.

III. STATISTICAL ANALYSIS OF RESONANCE PARAMETERS

The s -wave mean level spacing D_0 and neutron strength function S_0 can be determined from the distribution of the reduced neutron widths. For an s -wave resonance, the reduced neutron width is defined as the ratio of the neutron width to the square root of the resonance energy:

$$\Gamma_{\lambda,n}^0 = \frac{\Gamma_{\lambda,n}}{\sqrt{E_\lambda}}. \quad (5)$$

TABLE IV. Experimental uncertainties introduced in the resonance shape analysis.

Parameter	Uncertainty
Normalization capture yield	2.8%
Effective temperature	10 K
Transmission background	0.005–0.01
Transmission flight length	2.0 cm
Initial delay	5.0 ns
Sample composition	0.5%–0.8%

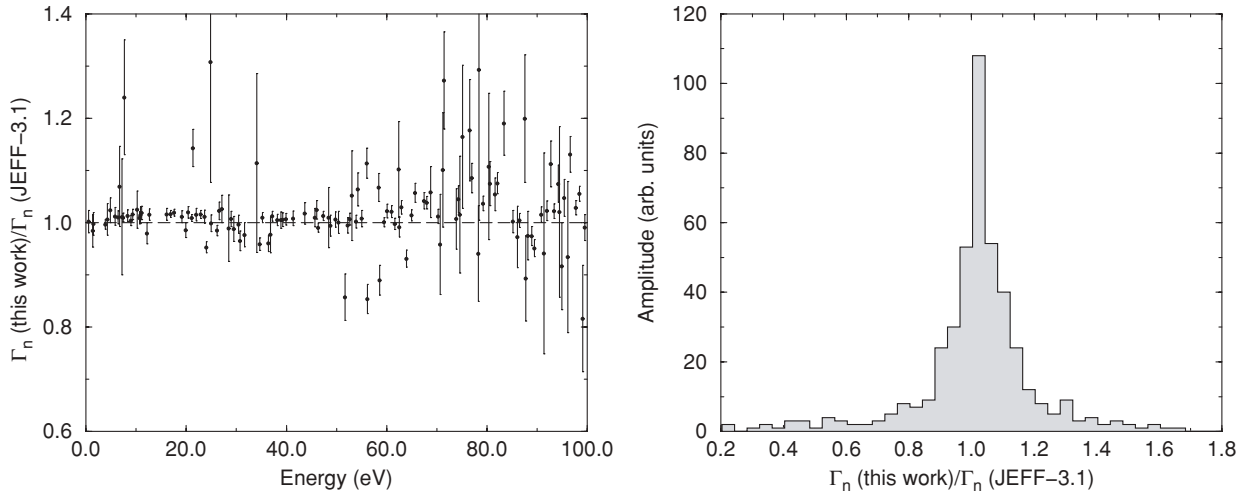


FIG. 2. Comparison of neutron width values obtained in this work and those recommended in the European library JEFF-3.1 below 100 eV. Top: ratio of the neutron widths as a function of the neutron energy. Bottom: distribution of this ratio.

The distribution of this parameter is a chi-square function with 1 degree of freedom [26]:

$$P(x)dx = \frac{e^{-(x/2)}}{\sqrt{2\pi x}} dx, \quad (6)$$

with

$$x = \frac{\Gamma_{\lambda,n}^0}{\langle \Gamma_{\lambda,n}^0 \rangle}, \quad (7)$$

where $\langle \Gamma_{\lambda,n}^0 \rangle$ stands for the average value of the s -wave reduced neutron width. The relationship among $\langle \Gamma_{\lambda,n}^0 \rangle$, D_0 , and S_0 can be written as follows:

$$\langle \Gamma_{\lambda,n}^0 \rangle = S_0 D_0, \quad (8)$$

with

$$D_0 = \frac{E_{\max} - E_{\min}}{N - 1}, \quad (9)$$

where N stands for the number of s -wave resonances between E_{\min} and E_{\max} . This number of resonances can be suggested from the cumulative distribution function of $P(x)$ [Eq. (6)]:

$$N(x_0) = N \int_{x_0}^{\infty} P(x)dx = N \left(1 - \text{erf} \sqrt{\frac{x_0}{2}} \right), \quad (10)$$

TABLE V. ^{237}Np average radiation width obtained in this work and reported in the literature.

Author(s)	Ref. no.	Value (meV)
Paya	[22]	40.0 ± 1.2
Mewissen <i>et al.</i>	[23]	41.2 ± 2.9
Weston and Todd	[12]	~ 40
Gressier	[1]	40.0 ± 2.0
Noguere <i>et al.</i>	[17]	39.5 ± 0.7
Mughaghab	[24]	40.7 ± 0.5
RIPL-2	[25]	40.8 ± 1.2
This work		39.3 ± 1.0

By using expressions (8) and (9), Eq. (10) becomes

$$N(X_0) = \left(\frac{E_{\max} - E_{\min}}{D_0} + 1 \right) \left(1 - \text{erf} \sqrt{\frac{X_0}{2S_0 D_0}} \right), \quad (11)$$

with

$$X_0 = x_0 S_0 D_0. \quad (12)$$

This distribution gives the number of resonances λ having a reduced neutron width $\Gamma_{\lambda,n}^0$ higher than a threshold value X_0 . This statistical approach is called the ESTIMA method. Detailed explanations are given elsewhere [3].

For the nuclear systems $n + ^{237}\text{Np}$, the only s -wave states of the compound nucleus allowed in the resonance range are those with total angular momenta $J = 2$ and $J = 3$. The corresponding statistical spin factors are $g_{J=2} = 5/12$ and $g_{J=3} = 7/12$. A satisfactory agreement between the theoretical curve [Eq. (11)] and the experimental distribution of the J -dependent reduced neutron widths was observed below $E_{\max} = 90$ eV. Results provided by the ESTIMA method are shown in Fig. 3. The s -wave neutron strength function and mean level spacing can be deduced from the J -dependent values by using the following relationships:

$$S_0 = \sum_{J=2}^3 g_J S_{0,J}, \quad (13)$$

$$D_0 = \left(\sum_{J=2}^3 \frac{1}{D_{0,J}} \right)^{-1}. \quad (14)$$

The combination of the J -dependent results provides

$$10^4 S_0 = 1.02 \pm 0.14, \\ D_0 = 0.60 \pm 0.03 \text{ eV}.$$

The quoted uncertainties take into account the uncertainties of the resonance parameters (Table III) and of the statistical analysis.

Figure 4 compares the final s -wave results with the “staircase” plots of the reduced neutron widths and of the

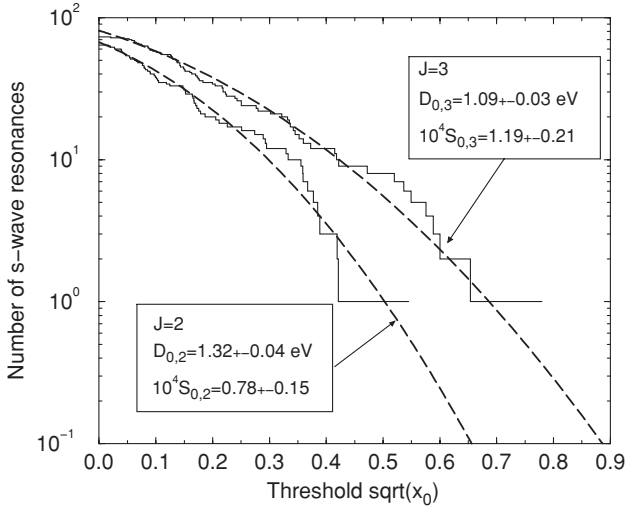


FIG. 3. Cumulative distribution functions of the reduced neutron widths determined in this work (solid lines) and calculated with Eq. (10) (dashed lines). The energy range for the statistical analysis is [$E_{\min} = 0.49$ eV; $E_{\max} = 90$ eV].

culated number of resonances. The discrepancies observed on the cumulated number of resonances confirm the increasing number of missing small resonances above 100 eV.

Table VI compares the average parameters obtained in this work with those reported in the literature. Our $10^4 S_0$ and D_0 results are consistent with the expected values close to unity and 0.6 eV, respectively.

IV. l -DEPENDENT MEAN LEVEL SPACING

For the nuclear system $n + {}^{237}\text{Np}$, the l -dependent mean level spacing D_l can be calculated as follows, assuming equal probability for both parities:

$$\frac{1}{D_0} = \frac{1}{2} \sum_{J=2}^3 \rho_J(B_n), \quad (15)$$

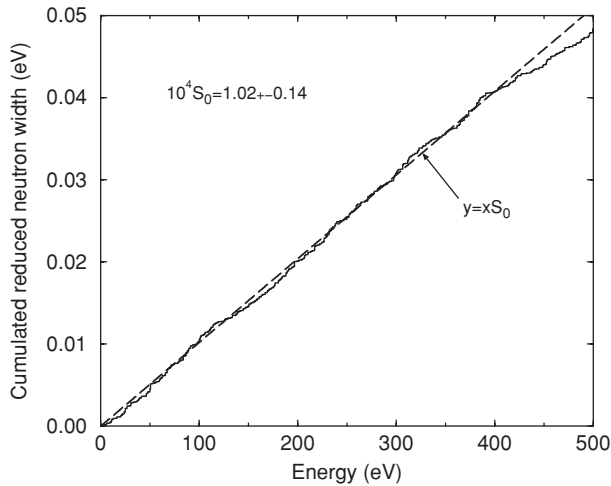


TABLE VI. ${}^{237}\text{Np}$ neutron strength function S_0 and mean level spacing D_0 reported in the literature and obtained in this work.

Author(s)	Ref. no.	E_{\max} (eV)	$10^4 S_0$	D_0 (eV)
Slaughter <i>et al.</i>	[27]	30	0.96 ± 0.13	1.15 ± 0.12
Mewissen <i>et al.</i>	[23]	100	1.02 ± 0.14	0.74 ± 0.06
Weston and Todd	[12]	100	1.02 ± 0.06	0.45 ± 0.10
Gressier	[1]	90	1.00 ± 0.07	0.58 ± 0.03
Mughaghab	[24]		1.02 ± 0.06	0.52 ± 0.04
RIPL-2	[25]		0.97 ± 0.07	0.57 ± 0.03
This work		90	1.02 ± 0.14	0.60 ± 0.03

$$\frac{1}{D_1} = \frac{1}{2} \sum_{J=1}^4 \rho_J(B_n), \quad (16)$$

$$\frac{1}{D_2} = \frac{1}{2} \sum_{J=0}^5 \rho_J(B_n). \quad (17)$$

In this work, the J -dependent level density $\rho_J(E)$ was calculated using the formula established by Gilbert and Cameron [28]:

$$\rho_J(E) = \rho(E) \frac{2J+1}{4\sigma^2(E)} \exp\left(-\frac{(J+1/2)^2}{2\sigma^2(E)}\right). \quad (18)$$

The parametrization of $\rho(E)$ is given by the constant-temperature approximation ($E < E_m$) and the Fermi-gas model ($E > E_m$),

$$\rho(E) = \begin{cases} \frac{1}{T} \exp\left(\frac{E-E_0}{T}\right), & E < E_m, \\ \frac{\exp(2\sqrt{a(E-\Delta)})}{12\sqrt{2}a^{1/4}(E-\Delta)^{5/4}\sigma(E)}, & E > E_m, \end{cases} \quad (19)$$

where $\sigma(E)$ stands for the spin cut-off parameter:

$$\sigma^2(E) = 0.0888A^{2/3}\sqrt{a(E-\Delta)}. \quad (20)$$

The pairing energy $\Delta = 0$ because the nuclear system $n + {}^{237}\text{Np}$ is characterized by odd values of N and Z .

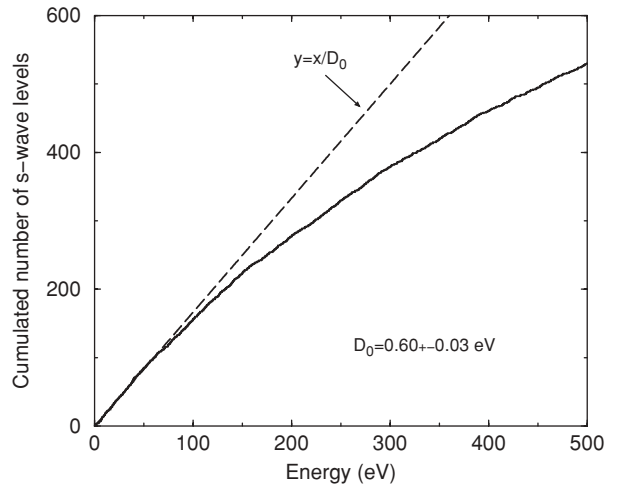


FIG. 4. Comparison of the results provided by the ESTIMA method (dashed line) and “staircase” plots of the s -wave reduced neutron widths (left) and of the cumulative number of s -wave resonances (right).

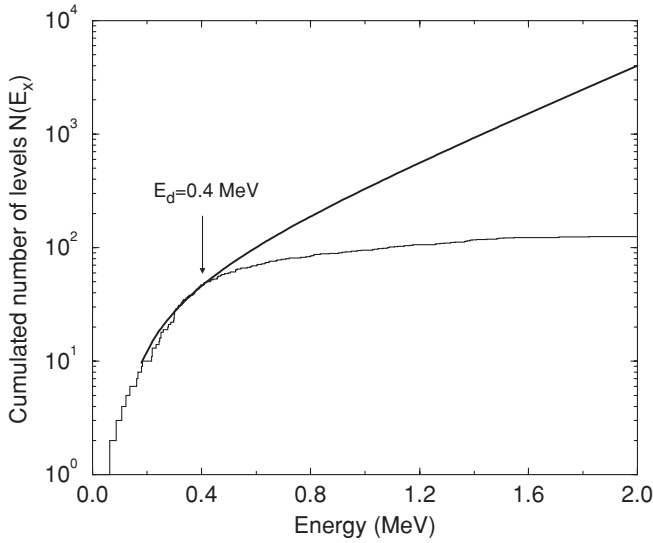


FIG. 5. Cumulated number of levels taken from RIPL [25] for the nuclear system $n + ^{237}\text{Np}$. The solid (lower) curve was calculated with Eq. (21).

The level density parameter a is calculated from the s -wave mean level spacing $D_0 = 0.60 \pm 0.03$ eV. By introducing the Fermi-gas model in Eq. (15), we obtain

$$a = 27.90 \pm 0.12 \text{ MeV}^{-1}.$$

The corresponding mean level spacings for $l = 1$ and $l = 2$ [Eqs. (16) and (17)] are

$$\begin{aligned} D_1 &= 0.309 \pm 0.015 \text{ eV}, \\ D_2 &= 0.218 \pm 0.011 \text{ eV}. \end{aligned}$$

The nuclear temperature T was determined by fitting the cumulative numbers of low-lying nuclear levels $N(E_x)$ with the following expressions [29,30]:

$$N(E_x) = N(E_d) + e^{-E_0/T} (e^{E_x/T} - e^{-E_d/T}), \quad (21)$$

$$E_0 = E_m - T \ln \left(\frac{T \exp(2\sqrt{a(E_m - \Delta)})}{12\sqrt{2}a^{1/4}(E_m - \Delta)^{5/4}\sigma(E_m)} \right), \quad (22)$$

$$E_m = \frac{T}{2}(aT - 3 + \sqrt{aT(aT - 6)}) + \Delta. \quad (23)$$

The value of the nuclear temperature depends on the upper energy level E_d , where the ‘‘continuum’’ is supposed to start. The solid (lower) curve in Fig. 5 was obtained for $E_d = 0.4 \pm$

TABLE VII. Parameters involved in the constant-temperature model for the nuclear system $n + ^{237}\text{Np}$.

Parameter	Value in this work
T	0.41 ± 0.01 MeV
E_m	3.33 ± 0.15 MeV
E_0	-1.36 ± 0.09 MeV

0.1 MeV. Results for T , E_m , and E_0 are reported in Table VII. The given uncertainties are dominated by the choice of E_d .

V. l -DEPENDENT NEUTRON STRENGTH FUNCTION

The l -dependent neutron average parameters of interest in this work are the neutron strength function S_l and the distant level parameter R_l^∞ . Within the frame of the average R -matrix theory proposed by Frohner [5], the neutron total cross section is given by

$$\sigma_t(E) = \frac{2\pi}{k^2} \sum_l (1 - \text{Re}[U_l(E)]), \quad (24)$$

in which U_l represents the collision matrix elements,

$$U_l(E) = e^{-2i\varphi_l(E)} \frac{1 + iP_l(E)R_l^\infty - s_l P_l(E)\pi}{1 - iP_l(E)R_l^\infty + s_l P_l(E)\pi}, \quad (25)$$

where P_l and φ_l are, respectively, the penetration factor of the centrifugal barrier and the phase shift of the incident wave scattered by a sphere. The parameter s_l stands for the pole strength function, which is closely related to the strength function S_l :

$$s_l = \frac{S_l \sqrt{E}}{2ka_c}. \quad (26)$$

Above a few tens of kilo-electron volts, the increasing contribution of the higher-order partial waves makes it impossible to separate the cross sections into l -dependent parameters. This problem was recently solved with the generalized SPRT method [31]. The latter method establishes simple relationships between the optical model and the average R -matrix parameters. According to this method, the energy dependence of the distant level parameter and pole strength function is given by

$$R_l^\infty(E) = \frac{2a_l(E) \cos[2\varphi_l(E)] + (1 - 2b_l(E)) \sin[2\varphi_l(E)]}{P_l(E)(1 + 2c_l^2(E) - 2b_l(E) + (1 - 2b_l(E)) \cos[2\varphi_l(E)] - 2a_l(E) \sin[2\varphi_l(E)])}, \quad (27)$$

$$s_l(E) = \frac{2(b_l(E) - c_l^2(E))}{\pi P_l(E)(1 + 2c_l^2(E) - 2b_l(E) + (1 - 2b_l(E)) \cos[2\varphi_l(E)] - 2a_l \sin[2\varphi_l(E)])}, \quad (28)$$

with

$$a_l^2(E) = c_l^2(E) - b_l^2(E), \quad (29)$$

$$b_l(E) = \frac{1}{2l+1} \sum_{j=l-1/2}^{l+1/2} \sum_{J=j-5/2}^{j+5/2} g_J \text{Im}[C_{lj}^J(E)], \quad (30)$$

TABLE VIII. Optical model parameters, uncertainties, and correlation matrix obtained in this work.

Parameter		Relative uncertainty	Correlation matrix							
r_0	(fm)	1.23 ± 0.02	1.6%	100						
a	(fm)	0.63 ± 0.03	5.3%	-8	100					
V_{HF}	(MeV)	-82.7 ± 4.4	5.3%	98	-8	100				
A_v	(MeV)	-15.2 ± 0.5	3.3%	9	-17	5	100			
A_s	(MeV)	-12.7 ± 0.9	7.1%	9	-6	5	4	100		
β_2		0.207 ± 0.010	4.8%	-37	11	-35	-16	-5	100	
β_4		0.102 ± 0.004	3.9%	-37	-8	-32	9	1	-34	100

$$c_l^2(E) = \frac{1}{2l+1} \sum_{j=l-1/2}^{l+1/2} \sum_{J=|j-5/2|}^{j+5/2} g_J |C_{lj}^J(E)|^2. \quad (31)$$

In the present work, the optical model code ECIS [7] was used to calculate the collision matrix elements C_{lj}^J involved in Eqs. (29) to (31). As suggested by the work on neptunium reported in Ref. [32], optical model parameters established by Morillon *et al.* [33,34] are suitable to reproduce the direct contribution in $n + {}^{237}\text{Np}$ reactions up to several tens of mega-electron volts (see Appendix).

Consistent l -dependent average parameters can be deduced from the reduced neutron width values $\Gamma_{\lambda,n}^0$ and the potential scattering R' by introducing Eq. (28) into Eq. (11) and Eq. (27) into Eq. (3). This statistical approach was successfully used to analyze the ${}^{242}\text{Pu}$ neutron cross sections [35] and the unresolved resonance range of the hafnium isotopes [36].

Realistic uncertainties in the average resonance and optical model parameters were determined by using a Monte Carlo technique specifically designed to derive model parameter uncertainties without changing the value of the parameters [37]. Optical model parameters of interest for the uncertainty propagation analysis are the reduced radius r_0 ,

the diffuseness a , the depths (V_{HF} , A_v , and A_s), and the deformation parameters (β_2 and β_4). A collection of ECIS results (total cross section, neutron transmission coefficient, collision matrix element, neutron strength function, distant level parameter, etc.) was generated by randomly varying these optical model parameters according to uniform distributions. Posterior values were selected according to the potential scattering length ($R' = 9.8 \pm 0.1$ fm) and neutron strength function ($10^4 S_0 = 1.02 \pm 0.14$) obtained in Secs. II and III. Final results, reported in Table VIII, were deduced from the first two moments of the posterior distributions. Figure 6 illustrates the strong correlation (~ 0.98) obtained between the reduced radius r_0 and the depth V_{HF} .

The distributions of the l -dependent average parameters [Eqs. (27) and (28)] are shown in Fig. 7. Table IX reports results for the s -, p -, and d -wave parameters. The s -wave distant level parameter $R_0^\infty = -0.18 \pm 0.03$ gives a potential scattering length $R' = 9.9 \pm 0.25$ fm [see Eq. (3)]. The latter uncertainty is twice as large as the uncertainty determined in the resonance range. By contrast, the final S_0 value of 1.01 ± 0.13 is in excellent agreement with the expected value of 1.02 ± 0.14 reported in Sec. III. Average parameters obtained in this work are summarized in Table X and compared with values compiled in the *Atlas of Neutron Resonances* [24] and RIPL-2 [25].

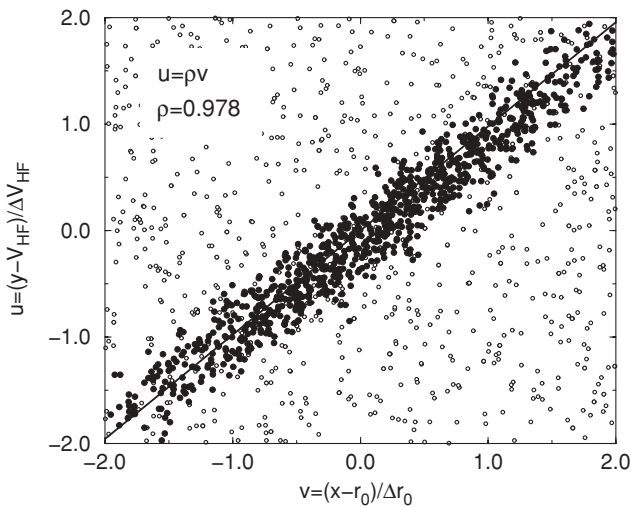


FIG. 6. Correlation between the Hartree-Fock contribution V_{HF} and the reduced radius r_0 . Open circles represent the uniform distribution of the prior values. Filled circles represent the posterior values obtained for $10^4 S_0 = 1.02 \pm 0.14$ and $R' = 9.8 \pm 0.1$ fm.

VI. NEUTRON CROSS SECTIONS

The parametrization established in this work (see Tables VIII and IX) was verified with experimental data retrieved from the EXFOR database [9]. For the total cross section, time-of-flight data measured by Gressier [1], Auchampaugh *et al.* [38], and Paya [22] were averaged over a

TABLE IX. Average R -matrix parameters, uncertainties, and correlation matrix obtained in this work.

Parameter		Relative uncertainty	Correlation matrix						
$10^4 S_0$	1.01 ± 0.13	12.9%	100						
$10^4 S_1$	1.81 ± 0.37	20.4%	19	100					
$10^4 S_2$	1.57 ± 0.23	14.6%	92	24	100				
R_0^∞	-0.18 ± 0.03	16.7%	-19	60	-38	100			
R_1^∞	0.18 ± 0.02	11.1%	-11	65	-15	85	100		
R_2^∞	-0.10 ± 0.03	30.0%	-4	61	-25	98	86	100	

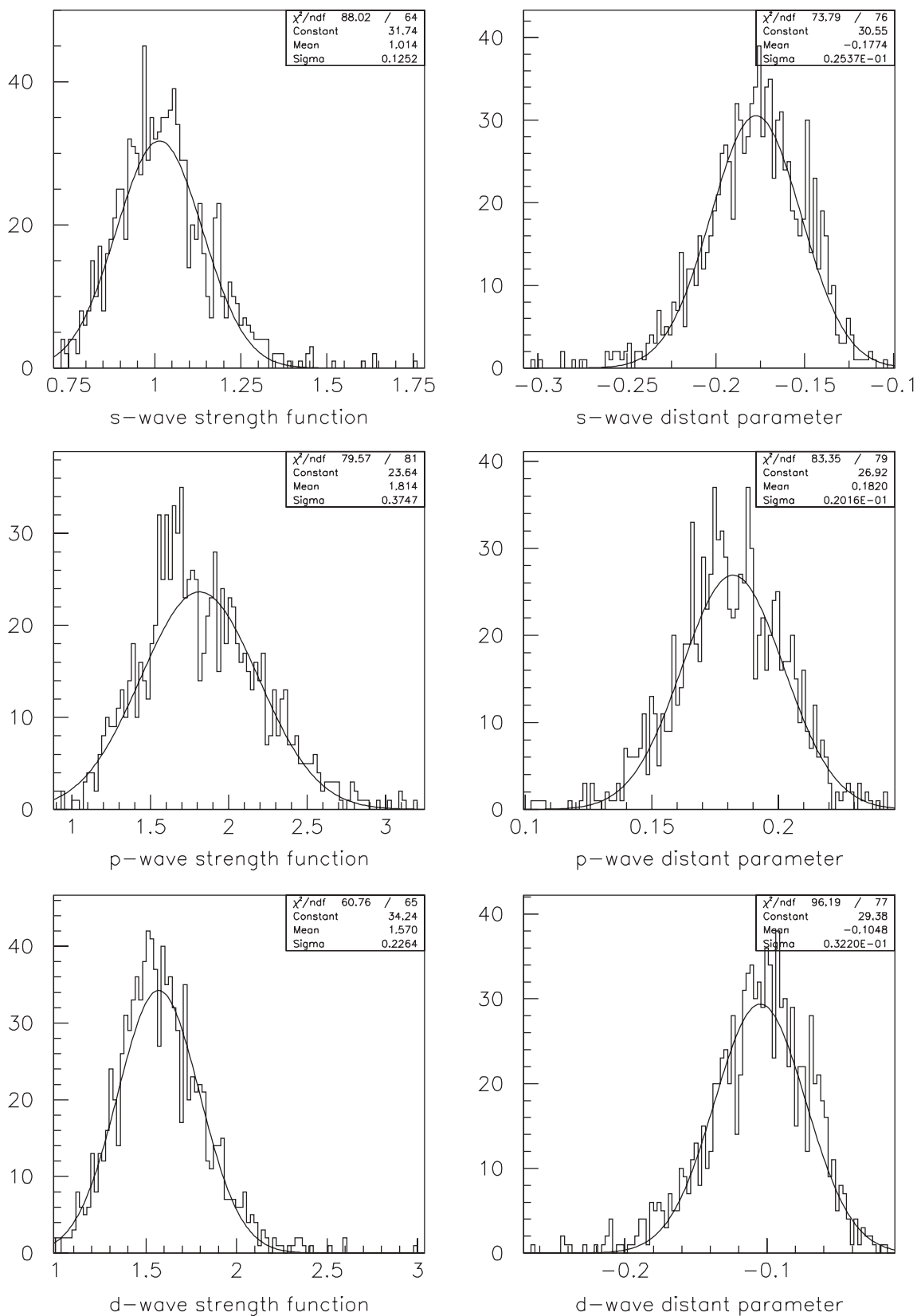


FIG. 7. Posterior distributions of the neutron strength function S_l (left-hand plots) and distant level parameters R_l^∞ (right-hand plots) for $l = 0, 1, 2$.

TABLE X. Comparison of l -dependent neutron strength functions obtained in this work (ESTIMA and SPRT methods) and reported in the literature.

	ESTIMA	SPRT	Mughaghab [24]	RIPL2 [25]
$10^4 S_0$	1.02 ± 0.14	1.01 ± 0.13	1.02 ± 0.06	0.97 ± 0.07
$10^4 S_1$		1.81 ± 0.37	2.0 ± 0.2	
$10^4 S_2$		1.57 ± 0.23		

suitable energy mesh and corrected for finite-sample-thickness effects. The SESH and CALENDF codes [39,40] were used to calculate this sample thickness correction by generating resonances with Monte Carlo techniques. The SESH code uses the single-level Breit-Wigner formalism to calculate neutron cross sections, while the CALENDF code uses the multilevel Breit-Wigner formalism. The latter is able to account for level-level interferences. This technique is routinely used within the neutron spectroscopy community [41,42] to calculate average total cross sections $\langle\sigma_t(E)\rangle$ from average transmission data $\langle T(E)\rangle$ by combining the sample thickness correction $C_T(E)$ and the sample thickness n (atoms per barn) as follows:

$$\langle\sigma_t(E)\rangle = -\frac{1}{n} \ln \frac{\langle T(E)\rangle}{C_T(E)}. \quad (32)$$

Correction factors $C_T(E)$ obtained for the Paya and Auchampaugh *et al.* data are compared in Fig. 8. A good agreement is obtained between the SESH and the CALENDF codes. The discrepancies remain lower than 5%. They become negligible above 2 keV. Similar calculations were performed for the transmission data measured at the GELINA facility.

The top plot in Fig. 9 compares the experimental data with the total cross section provided by the optical model code ECIS [7]. Calculations performed with and without correlations between the optical model parameters demonstrate the significant impact of our retroactive analysis up to 100 keV.

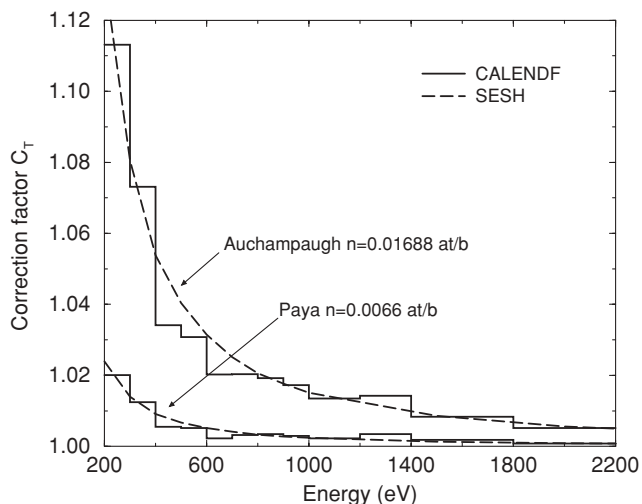


FIG. 8. Sample thickness corrections calculated with the SESH and CALENDF codes for transmission data measured by Paya [22] and Auchampaugh *et al.* [38].

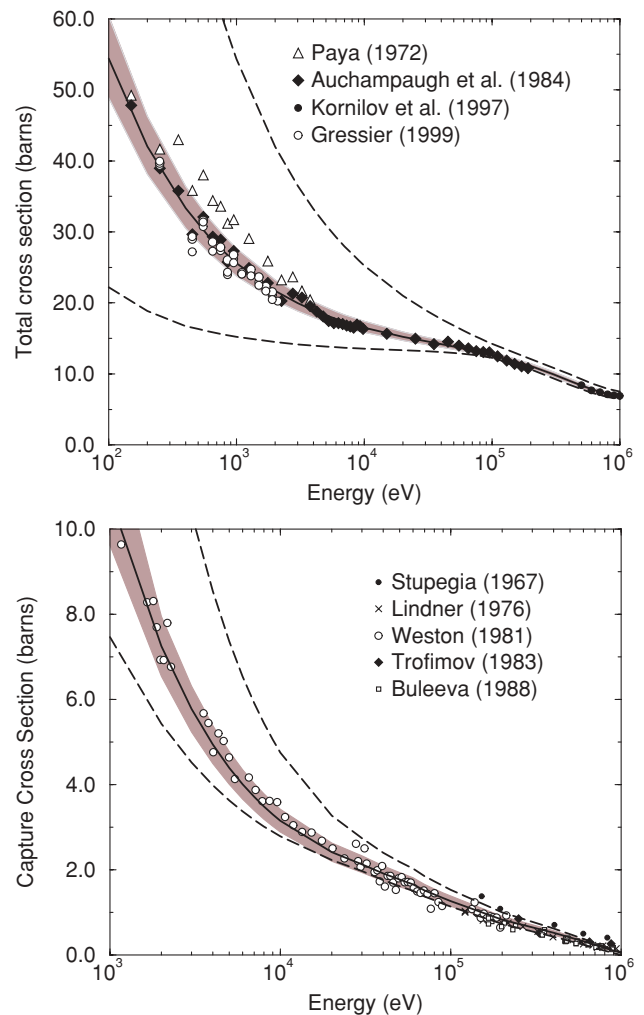


FIG. 9. (Color online) ^{237}Np cross sections (solid line) and uncertainties (shaded area) calculated by ECIS and TALYS. Dashed lines represent the uncertainties calculated without correlations between the model parameters. Experimental data were retrieved from the EXFOR database [9].

The good agreement observed between the data measured by Auchampaugh *et al.* and those measured by Gressier confirms the correct parametrization of the direct interaction used in this work.

The bottom plot in Fig. 9 shows the ^{237}Np capture cross section calculated with the statistical model code TALYS [8]. The correlations among the optical model parameters (Table VIII), the uncertainty of 1.0 meV quoted for the average radiation width (Table V), and the 5% relative uncertainty obtained in the mean level spacing (Table VI) were propagated through the TALYS calculations via direct Monte Carlo techniques [18]. The good agreement obtained with the capture cross section measured at the ORELA facility [12] confirms the magnitude of the ^{237}Np γ -ray strength function $10^4 S_\gamma = 655 \pm 37$ provided by the statistical analysis of the resolved resonance parameters.

The ^{237}Np total and capture cross sections obtained in this work are given in Table XI. Results provided by the ECIS and TALYS codes are compared with those calculated

TABLE XI. ^{237}Np total and capture cross sections (barns) calculated with the ECIS, TALYS, and CONRAD codes below 200 keV.

Energy (keV)	Total cross section		Capture cross section	
	CONRAD	ECIS	CONRAD	TALYS
0.5	31.11	31.23 ± 2.64	16.11	15.90 ± 1.76
0.6	29.47	29.58 ± 2.43	14.54	14.35 ± 1.57
0.8	27.15	27.28 ± 2.13	12.35	12.19 ± 1.30
1.0	25.57	25.71 ± 1.93	10.88	10.74 ± 1.12
2.0	21.67	21.82 ± 1.43	7.33	7.25 ± 0.71
3.0	19.94	20.09 ± 1.22	5.85	5.78 ± 0.54
4.0	18.92	19.07 ± 1.09	5.00	4.94 ± 0.45
5.0	18.21	18.37 ± 1.00	4.44	4.39 ± 0.39
6.0	17.70	17.85 ± 0.93	4.06	4.00 ± 0.35
7.0	17.30	17.45 ± 0.88	3.76	3.71 ± 0.32
8.0	16.97	17.12 ± 0.84	3.53	3.49 ± 0.30
9.0	16.70	16.85 ± 0.80	3.34	3.30 ± 0.28
10.0	16.47	16.62 ± 0.77	3.19	3.15 ± 0.27
20.0	15.19	15.32 ± 0.60	2.45	2.42 ± 0.22
30.0	14.57	14.68 ± 0.52	2.16	2.13 ± 0.20
40.0	14.16	14.24 ± 0.47	1.93	1.91 ± 0.18
50.0	13.83	13.90 ± 0.44	1.79	1.77 ± 0.17
60.0	13.56	13.61 ± 0.41	1.65	1.67 ± 0.15
70.0	13.33	13.35 ± 0.39	1.51	1.52 ± 0.14
80.0	13.11	13.12 ± 0.38	1.41	1.42 ± 0.13
90.0	12.91	12.90 ± 0.37	1.32	1.34 ± 0.12
100.0	12.72	12.70 ± 0.36	1.25	1.27 ± 0.12
200.0	11.20	11.10 ± 0.34	0.79	0.83 ± 0.08

with the CONRAD code [6]. The latter uses the average R -matrix theory [Eqs. (24) and (25)] to calculate the total cross section with the average parameters reported in Table IX. The same code calculates the compound nucleus reactions (capture, elastic, inelastic, and fission reactions) via the Hauser-Feshbach formula with width fluctuation corrections based on the Moldauer's prescriptions. The good agreement between ECIS/CONRAD and TALYS/CONRAD demonstrates the correct description of the cross sections with the l -dependent average parameters established in this work.

VII. CONCLUSIONS

Results presented in this work demonstrate the performance of the combined analysis of the resolved and unresolved resonance ranges to predict the behavior of the neutron-induced capture reaction up to several tens of kilo-electron volts. The good agreement between the theoretical and the experimental values is confirmed by the uncertainties obtained with Monte Carlo techniques.

The analysis of several time-of-flight data provided a potential scattering length $R' = 9.8 \pm 0.1$ fm, an average radiation width $\langle \Gamma_\gamma \rangle = 39.3 \pm 1.0$ meV, an s -wave mean level spacing $D_0 = 0.60 \pm 0.03$ eV, and an s -wave neutron strength function $10^4 S_0 = 1.02 \pm 0.14$. For higher-order partial waves ($l > 0$), the statistical analysis of the resonances with the generalized SPRT method led to p - and d -wave neutron strength functions equal to $10^4 S_1 = 1.81 \pm 0.37$ and $10^4 S_2 = 1.57 \pm 0.23$. By

introducing these l -dependent average parameters in the average R -matrix code CONRAD, we obtained total and capture cross sections in excellent agreement with the ECIS and TALYS calculations.

Investigations of the complex nuclear mechanisms involved above the mega-electron volt energy range are in progress. Works performed by A. Tudora at the Faculty of Physics of the University of Bucharest will be used to describe the fission process.

ACKNOWLEDGMENTS

The author wishes to express his appreciation for the work of A. Lepretre, F. Gunsing, A. Brusegan, and P. Siegler. Special thanks go to V. Gressier, who performed the transmission measurement at the GELINA facility. I also express my gratitude to A. Tudora for her relevant advice. The author thanks P. Schillebeeckx and O. Litaize for the correction of this work.

APPENDIX: OPTICAL MODEL POTENTIAL FOR ECIS CALCULATIONS

This Appendix presents the optical model parametrization used to calculate the collision matrix elements C_{ij}^J involved in Eqs. (29) to (31). The dispersive optical potential proposed by Morillon *et al.* [33,34] can be written as

$$\begin{aligned}
 V(r, E) = & [(V_v(E) + \Delta V_v(E)) + iW_v(E)]f(r, r_0, a) \\
 & - 4a[\Delta V_s(E) + iW_s(E)]\frac{df(r, r_0, a)}{dr} \\
 & - [(V_{so}(E) + \Delta V_{so}(E)) + iW_{so}(E)]\left(\frac{\hbar}{m_\pi c}\right)^2 \\
 & \times \frac{1}{r}\frac{df(r, r_0, a)}{dr}\vec{\tau} \cdot \vec{s}, \quad (A1)
 \end{aligned}$$

where the Woods-Saxon form factors $f(r, r_0, a)$ for the volume (v), surface (s), and spin-orbit (so) potentials share the same geometrical parameters (reduced radius r_0 , diffuseness a).

TABLE XII. Optical model parameters established by Morillon *et al.* Values of parameters are reported in Refs [33] and [34].

Parameter	Value
r_0	1.231 fm
a	0.633 fm
V_{HF}	-82.8 MeV
β	1.114 fm
γ	0.093 fm
A_v	-15.24 MeV
B_v	90.44 MeV
A_s	-12.73 MeV
B_s	13.0 MeV
C_s	0.025 MeV

In the dispersion relation treatment, $\Delta V_i(E)$ is used to connect the real $V_i(E)$ and imaginary $W_i(E)$ terms of each component ($i = v, s, \text{so}$). For the spin-orbit contributions, $V_{\text{so}}(E)$ and $W_{\text{so}}(E)$ were taken from Ref. [43]. For the real part of the surface potential the Hartree-Fock contribution of the mean field is given by

$$V_v(E) = V_{\text{HF}} e^{\left(-\frac{\mu\beta^2|E-E_F|}{2\hbar^2}\right)} e^{\left(\frac{4\mu^2\gamma^2|E-E_F|^2}{\hbar^4}\right)}. \quad (\text{A2})$$

This contribution is defined by the depth V_{HF} , the reduced mass of the system μ , and the nonlocality ranges β and γ . For the volume and surface imaginary terms, the energy dependences are symmetric about the Fermi energy

E_F :

$$W_v(E) = \frac{A_v(E - E_F)^2}{(E - E_F)^2 + B_v^2}, \quad (\text{A3})$$

$$W_s(E) = \frac{A_s(E - E_F)^2}{(E - E_F)^2 + B_s^2} \exp(-C_s(E - E_F)). \quad (\text{A4})$$

Optical model parameters established by Morillon *et al.* [33,34] are given in Table XII. Parameters of interest in this work are the reduced radius r_0 , the diffuseness a , and the depths V_{HF} , A_v , and A_s . For coupled-channel calculations, deformation parameters β_2 and β_4 were retrieved from the Moller and Nix database [44]:

$$\beta_2 = 0.215 \quad \text{and} \quad \beta_4 = 0.102.$$

-
- [1] V. Gressier, CEA/DSM Saclay Report DAPNIA/SPHN-99-04T (1999).
- [2] A. Lepretre, A. Brusegan, N. Herault, G. Noguere, and P. Siegler, CEA/DSM Saclay Report DAPNIA-02-374 (2002).
- [3] F. Gunsing, A. Lepretre, C. Mounier, C. Raepsaet, A. Brusegan, and E. Macavero, *Phys. Rev. C* **61**, 054608 (2000).
- [4] G. Noguere, O. Bouland, A. Brusegan, P. Schillebeeckx, P. Siegler, A. Lepretre, N. Herault, and G. Rudolf, *Phys. Rev. C* **74**, 054602 (2006).
- [5] F. H. Frohner, *Nucl. Sci. Eng.* **103**, 119 (1989).
- [6] C. De Saint Jean, B. Habert, O. Litaize, G. Noguere, and C. Suteau, in *Proceedings of the International Conference on Nuclear Data for Science and Technology, Nice, France, 2007*, edited by O. Bersillon *et al.* (EDP Sciences, 2008).
- [7] J. Raynal, in *Proceedings of the Specialists' Meeting on the Neutron Nucleus Optical Model up to 200 MeV, Bruyres-le-Châtel, France, 1996* (Nuclear Energy Agency, Paris, 1997).
- [8] A. J. Koning, S. Hilaire, and M. C. Duijvestijn, in *Proceedings of the International Conference on Nuclear Data for Science and Technology, Santa Fe, New Mexico, 2004*, edited by R. C. Haight *et al.* (American Institute of Physics, Melville, NY, 2005).
- [9] H. Henriksson, O. Schwerer, D. Rochman, M. V. Mikhaylyukova, and N. Otuka, in *Proceedings of the International Conference on Nuclear Data for Science and Technology, Nice, France, 2007*, edited by O. Bersillon *et al.* (EDP Sciences, 2008).
- [10] C. W. Reich and M. S. Moore, *Phys. Rev.* **111**, 929 (1958).
- [11] A. Koning *et al.*, in *Proceedings of the International Conference on Nuclear Data for Science and Technology, Nice, France, 2007*, edited by O. Bersillon *et al.* (EDP Sciences, 2008).
- [12] L. W. Weston and J. H. Todd, *Nucl. Sci. Eng.* **79**, 184 (1981).
- [13] K. Kobayashi, S. Lee, S. Yamamoto, H. J. Cho, and Y. Fujita, *Nucl. Sci. Tech.* **39**, 111 (2002).
- [14] O. Shcherbakov, K. Furutaka, S. Nakamura, H. Sakane, K. Kobayashi, S. Yamamoto, J. I. Hori, and H. Harada, *Nucl. Sci. Tech.* **42**, 135 (2005).
- [15] E. I. Esch, R. Reifarth, E. M. Bond, T. A. Bredeweg, A. Couture, S. E. Glover, U. Greife, R. C. Haight, A. M. Hatarik, R. Hatarik, M. Jandel, T. Kawano, A. Mertz, J. M. O'Donnell, R. S. Rundberg, J. M. Schwantes, J. L. Ullmann, D. J. Vieira, J. B. Wilhelmy, and J. M. Wouters, *Phys. Rev. C* **77**, 034309 (2008).
- [16] M. C. Moxon and J. B. Brisland, REFIT computer code. Harwell Laboratory Report No. CBNM/ST/90-131/1 (1990).
- [17] G. Noguere, D. Bernard, C. De Saint Jean, B. Iooss, F. Gunsing, K. Kobayashi, S. F. Mughabghab, and P. Siegler, *Nucl. Sci. Eng.* **160**, 108 (2008).
- [18] G. Noguere and J.-Ch. Sublet, *Ann. Nucl. Eng.* **35**, 2259 (2008).
- [19] C. De Saint Jean, G. Noguere, B. Habert, and B. Iooss, *Nucl. Sci. Eng.* **161**, 363 (2009).
- [20] O. Bringer, I. Al Mahamid, S. Chabod, F. Chartier, E. Dupont, A. Letourneau, P. Mutti, L. Oriol, S. Panebianco, and C. Veysire, in *Proceedings of the International Conference on Nuclear Data for Science and Technology, Nice, France, 2007*, edited by O. Bersillon *et al.* (EDP Sciences, 2008).
- [21] M. Herman, ENDF-102 Data Formats and Procedures for the Evaluated Nuclear Data File ENDF-6, Brookhaven National Laboratory Report BNL-NCS-44945-05-Rev (2005).
- [22] D. Paya, Ph.D. thesis, Université de Orsay, France, 1972.
- [23] L. Mewissen, F. Poortmans, E. Cornelis, G. Vanpraet, A. Angeletti, G. Rohr, and H. Weigmann, *Nucl. Sci. Eng.* **70**, 155 (1979).
- [24] S. F. Mughabghab, *Atlas of Neutron Resonances*, 5th ed. (Elsevier, Amsterdam, 2006).
- [25] T. Belgia *et al.*, IAEA Nuclear Data Services Report IAEA-TECDOC-1506 (2005).
- [26] C. E. Porter and R. G. Thomas, *Phys. Rev.* **104**, 483 (1956).
- [27] G. G. Slaughter, J. A. Harvey, and R. C. Block, *Bull. Am. Phys. Soc.* **6**, 70 (1961).
- [28] A. Gilbert and A. G. W. Cameron, *Can. J. Phys.* **43**, 1446 (1965).
- [29] G. Vladuca, A. Tudora, F.-J. Hamsch, S. Oberstedt, and I. Ruskov, *Nucl. Phys. A* **720**, 274 (2003).
- [30] G. Vladuca, F.-J. Hamsch, A. Tudora, S. Oberstedt, A. Oberstedt, F. Tovesson, and D. Filipescu, *Nucl. Phys. A* **740**, 3 (2004).
- [31] E. Rich, G. Noguere, C. De Saint Jean, and A. Tudora, *Nucl. Sci. Eng.* **162**, 76 (2009).
- [32] G. Vladuca, A. Tudora, B. Morillon, and D. Filipescu, *Nucl. Phys. A* **767**, 112 (2006).
- [33] B. Morillon and P. Romain, *Phys. Rev. C* **70**, 014601 (2004).
- [34] B. Morillon and P. Romain, *Phys. Rev. C* **74**, 014601 (2006).
- [35] E. Rich, A. Tudora, G. Noguere, J. Tommasi, and J.-F. Lebrat, *Nucl. Sci. Eng.* **162**, 178 (2009).

- [36] G. Noguere, E. Rich, C. De Saint Jean, O. Litaize, P. Siegler, and V. Avrigeanu, [Nucl. Phys. A **831**, 106 \(2009\)](#).
- [37] B. Habert, C. De Saint Jean, G. Noguere, L. Leal, and Y. Rugama (accepted for publication in Nucl. Sci. Eng.).
- [38] G. F. Auchampaugh, M. S. Moore, J. D. Moses, R. O. Nelson, R. C. Extermann, C. E. Olsen, N. W. Hill, and J. A. Harvey, [Phys. Rev. C **29**, 174 \(1984\)](#).
- [39] F. H. Froehner, SESH computer code. General Atomic Report GA-8380 (1968).
- [40] J-C.H. Sublet, P. Ribon, and M. Coste-Delclaux, User manual for CEA/DEN Cadarache Report CEA-R-6131 (2006).
- [41] H. Derrien, L. C. Leal, and N. M. Larson, in Proceedings of PHYSOR-2006 Topical Meeting on Reactor Physics, Vancouver, Canada (2006).
- [42] S. Marrone *et al.*, [Phys. Rev. C **73**, 034604 \(2006\)](#).
- [43] A. J. Koning and J. P. Delaroche, [Nucl. Phys. A **713**, 231 \(2003\)](#).
- [44] P. Moller, J. R. Nix, and W. J. Swiatecki, [At. Data Nucl. Data Tables **59**, 185 \(1995\)](#).

Appendix C

Average cross section of Hafnium



Average neutron parameters for hafnium

G. Noguere^{a,*}, E. Rich^a, C. De Saint Jean^a, O. Litaize^a, P. Siegler^b,
V. Avrigeanu^c

^a CEA, DEN Cadarache, 13108 Saint Paul les Durance, France

^b EC-JRC-IRMM, 2440 Geel, Belgium

^c “Horia Hulubei” National Institute for Physics and Nuclear Engineering, Bucharest, Romania

Received 16 March 2009; received in revised form 17 August 2009; accepted 28 August 2009

Available online 10 September 2009

Abstract

The neutron transmission of natural hafnium samples have been measured within the 2 eV to 50 keV energy range at the white neutron source GELINA of the Institute for Reference Materials and Measurements (IRMM) in Geel, Belgium. Data sets for two temperatures (77 K and 300 K) and three sample thicknesses (1 mm, 2 mm, 15 mm) have been simultaneously analyzed in terms of Reich–Moore parameters. The ESTIMA technique in association with the generalized SPRT method were used to obtain a consistent set of l -dependent average resonance parameters. For each hafnium isotope, scattering radius R' , neutron strength function S_l , distant level parameter R_l^∞ , mean level spacing D_l and average radiation width $\langle \Gamma_\gamma \rangle$ are given and compared with results reported in the literature. The capture and total cross sections calculated by the CONRAD code using this set of average parameters were successfully compared to experimental data retrieved from EXFOR.

© 2009 Elsevier B.V. All rights reserved.

PACS: 24.10.-I; 28.20.-v; 29.30.Hs

Keywords: NUCLEAR REACTIONS $^{174,176,177,178,179,180}\text{Hf}(n,\gamma)$, $E = 0.002\text{--}50$ keV; measured transmission and capture σ at the GELINA white neutron source facility; deduced resonance parameters using Reich–Moore interpretation and the REFIT code. Comparison with data

* Corresponding author.

E-mail address: gilles.noguere@cea.fr (G. Noguere).

1. Introduction

Hafnium is a ductile metal which does not exist as a free element in nature. The hafnium isotopes ^{174}Hf , ^{176}Hf , ^{177}Hf , ^{178}Hf , ^{179}Hf and ^{180}Hf are found combined in zirconium compounds with a respective abundance of 0.16%, 5.26%, 18.60%, 27.28%, 13.62% and 35.08%. In the neutron epi-thermal energy range, experimental works on natural and isotopic hafnium samples are scarce in the literature. Available data are rather old and the given results are often incomplete.

The first resonance spectroscopy which has established resolved resonance parameters for the hafnium isotopes over a wide energy range was reported by Fuketa et al. [1,2]. Single level parameters were extracted up to 1.2 keV from neutron transmission data of natural and isotopically enriched samples measured at the 45 m-flight path of the Oak Ridge National Laboratory fast chopper, and at the 25 m-flight path of the Linac facility of the Rensselaer Polytechnic Institute (RPI). Recently, the public release of a classified Multi-Level analysis, performed by Moxon on data measured at the Linac facility of the Harwell laboratory [3], provides one of the most reliable set of resonance parameters for ^{174}Hf , ^{176}Hf , ^{177}Hf , ^{178}Hf and ^{179}Hf below 30 eV. In his work, Moxon reports for the first time a strong $^{176,178}\text{Hf}$ doublet near 8 eV. For ^{177}Hf , resonance parameters used in the Evaluated Neutron Data Files are mainly based on results obtained in the mid 70s from high resolution neutron time-of-flight measurements performed at the Columbia University Nevis synchrotron by Liou et al. [4], and at the GELINA facility of the Institute for Reference Materials and Measurements (IRMM) by Rohr et al. [5]. The given resonance parameters are in good agreement within the energy range of overlap of both sets of data (below 300 eV). The last relevant transmission and capture measurements were performed at the RPI facility up to 200 eV [6]. The analysis performed by Trbovich with the modern R-matrix code SAMMY [7] provided a consistent set of parameters for a large number of $^{177,179}\text{Hf}$ resonances. Complementary studies over a larger energy range are required for improving the average nuclear properties of the even/even Hf isotopes, characterized by a higher mean level spacing.

In this paper, an attempt was made to establish an unambiguous set of l -dependent average parameters for the six Hf isotopes by using six transmission data measured at the Doppler station of the GELINA facility at low (77 K) and room (300 K) temperatures. These measurements were firstly performed to test Hf nuclear data by comparison of measured and calculated average transmission spectra [8]. Preliminary analysis [9,10] have demonstrated the possibilities to extract resonance energies and partial widths up to 1 keV.

The strength and originality of the present work lie in the Reich–Moore interpretation of the resolved resonance range with the shape analysis code REFIT [11] in association with optical model calculations based on parameters established by Morillon et al. [12,13] with deformation parameters initially proposed by Avrigeanu et al. [14,15]. Links between the collision matrix elements calculated by the optical model code ECIS [16] and the average R-Matrix parameters (neutron strength function S_l and distant level parameters R_l^∞) were established by using the ESTIMA [17] and SPRT methods [18]. The consistency of the resulting mean level spacing D_l and average radiation width $\langle\Gamma_\gamma\rangle$ was tested by comparing experimental capture cross sections retrieved from EXFOR [19] with statistical model calculations performed with the TALYS [20] and CONRAD [21] codes.

2. Experimental techniques

The transmission experiments were performed at the Doppler station of the 150 MeV pulsed neutron source GELINA of the IRMM. A scheme of the experimental areas is shown in Fig. 1.

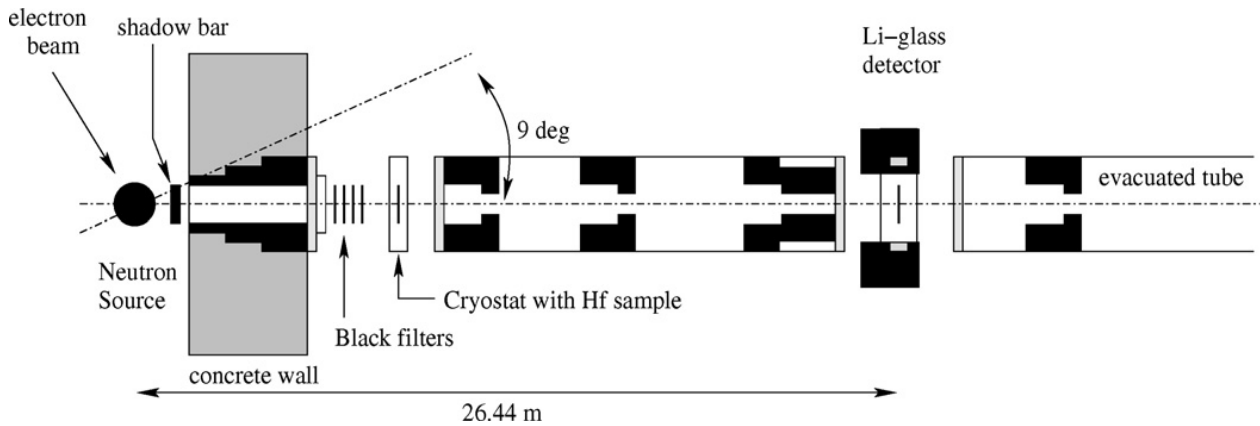


Fig. 1. Scheme of the Doppler station of the GELINA facility.

Table 1

Thicknesses of the three hafnium samples at different temperatures.

Sample thickness	300 ± 1 K (atom/barn)	77 ± 1 K (atom/barn)
e = 1 mm	0.00475 ± 0.00005	0.00476 ± 0.00005
e = 2 mm	0.00938 ± 0.00006	0.00941 ± 0.00006
e = 15 mm	0.06645 ± 0.00009	0.06664 ± 0.00009

Neutrons are produced by using (γ, xn) and (γ, f) processes induced by electrons incident on a rotating U-target. Fast neutrons are moderated by a 36 mm water slab in a 2 mm Be canning. The accelerator conditions were 1 ns pulse-width at 800 Hz repetition rate. Neutrons produced by the target-moderator assembly were crossing a filter setup and the Hf samples in the cryostatic sample changer located at 10 m from the neutron source. They were detected at 26.443 ± 0.005 m with a 110 mm diameter and 10 mm thick Li-glass detector (NE912). The scintillator was viewed by two 5" EMI 9823 photo-multiplier tubes which were placed orthogonal to the beam axis and out of the neutron beam itself.

The natural hafnium samples were metal discs with diameter of 55 mm and thickness of 1 mm. The hafnium content was given by the manufacturer to be 97%. The largest impurity was 2.8% zirconium. The discs were combined to generate the three different sample thicknesses given in Table 1. For the measurements at 77 K, the sample thickness was calculated using a linear expansion coefficient of $\alpha = 6.0 \times 10^{-6} \text{ K}^{-1}$. The samples are moved "in" (sample-in) and "out" (sample-out) of the neutron beam by an electro-mechanical sample changer. The sample position is located after 600 mm borax-resin collimator with an aperture of 40 mm.

The low temperature measurements were performed using a cryostat based on a Gifford–McMahon cycle. Temperature stabilization was assured by monitoring the temperature with two platinum temperature sensors and adjusting the current through a heating resistor close to the sample position. This allows sample temperatures between 10 K and 350 K with an accuracy and stability better than 1 K. In order to avoid differences in the transmission spectra due to temperature differences between materials of the sample holder, both sample-in and sample-out positions were cooled and stabilized.

To avoid slow neutron background from the previous accelerator cycle, an anti-overlap filter was placed in the neutron beam in front of the sample changer. It was made from 0.0053 atoms/b rhodium disc and a 0.032 atoms/b cadmium sheet. To reduce the influence of the γ -flash, coming

from the neutron producing target, a 5 mm thick high purity lead filter was permanently placed in the beam.

3. Data reduction

Transmission experiments measure the attenuation of the incident neutron flux going through a sample. Measurements are routinely performed in cycles with a preset count rate for the sample-in and sample-out positions. This resulted in a cycle length of about 10 minutes, which minimized the effects of the inherent instabilities of the neutron flux. The transmission factor is then obtained from the ratio of the sum of the sample-in $C_{in,i}$ and sample-out $C_{out,i}$ measurements, both corrected for the dead time (a_{in} and a_{out}) and background contributions (B_{in} and B_{out}):

$$T(t) = N \frac{a_{in}(t) \sum_i C_{in,i}(t) - B_{in}(t)}{a_{out}(t) \sum_i C_{out,i}(t) - B_{out}(t)} \quad (1)$$

in which i labels the cycle numbers and N stands for the normalization factor. The latter accounts for the differences in integrated intensities of the incident neutron beam during the sample-in and sample-out cycles. The normalization was obtained by monitoring the neutron flux using two BF_3 proportional counters located in the concrete roof above the neutron source. These detectors give an accurate normalization of the transmission spectra with a dispersion of about 0.5%.

The electronic dead time of the acquisition system was measured and recorded online. For the present experiments, corrections were well below 3%. After summation of the corresponding sample-in and sample-out cycles, the raw data were corrected for the timing offset and the compressed time channels were transferred to a linear scale.

The time dependent background was determined with the black resonance technique. Black resonances of Cd, Rh and Hf were adjusted in order to obtain the real transmission value for the minima. In a second stage, the time dependence of the background was fitted on the reconstructed values and subtracted from the raw data. Typical values for the background were 4.5% at 1 keV and 1.1% at 5 eV. For practical purpose, the black resonance regions were smoothed in order to avoid oscillations in the final TOF transmission spectra.

At this stage of the analysis, the contribution of the 2.8% impurity of zirconium in the hafnium sample was corrected. The experimental transmission data were divided by the theoretical transmission of the natural zirconium reconstructed by taken into account the sample temperature and experimental resolution. Final transmission spectra are shown in Fig. 2 as a function of the incident neutron energy.

4. Resonance shape analysis

The six transmission spectra measured at the GELINA facility were analyzed with the simultaneous fitting procedure of the REFIT code [11]. The transmission data were interpreted in term of Reich–Moore parameters by using the following expression:

$$T(E) = \int_0^{\infty} R(E, E') T_{th}(E') dE' \quad (2)$$

with

$$T_{th}(E) = \exp \left[- \sum_i n_i \sigma_i(E) \right] \quad (3)$$

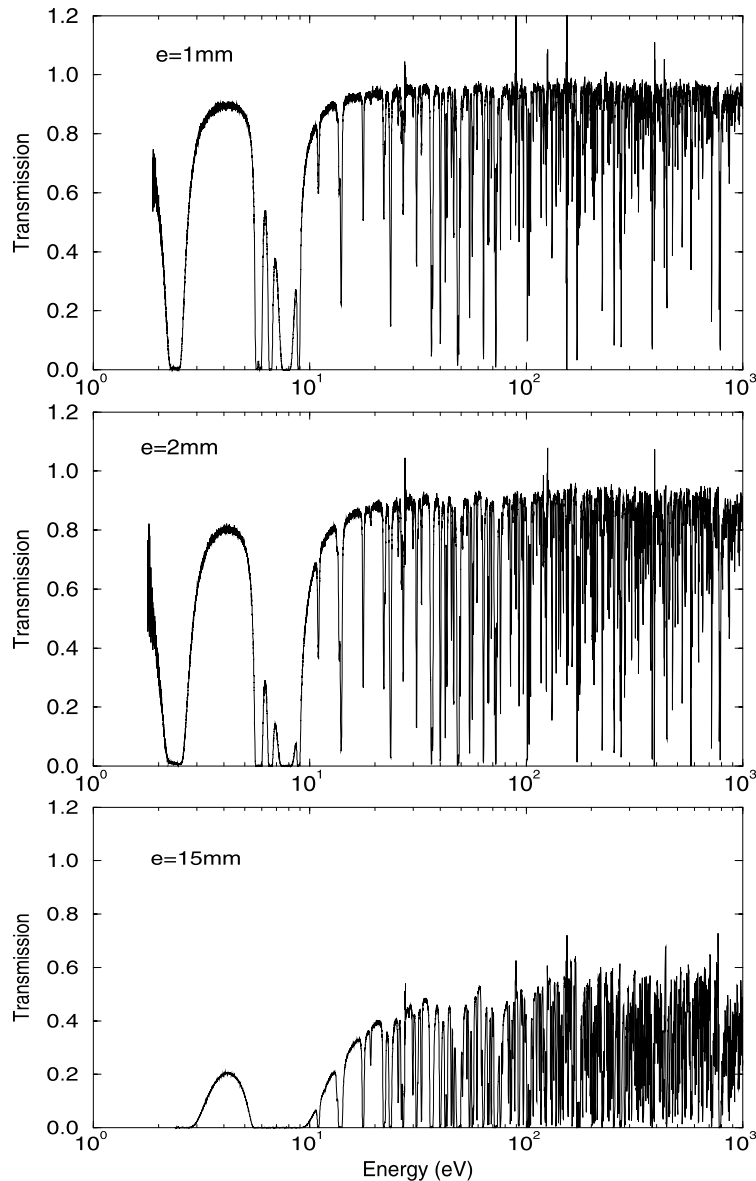


Fig. 2. Transmission spectra measured at the GELINA facility at 300 K.

in which i labels the contribution of the six Hf isotopes, n_i represents the atomic surface density in atom per barn, σ_i is the Doppler broadened total cross section and R accounts for the experimental resolution of the Doppler station.

The determination of meaningful nuclear resonance parameters from neutron time-of-flight data requires a correct description of the energy resolution of the facility as a function of neutron energies. In the REFIT code, the variance and the skewness of the resolution function are determined by two parameters λ_1 and λ_2 . They represent the “effective” mean free path of the neutron respectively in the water slab and in the vicinity of the target-moderator assembly. The value of $\lambda_1 = 5.7 \pm 0.7$ mm was calculated from ^{56}Fe capture data measured at the GELINA facility [22]. This result was confirmed by Monte-Carlo simulations [23,24]. For the determination of λ_2 , we have used a technique proposed in Ref. [25], that consists to fit the bottom of the nearly black resonances. The analysis of the transmission data of the 15-mm thick sample leads to $\lambda_2 = 55.6 \pm 2.1$ mm. Example of resolution function given in distance is presented in Fig. 3.

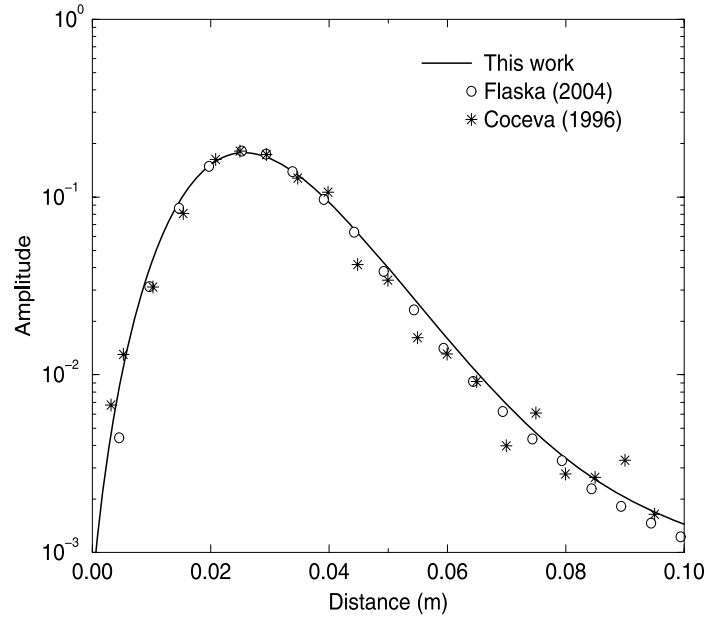


Fig. 3. Experimental resolution function at 10 eV as a function of the flight distance calculated in this work and compared with independent Monte-Carlo simulations [23,24].

Table 2
Debye temperature for mono-atomic hafnium crystal.

Author	Year	Ref.	Θ_D (K)
Wolcott	1955	[28]	261
Kneip	1963	[29]	252.3 ± 0.9 251.5 ± 1.2
Betterton	1968	[30]	252 ± 1
Gao	1999	[32]	250
Ostanin ^a	2000	[31]	215
Feranchuk ^a	2002	[33]	280
Average value			251.7
Standard deviation			19.3

^a Calculated value.

The contribution of the Doppler effect was taken into account by using the Free Gas Model with an effective temperature [26]. The effective temperature T_{eff} corresponding to $T = 300 \pm 1$ K was calculated using a simple Einstein model valid for pure element above room temperature:

$$T_{eff} = T_E \coth\left(\frac{T_E}{T}\right) \quad (4)$$

The first two term of the Taylor expansion of this expression suffice and give [27]:

$$T_{eff} \simeq T \left[1 + \frac{1}{3} \left(\frac{T_E}{T} \right)^2 \right] \quad (5)$$

where T_E stands for the Einstein temperature which is related to the Debye temperature $T_E = \frac{3}{8}\theta_D$. Table 2 reports experimental and calculated values of Debye temperature for hafnium found in the literature. Although large discrepancies are observed, the average value remains consistent with the value of 252 K reported in Ref. [34]. By introducing the average value of θ_D and its standard deviation in Eq. (5), we obtain an effective temperature equal to $T_{eff} = 309.8 \pm 1.8$ K.

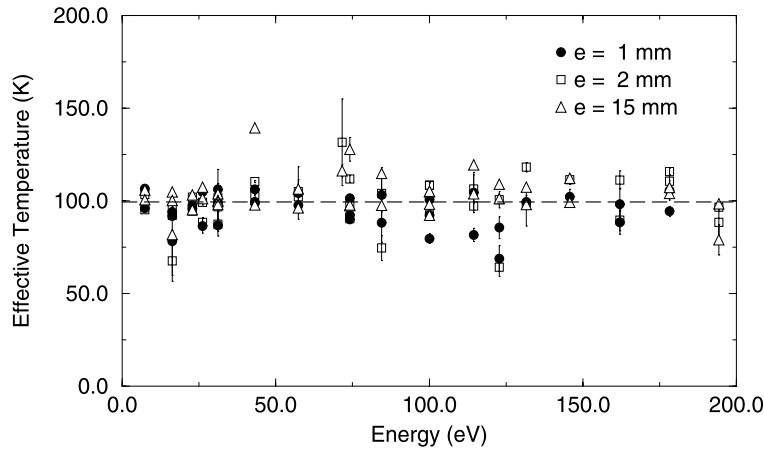


Fig. 4. Effective temperature determined with the REFIT code [11].

For the transmission spectra measured at 77 K, T_{eff} was fitted on the data together with the resonance parameters. Results are shown in Fig. 4 as a function of the incident neutron energy. The average value is $T_{eff} = 99.4$ K and the standard deviation is close to 11.5 K.

Examples of transmission data are shown in Fig. 5 together with the least-square adjusted theoretical curves. The strength of the present analysis lies in the successful use of transmission data measured at low temperature. Their simultaneous analysis within the fitting algorithm of the REFIT code allowed confirmation of the existence of broad multiplets of overlapping resonances (Fig. 6).

The final resonance shape analysis accounts for the contribution of a large variety of nuisance parameters (effective temperature, parameters of the resolution function, flight path length, atomic surface density). Realistic variance and covariance between the model parameters were calculated by means of Monte-Carlo techniques relying on conditional probabilities. Detail explanations can be found elsewhere [35,36]. The resonance energies and partial widths for the even/even hafnium isotopes are given in Table 3. Those obtained below 200 eV for $^{177,179}\text{Hf}$ are listed in Tables 4 and 5. The complete set of hafnium parameters is reported in Ref. [37]. Our results are compared with the parameters available in the latest version of the European library JEFF-3.1.1 [38]. Below 200 eV, parameters of JEFF-3.1.1 were established by Trbovich et al. [6] from the resonance shape analysis of data measured at the RPI facility. The agreement between both sets of neutron widths is close to 5% in average. However, owing to the complex overlapping resonant structures of the natural hafnium cross sections, huge local discrepancies greater than 15% can be observed, especially for the less abundant ^{174}Hf isotope.

The analysis of the 15 mm-thick sample allowed the simultaneous adjustment of the neutron and radiation widths for several broad s -wave resonances mainly observed below 100 eV. For the $n+^{177}\text{Hf}$ and $n+^{179}\text{Hf}$ nuclear systems, we were able to extract Γ_γ values for 28 and 13 resonances respectively. Their independent behavior with the neutron energy is shown in Fig. 7. For the even/even hafnium isotopes, the number of individual Γ_γ accessible by means of the shape analysis method is more limited because of their larger mean level spacing and the increasing competition with the experimental resolution. Two radiation width values were obtained for the $n+^{180}\text{Hf}$ nuclear system, and three values for $n+^{174}\text{Hf}$, $n+^{176}\text{Hf}$ and $n+^{178}\text{Hf}$. The average radiation widths $\langle\Gamma_\gamma\rangle$ obtained in this work are compared in Table 6 with results compiled in Refs. [39,40]. Agreement between the different values remains within the limit of the given uncertainties, excepted in the case of the compound system $n+^{179}\text{Hf}$.

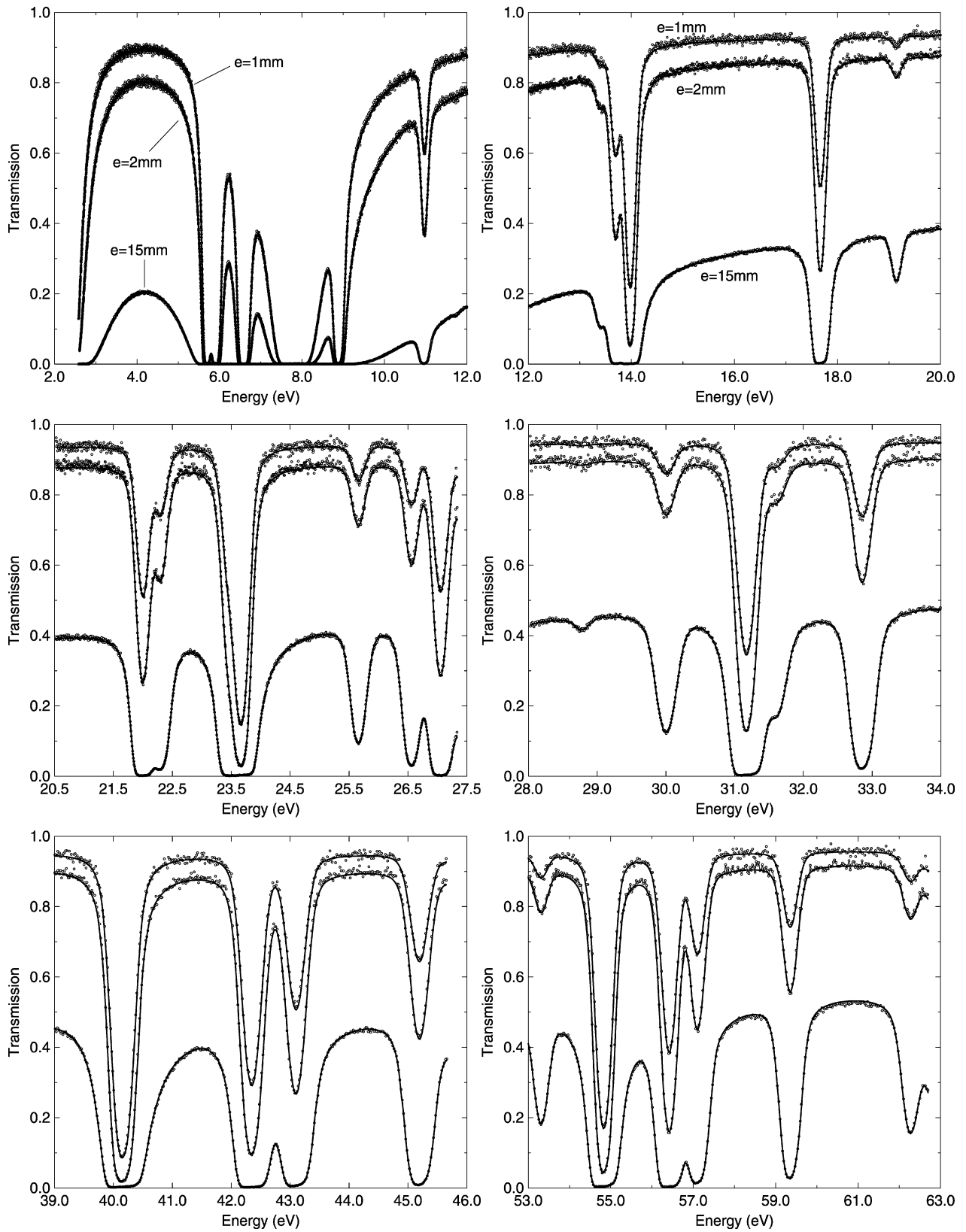


Fig. 5. Examples of theoretical curves adjusted with the REFIT code on the transmission data measured at the Doppler station of the GELINA facility ($T = 300\text{ K}$).

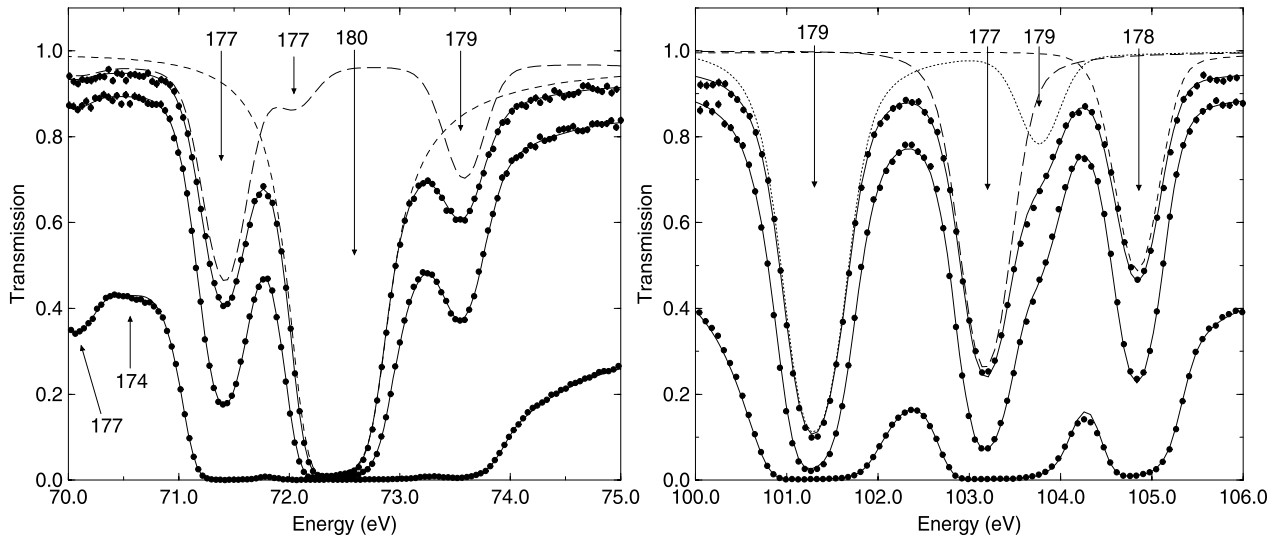


Fig. 6. Examples of multiplets of overlapping resonances around 72 eV and 103 eV. The label numbers denote the mass number of the target nucleus.

Table 3

Resonance parameters for the even/even hafnium isotopes obtained below 1 keV.

Energy (eV)	J^π	This work		JEFF-3.1.1	
		Γ_γ (meV)	Γ_n (meV)	Γ_γ (meV)	Γ_n (meV)
Nuclear system n+ ¹⁷⁴ Hf					
4.06 ± 0.04	1/2 ⁺	52.0	0.015	52.0	0.015
13.38 ± 0.02	1/2 ⁺	54.4 ± 2.6	3.7 ± 0.1	65.0	5.7
29.98 ± 0.05	1/2 ⁺	58.7 ± 3.5	31.6 ± 0.2	65.0	36.3
70.53 ± 0.11	1/2 ⁺	59.2	10.2 ± 0.4	65.0	24.0
77.81 ± 0.12	1/2 ⁺	71.6 ± 9.4	68.6 ± 1.2	51.0	83.0
106.97 ± 0.17	1/2 ⁺	59.2	90.4 ± 1.3	65.0	117.0
124.6	1/2 ⁺			65.0	680.0
147.69 ± 0.23	1/2 ⁺	59.2	116.5 ± 5.0	102.0	358.0
153.42 ± 0.23	1/2 ⁺	59.2	219.0 ± 17.0	65.0	219.0
211.56 ± 0.33	1/2 ⁺	59.2	112.3 ± 5.2	60.0	180.0
Nuclear system n+ ¹⁷⁶ Hf					
7.89 ± 0.01	1/2 ⁺	61.8	10.1	61.8	10.1
48.24 ± 0.07	1/2 ⁺	51.2 ± 4.3	108.5 ± 1.7	49.0	107.0
53.27 ± 0.08	1/2 ⁺	50.7 ± 6.7	1.4 ± 0.1	55.0	1.7
67.23 ± 0.10	1/2 ⁺	55.2	26.0 ± 0.6	55.0	26.0
124.05 ± 0.19	1/2 ⁺	57.0 ± 2.7	45.9 ± 2.4	55.0	32.0
177.15	1/2 ⁺			55.0	86.0
201.72 ± 0.32	1/2 ⁺	55.2	33.4 ± 2.8	51.0	39.0
243.53 ± 0.38	1/2 ⁺	55.2	18.5 ± 2.0	51.0	22.0
255.02 ± 0.39	1/2 ⁺	55.2	95.0	51.0	95.0
286.79 ± 0.45	1/2 ⁺	55.2	216.2 ± 4.6	51.0	285.0
304.62 ± 0.48	1/2 ⁺	55.2	17.3 ± 0.4	51.0	21.0
347.21 ± 0.54	1/2 ⁺	55.2	167.0 ± 4.1	51.0	173.0
435.66 ± 0.67	1/2 ⁺	55.2	167.0	51.0	167.0
444.12 ± 0.72	1/2 ⁺	55.2	122.7 ± 44.6	51.0	173.0
557.13 ± 0.86	1/2 ⁺	55.2	335.0	51.0	335.0
626.13 ± 0.97	1/2 ⁺	55.2	512.0 ± 154.1	51.0	640.0
659.37 ± 1.02	1/2 ⁺	55.2	58.2 ± 3.5	51.0	270.0
873.03 ± 1.35	1/2 ⁺	55.2	236.9 ± 15.5	51.0	280.0

Table 3 (continued)

Energy (eV)	J^π	This work		JEFF-3.1.1	
		Γ_γ (meV)	Γ_n (meV)	Γ_γ (meV)	Γ_n (meV)
928.15 ± 1.44	$1/2^+$	55.2	286.5 ± 17.6	51.0	145.0
958.87 ± 1.48	$1/2^+$	55.2	489.9 ± 10.2	51.0	300.0
994.04 ± 1.54	$1/2^+$	55.2	186.1 ± 10.7	51.0	270.0
1068.5 ± 1.65	$1/2^+$	55.2	449.5 ± 13.3	51.0	250.0
Nuclear system n+ ^{178}Hf					
7.79 ± 0.01	$1/2^+$	56.9 ± 0.6	49.7 ± 0.3	53.0	53.8
28.76 ± 0.05	$1/2^+$	54.6	$\simeq 0.009$		
104.86 ± 0.16	$1/2^+$	54.8 ± 4.1	8.3 ± 0.2	53.0	7.2
164.73 ± 0.25	$1/2^+$	54.6	13.5	53.0	13.5
255.36 ± 0.39	$1/2^+$	54.6	239.9 ± 2.4	45.0	220.0
275.09 ± 0.43	$1/2^+$	52.3 ± 8.9	225.5 ± 3.0	52.0	230.0
351.78 ± 0.55	$1/2^+$	54.6	9.2 ± 0.3	51.0	160.0
382.56 ± 0.60	$1/2^+$	54.6	442.5 ± 10.5	59.0	425.0
445.81 ± 0.70	$1/2^+$	54.6	137.8 ± 3.4	51.0	160.0
502.02 ± 0.78	$1/2^+$	54.6	66.5 ± 2.5	51.0	850.0
526.27 ± 0.82	$1/2^+$	54.6	223.6 ± 7.1	44.0	130.0
577.56 ± 0.89	$1/2^+$	54.6	360.0	54.0	360.0
604.88 ± 0.95	$1/2^+$	54.6	60.1 ± 2.1	51.0	15.0
720.16 ± 1.13	$1/2^+$	54.6	1138.9 ± 13.2	51.0	1050.0
780.74 ± 1.22	$1/2^+$	54.6	795.2 ± 12.4	49.0	1300.0
869.69 ± 1.35	$1/2^+$	54.6	285.1 ± 9.1	46.0	190.0
893.90 ± 1.38	$1/2^+$	54.6	68.6 ± 2.9	50.0	8.0
1090.0 ± 1.70	$1/2^+$	54.6	661.8 ± 15.7	47.0	550.0
1155.4 ± 1.81	$1/2^+$	54.6	1972.3 ± 20.2	51.0	1160.0
1180.1 ± 1.85	$1/2^+$	54.6	891.5 ± 20.9	51.0	190.0
Nuclear system n+ ^{180}Hf					
72.43 ± 0.11	$1/2^+$	34.7 ± 2.3	65.5 ± 0.9	28.9	63.3
171.92 ± 0.27	$1/2^+$	51.9 ± 16.8	118.1 ± 4.7	52.0	115.0
447.24 ± 0.70	$1/2^+$	43.3	204.4 ± 9.9	46.0	210.0
474.99 ± 0.74	$1/2^+$	43.3	161.0 ± 6.1	41.0	130.0
584.40 ± 0.91	$1/2^+$	43.3	69.6 ± 6.6	46.0	78.0
788.49 ± 1.23	$1/2^+$	43.3	2020.5 ± 13.1	51.0	1900.0
919.99 ± 1.43	$1/2^+$	43.3	85.4 ± 3.8	42.0	65.0
1169.8 ± 1.83	$1/2^+$	43.3	431.9 ± 13.5	51.0	680.0

5. Statistical analysis of the Reich–Moore parameters

Inherent difficulties in assessing unambiguous average resonance parameters from neutron spectroscopy measurements are not only the correct determination of the s -wave parameters but also the generalization of the obtained results to higher order partial waves ($l = 1, 2, 3, \dots$). These difficulties can be partially solved with a sequential (and iterative) analysis of the low and high neutron energy ranges. The consistency of the final results depends mainly of the quality of the experimental data available in the unresolved resonance range, and of the choice of the optical model parameters established for the nuclei involved in the nuclear reactions of interest.

In the present work, we decided to focus our attention on the links between the average resonance parameters of the hafnium isotopes (i.e. neutron strength function S_l , mean level spacing D_l , distant level parameters R_l^∞) and the systematic behavior of the deformation parameters needed for coupled channel calculations.

Table 4
 ^{177}Hf resonance parameters obtained below 200 eV.

Energy (eV)	J^π	This work		JEFF-3.1.1	
		Γ_γ (meV)	Γ_n (meV)	Γ_γ (meV)	Γ_n (meV)
1.10	3.0 ⁻			65.2	2.2
2.39 ± 0.01	4.0 ⁻	60.7	8.0	60.7	8.0
5.90 ± 0.01	3.0 ⁻	64.0 ± 1.2	5.4 ± 0.1	62.0	5.3
6.58 ± 0.01	4.0 ⁻	54.5 ± 2.0	8.6 ± 0.2	55.6	8.2
8.88 ± 0.01	4.0 ⁻	60.7 ± 1.3	5.8 ± 0.1	57.3	5.9
10.96 ± 0.02	3.0 ⁻	62.2 ± 2.1	0.5 ± 0.1	57.0	0.5
11.74 ± 0.02	3.0 ⁻	58.9	~ 0.005		
13.68 ± 0.02	4.0 ⁻	60.7 ± 2.4	0.6 ± 0.1	57.0	0.6
13.97 ± 0.02	3.0 ⁻	63.7 ± 1.0	3.0 ± 0.1	57.0	2.7
21.99 ± 0.03	4.0 ⁻	55.1 ± 2.0	1.8 ± 0.1	57.0	1.8
22.29 ± 0.03	3.0 ⁻	64.8 ± 3.2	0.8 ± 0.1	57.0	0.8
23.43 ± 0.04	4.0 ⁻	52.5 ± 1.4	1.2 ± 0.1	57.0	1.3
25.64 ± 0.04	3.0 ⁻	60.6 ± 3.6	0.5 ± 0.1	57.0	0.5
27.04 ± 0.04	3.0 ⁻	60.4 ± 4.6	3.0 ± 0.1	57.0	2.8
31.60 ± 0.05	3.0 ⁻	58.9	0.3 ± 0.1	57.0	0.4
32.84 ± 0.05	4.0 ⁻	58.5 ± 3.2	1.3 ± 0.1	57.0	1.3
36.10 ± 0.06	3.0 ⁻	49.9 ± 4.5	3.2 ± 0.1	57.0	3.5
36.97 ± 0.06	4.0 ⁻	58.6 ± 3.2	9.6 ± 0.1	57.0	8.9
43.07 ± 0.07	4.0 ⁻	65.2 ± 2.5	5.0 ± 0.1	57.0	5.1
45.16 ± 0.07	4.0 ⁻	57.6 ± 4.0	3.2 ± 0.1	57.0	3.4
46.26 ± 0.07	4.0 ⁻	58.9	7.0	57.0	7.0
48.84 ± 0.08	3.0 ⁻	63.1 ± 4.4	40.6 ± 0.6	57.0	36.0
49.61 ± 0.08	4.0 ⁻	53.8 ± 4.5	5.9 ± 0.1	57.0	5.9
54.79 ± 0.09	4.0 ⁻	50.4 ± 1.7	21.0 ± 0.4	57.0	20.6
56.38 ± 0.09	3.0 ⁻	62.6 ± 2.4	14.4 ± 0.2	57.0	14.2
57.06 ± 0.09	4.0 ⁻	62.0 ± 4.7	4.2 ± 0.1	57.0	4.2
59.31 ± 0.09	3.0 ⁻	70.4 ± 4.6	4.2 ± 0.1	57.0	4.2
62.22 ± 0.09	3.0 ⁻	58.9	1.4 ± 0.1	57.0	1.6
63.56 ± 0.10	4.0 ⁻	54.3	70.2	54.3	70.2
66.78 ± 0.10	3.0 ⁻	58.9	41.6 ± 4.2	119.0	41.6
70.06 ± 0.11	4.0 ⁻	58.9	0.4 ± 0.1	57.0	0.7
71.41 ± 0.11	4.0 ⁻	53.5 ± 4.6	13.8 ± 0.2	57.0	14.1
72.26 ± 0.11	3.0 ⁻	58.9	1.7 ± 0.3	72.0	2.2
75.71 ± 0.12	3.0 ⁻	58.9	2.8 ± 0.1	57.0	2.9
76.11 ± 0.12	4.0 ⁻	57.3 ± 7.0	15.6 ± 0.2	57.0	15.0
82.42 ± 0.13	4.0 ⁻	58.9	0.4 ± 0.1	57.0	0.6
84.78 ± 0.13	4.0 ⁻	58.9	23.5	57.0	23.5
85.26 ± 0.13	3.0 ⁻	58.9	0.4	57.0	0.4
86.84 ± 0.14	4.0 ⁻	58.9	1.0 ± 0.1	57.0	1.1
88.65 ± 0.14	3.0 ⁻	58.9	5.4 ± 0.1	57.0	4.6
93.25 ± 0.15	3.0 ⁻	58.9	5.1 ± 0.1	57.0	4.7
97.17 ± 0.15	4.0 ⁻	56.4 ± 4.0	19.7 ± 0.5	98.0	17.4
99.13 ± 0.15	4.0 ⁻	58.9	0.9 ± 0.1		
103.19 ± 0.16	3.0 ⁻	58.9	59.1 ± 0.6	57.0	59.0
111.62 ± 0.17	3.0 ⁻	58.9	2.4 ± 0.1	57.0	2.3
112.01 ± 0.17	4.0 ⁻	58.9	3.9 ± 0.1	57.0	4.1
115.23 ± 0.18	4.0 ⁻	58.9	3.8 ± 0.1	57.0	4.1
121.34 ± 0.19	3.0 ⁻	58.9	4.4 ± 0.1	57.0	4.2
122.10	3.0 ⁻			57.0	2.5
122.18	3.0 ⁻			57.0	0.5

Table 4 (continued)

Energy (eV)	J^π	This work		JEFF-3.1.1	
		Γ_γ (meV)	Γ_n (meV)	Γ_γ (meV)	Γ_n (meV)
123.86 ± 0.19	3.0 ⁻	58.9	11.2 ± 1.4	57.0	8.0
126.38 ± 0.20	4.0 ⁻	58.9	0.8	57.0	0.8
131.77 ± 0.21	3.0 ⁻	56.7 ± 5.1	63.1 ± 1.5	67.0	59.0
134.22 ± 0.21	4.0 ⁻	58.9	3.7 ± 0.1	57.0	4.2
136.38 ± 0.21	3.0 ⁻	58.9	0.6 ± 0.1	57.0	1.7
138.09 ± 0.21	4.0 ⁻	58.9	10.0 ± 0.6	57.0	16.2
141.28 ± 0.22	4.0 ⁻	58.9	22.2 ± 0.4	57.0	21.1
143.23 ± 0.23	3.0 ⁻	58.9	3.8 ± 0.2	57.0	3.7
143.90 ± 0.23	4.0 ⁻	58.9	14.3 ± 0.3	57.0	9.5
145.72 ± 0.23	3.0 ⁻	58.9	7.2 ± 0.1	57.0	7.6
148.70 ± 0.23	3.0 ⁻	58.9	21.1 ± 0.4	57.0	21.0
151.21 ± 0.23	4.0 ⁻	58.9	0.2 ± 0.1	57.0	0.7
152.69 ± 0.24	4.0 ⁻	58.9	3.8	57.0	3.8
154.90 ± 0.24	3.0 ⁻	58.9	1.5	57.0	1.5
160.17 ± 0.25	4.0 ⁻	58.9	3.3 ± 0.1	57.0	3.9
163.20 ± 0.26	3.0 ⁻	58.9	47.1 ± 1.0	57.0	45.8
167.52 ± 0.26	3.0 ⁻	58.9	8.0 ± 0.2	57.0	9.3
171.25 ± 0.26	3.0 ⁻	58.9	14.0 ± 1.0	57.0	10.0
174.36 ± 0.27	4.0 ⁻	58.9	55.0 ± 0.5	57.0	27.0
176.28 ± 0.28	3.0 ⁻	58.9	58.2 ± 0.8	57.0	45.0
177.07 ± 0.28	4.0 ⁻	58.9	43.1 ± 0.4	57.0	9.0
179.31	4.0 ⁻			57.0	0.5
181.27 ± 0.28	4.0 ⁻	58.9	4.8 ± 0.1	57.0	5.6
184.85 ± 0.29	4.0 ⁻	58.9	1.1 ± 0.1	57.0	1.7
188.45 ± 0.29	4.0 ⁻	58.9	1.8	57.0	1.8
193.03 ± 0.30	4.0 ⁻	58.9	15.0	57.0	15.0
194.30 ± 0.30	3.0 ⁻	58.9	8.4 ± 0.3	57.0	9.8
199.39 ± 0.31	4.0 ⁻	58.9	19.7 ± 0.9	57.0	21.0
202.03 ± 0.31	4.0 ⁻	58.9	14.9 ± 1.2	65.0	19.2

Table 5

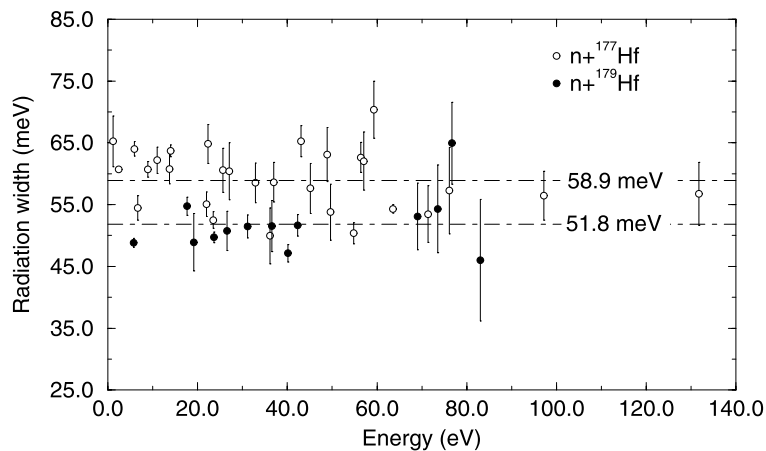
¹⁷⁹Hf resonance parameters below 200 eV.

Energy (eV)	J^π	This work		JEFF-3.1.1	
		Γ_γ (meV)	Γ_n (meV)	Γ_γ (meV)	Γ_n (meV)
5.69 ± 0.01	5.0 ⁺	48.8 ± 0.7	4.3 ± 0.1	47.0	4.3
17.66 ± 0.03	4.0 ⁺	54.7 ± 1.5	2.2 ± 0.1	52.0	2.1
19.13 ± 0.03	5.0 ⁺	48.9 ± 4.6	0.1 ± 0.1	52.0	0.1
23.66 ± 0.04	5.0 ⁺	49.7 ± 0.9	8.6 ± 0.1	52.0	7.5
26.54 ± 0.04	4.0 ⁺	50.7 ± 3.2	1.2 ± 0.1	52.0	1.3
27.42 ± 0.04	5.0 ⁺	51.8	0.4	52.0	0.4
31.16 ± 0.05	4.0 ⁺	51.5 ± 1.8	8.5 ± 0.1	52.0	8.1
36.51 ± 0.06	5.0 ⁺	51.5 ± 4.1	28.7 ± 0.4	52.0	26.0
40.13 ± 0.06	5.0 ⁺	47.1 ± 1.4	26.3 ± 0.4	61.0	23.5
42.32 ± 0.07	4.0 ⁺	51.6 ± 1.7	15.9 ± 0.2	52.0	15.3
50.79 ± 0.08	5.0 ⁺	51.8	1.1 ± 0.1	52.0	1.1
51.14 ± 0.08	4.0 ⁺	51.8	0.6 ± 0.1	52.0	0.7
54.08	4.0 ⁺			52.0	0.3
69.07 ± 0.11	4.0 ⁺	53.1 ± 5.4	10.7 ± 0.2	52.0	10.6
73.57 ± 0.12	4.0 ⁺	54.3 ± 7.1	9.5 ± 0.1	52.0	9.2

(continued on next page)

Table 5 (continued)

Energy (eV)	J^π	This work		JEFF-3.1.1	
		Γ_γ (meV)	Γ_n (meV)	Γ_γ (meV)	Γ_n (meV)
76.68 ± 0.12	5.0 ⁺	64.9 ± 6.6	3.3 ± 0.1	52.0	3.3
83.00 ± 0.13	4.0 ⁺	46.0 ± 9.8	4.5 ± 0.1	52.0	4.7
85.43 ± 0.13	4.0 ⁺	51.8	11.5 ± 0.4	52.0	11.8
92.12 ± 0.14	4.0 ⁺	51.8	11.1 ± 0.2	52.0	11.7
92.74 ± 0.15	5.0 ⁺	51.8	28.4 ± 0.5	52.0	27.0
101.32 ± 0.16	5.0 ⁺	51.8	116.9 ± 1.4	52.0	113.8
103.77 ± 0.16	5.0 ⁺	51.8	10.2 ± 0.2	52.0	9.8
107.85 ± 0.17	4.0 ⁺	51.8	11.7 ± 0.4	52.0	9.5
117.23 ± 0.18	5.0 ⁺	51.8	34.5 ± 0.8	44.0	31.0
120.33 ± 0.19	4.0 ⁺	51.8	3.5	52.0	3.5
121.96 ± 0.19	4.0 ⁺	51.8	7.6 ± 0.1	52.0	3.7
122.63 ± 0.19	5.0 ⁺	51.8	17.1 ± 0.3	52.0	15.8
130.01 ± 0.20	4.0 ⁺	51.8	9.4 ± 0.2	52.0	10.2
137.36 ± 0.21	5.0 ⁺	51.8	32.9 ± 0.7	52.0	36.6
144.31 ± 0.23	5.0 ⁺	51.8	25.2 ± 0.8	52.0	32.0
147.07 ± 0.23	4.0 ⁺	51.8	14.3 ± 0.3	52.0	15.2
156.29 ± 0.24	5.0 ⁺	51.8	47.4 ± 1.2	58.0	45.0
158.82 ± 0.25	4.0 ⁺	51.8	3.4 ± 0.2	52.0	4.7
165.74 ± 0.26	5.0 ⁺	51.8	23.6 ± 0.7	52.0	23.7
174.98 ± 0.27	4.0 ⁺	51.8	31.2 ± 0.7	52.0	77.0
177.89 ± 0.28	5.0 ⁺	51.8	61.2 ± 1.4	52.0	66.0
182.69 ± 0.29	4.0 ⁺	51.8	33.6 ± 1.0	52.0	32.8
188.72 ± 0.29	4.0 ⁺	51.8	6.1	52.0	6.1
189.86 ± 0.30	5.0 ⁺	51.8	22.3 ± 0.8	52.0	20.2
191.25	4.0 ⁺			52.0	0.9
198.00 ± 0.31	5.0 ⁺	51.8	14.0 ± 0.4	52.0	16.1
202.67 ± 0.32	5.0 ⁺	51.8	61.7 ± 3.8	66.0	81.8

Fig. 7. Individual ^{177}Hf and ^{179}Hf radiation widths obtained in this work.

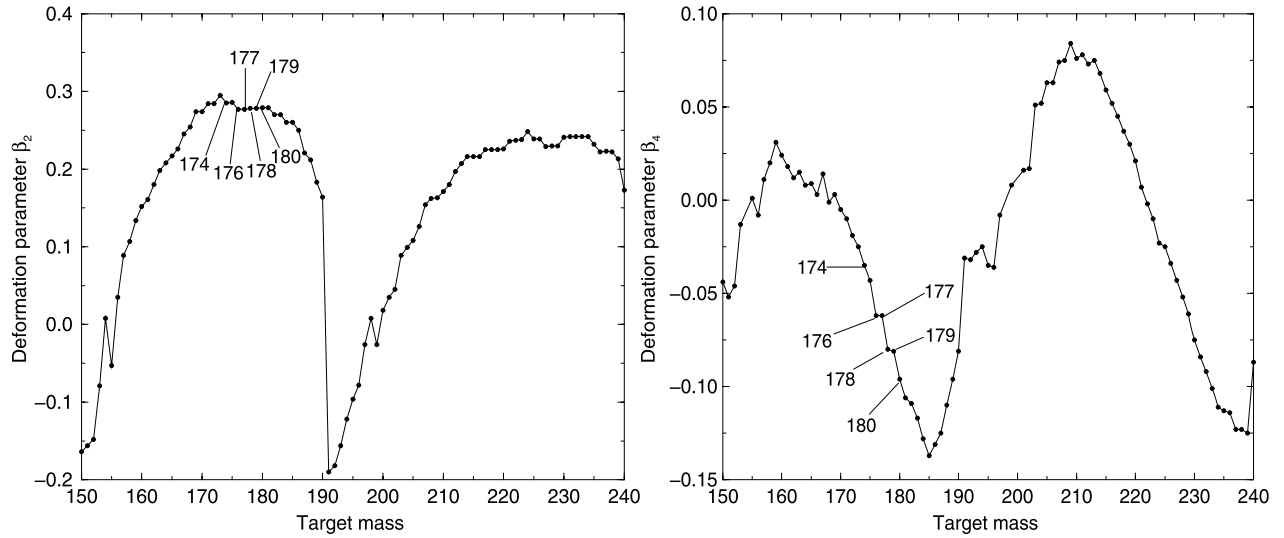
5.1. The ESTIMA and SPRT methods

For modeling neutron induced reactions on the deformed hafnium nuclei, the coupled-channels model of the ECIS code was used with optical model parameters retrieve from the RIPL-2 database [40]. Some inconclusive calculations performed with phenomenological poten-

Table 6

Average radiation widths for the nuclear systems of interest for this work.

Nuclear systems	Mughabghab [39]	RIPL-2 [40]	This work
n+ ¹⁷⁴ Hf	60.0 ± 1.0 meV		59.2 ± 3.4 meV
n+ ¹⁷⁶ Hf	59.0 ± 3.0 meV	60.0 ± 10.0 meV	55.2 ± 2.5 meV
n+ ¹⁷⁷ Hf	65.0 ± 5.0 meV	66.0 ± 10.0 meV	58.9 ± 2.3 meV
n+ ¹⁷⁸ Hf	53.0 ± 1.5 meV	54.0 ± 5.0 meV	54.6 ± 3.9 meV
n+ ¹⁷⁹ Hf	62.0 ± 6.0 meV	66.0 ± 5.0 meV	51.8 ± 3.1 meV
n+ ¹⁸⁰ Hf	50.0 ± 5.0 meV	50.0 ± 5.0 meV	43.3 ± 8.2 meV

Fig. 8. Systematic behavior of the β_2 and β_4 deformation parameters retrieve from the Moller and Nix data base [41].

tial established in the mid 80s lead us to choose the more recent dispersive and global optical model of Morillon et al. [12,13] established for target mass ranging from $A = 24$ to 209.

For the deformation parameters, prior β_2 and β_4 values were retrieved from the Moller and Nix data base [41]. As shown in Fig. 8, values of β_2 for the ^{174,176,177,178,179,180}Hf isotopes are close to 0.27. Therefore, β_2 has to be considered as a free parameter under the condition to get a nearly constant final value for all the stable hafnium isotopes. This condition was achieved by using phenomenological relationships between the deformation parameters and the s -wave neutron strength functions provided by the ESTIMA and SPRT methods.

Relationships between these model parameters for neutron orbital angular momentum $l = 0, 1$ were firstly given through the low energy approximation of the SPRT approach [42]. Its generalization was recently derived from the real and imaginary parts of the collision matrix elements calculated by ECIS [18]. For deformed nuclei, the l -dependent neutron strength function S_l and distant level parameter R_l^∞ at the binding energy can be formally expressed as a function of the channel radius a_c and of the deformation parameters β_i ($i = 2, 4$):

$$S_l = \lim_{E \rightarrow 0} S_l(E, a_c, \beta_i) \quad (6)$$

$$R_l^\infty = \lim_{E \rightarrow 0} R_l^\infty(E, a_c, \beta_i) \quad (7)$$

According to the rules used in the Evaluated Nuclear Data Files [43], a reasonable choice for the channel radius a_c is:

$$a_c = 1.23 \left(\frac{A}{m_n} \right)^{1/3} + 0.8 \quad \text{in fm} \quad (8)$$

For s -wave channel, the relationship between the potential scattering length, the distant level parameters and the channel radius is explicitly defined as:

$$R' = a_c (1 - R_0^\infty) \quad (9)$$

In absence of resonances, equivalent expressions are obtained with the low energy approximation of the Reich–Moore and Multi-Level Breit–Wigner formalisms. Therefore, distant level parameters reported in this work can be used to describe the contribution of the direct interaction in the resolved resonance range.

The generalized SPRT method provides l dependent model parameters that can be directly compared with those deduced from the statistical ESTIMA analysis of the resolved resonance parameters [17]. The latter analysis is routinely used within the low neutron energy spectroscopy community [44,45] to suggest the neutron strength function S_0 and mean level spacing D_0 from a confident s -wave resonance sample by taking into account experimentally missed small resonances.

The determination of the s -wave average parameters is sensitive to the contamination of p -wave resonances. The quantity usually measured in capture or transmission measurements is the product of the statistical spin factor g_J with the neutron width Γ_n . Therefore, the posterior probability that a resonance with a given $g_J \Gamma_n$ value is a p -wave resonance can be formally expressed as follow:

$$P(l = 1 | g_J \Gamma_n) \propto P(g_J \Gamma_n | l = 1) P(l = 1) \quad (10)$$

In which $P(l = 1)$ stands for the probability that a resonance is a p -wave resonance. Such a probabilistic method fails to provide unique l assignments since there is an overlap between the weak s -wave and the strong p -wave resonances. A confident sample of s -wave resonances is suggested according to a threshold probability $P(l = 1 | g_J \Gamma_n) > P_B$. Below P_B , the s - and p -wave probability become indistinctive. Within the ESTIMA method, the P_B threshold is chosen to minimize the discrepancies between the experimental and calculated integral of the Porter–Thomas reduced neutron width distribution $P(x)$:

$$N(x_0) = N \int_{x_0}^{\infty} P(x) dx = N \operatorname{erfc} \left(\sqrt{\frac{x_0}{2}} \right) \quad (11)$$

with

$$x = \frac{g_J \Gamma_n^0}{\langle g_J \Gamma_n^0 \rangle} \quad (12)$$

Expression $N(x_0)$ stands for the number of s -wave resonances having $x > x_0$ in which N and $\langle g_J \Gamma_n^0 \rangle$ are free parameters. They represent respectively the estimated number of resonances for $x_0 = 0$ and the average value of the s -wave reduced neutron width. The s -wave mean level spacing D_0 and neutron strength function S_0 are calculated as follows:

$$D_0 = \frac{E_{max} - E_{min}}{N - 1} \quad (13)$$

$$S_0 = \frac{\langle g_J \Gamma_n^0 \rangle}{D_0} \quad (14)$$

In which E_{min} and E_{max} represent the lower and upper energy limits of the resolved resonance range under investigation.

Expressions (6), (7), (13) and (14) show the relationships that exist on the one hand between β_i ($i = 2, 4$), S_l and R_l^∞ via the generalized SPRT method, and on the other hand between S_0 and D_0 via the ESTIMA method. The combination of the two methods gives constraints for the determination of the deformation parameters (involved in the description of the direct interactions) and of the mean level spacing (involved in the statistical modeling of the compound nucleus reactions).

5.2. Deformation parameters

The magnitude of the deformation parameters β_2 and β_4 was deduced from the statistical analysis of the ^{177}Hf and ^{179}Hf resonance parameters. An iterative analysis was needed to adopt the coupling scheme and to establish consistent ESTIMA parameters such as P_B and E_{max} (Eq. (13)). Minima in the variance of the neutron strength functions were observed for $E_{max}(^{177}\text{Hf}) < 200$ eV and $E_{max}(^{179}\text{Hf}) < 300$ eV. The Bayesian formulation of the probability $P(l = 1 | g_J \Gamma_n)$ given in Eq. (10) suggests that all the levels measured below these energy limits are s -wave resonances. The ESTIMA results are shown in Fig. 9. The corresponding results are reported on the “staircase” plots of the s -wave reduced neutron widths and on the cumulative number of resonances. The slope of the curves yields respectively the s -wave neutron strength function S_0 and the level density $1/D_0$. Above E_{max} , we can observe a rapid increase of the number of missing resonances. At 500 eV, it represents approximately more than 40% of the observed levels.

The generalized expression of the SPRT method, given in Eqs. (6) and (7), were used to link the ESTIMA results and the deformation parameters. Fig. 10 illustrates the SPRT results for the $n+^{177}\text{Hf}$ and $n+^{179}\text{Hf}$ nuclear systems. By combining these results with the systematic behavior shown in Fig. 8, we were able to optimize a consistent set of β_2 and β_4 parameters accordingly to prior values proposed by Avrigeanu et al. [14,15]. Our study suggests to normalize the β_2 and β_4 parameters of Moller and Nix with correction factors of 0.86 ± 0.11 and 0.42 ± 0.06 respectively. Final model parameters are listed in Table 7. Values of the $^{177,179}\text{Hf}$ neutron strength functions ($10^4 S_0 = 2.48$ and $10^4 S_0 = 2.15$) are consistent with those reported in Fig. 9 ($10^4 S_0 = 2.51$ and $10^4 S_0 = 2.11$). The given uncertainties are dominated by the accuracy of the statistical formalism used within the ESTIMA approach. The simultaneous analysis of the integral formulation of the Porter–Thomas distribution (Eq. (11)) with the “staircase” plot of the reduced neutron width could reduce the relative uncertainty of each parameter down to 10%. This improved ESTIMA approach is under study in the frame of the CONRAD code.

Table 8 compares our neutron strength function and potential scattering length values with those compiled in Refs. [39,40]. If R' results are in reasonable agreement, the l -dependent neutron strength functions are characterized by larger discrepancies. For $l = 0$, an excellent agreement is observed for $n+^{177}\text{Hf}$, $n+^{178}\text{Hf}$ and $n+^{180}\text{Hf}$, while results proposed by Mughabghab for S_2 are systematically lower. The order of magnitude of our results was verified with optical model parameters as used in Ref. [15]. The generalized SPRT method leads to d -wave strength function close to 3.0×10^{-4} and distant level parameters compatible with those reported in Table 7.

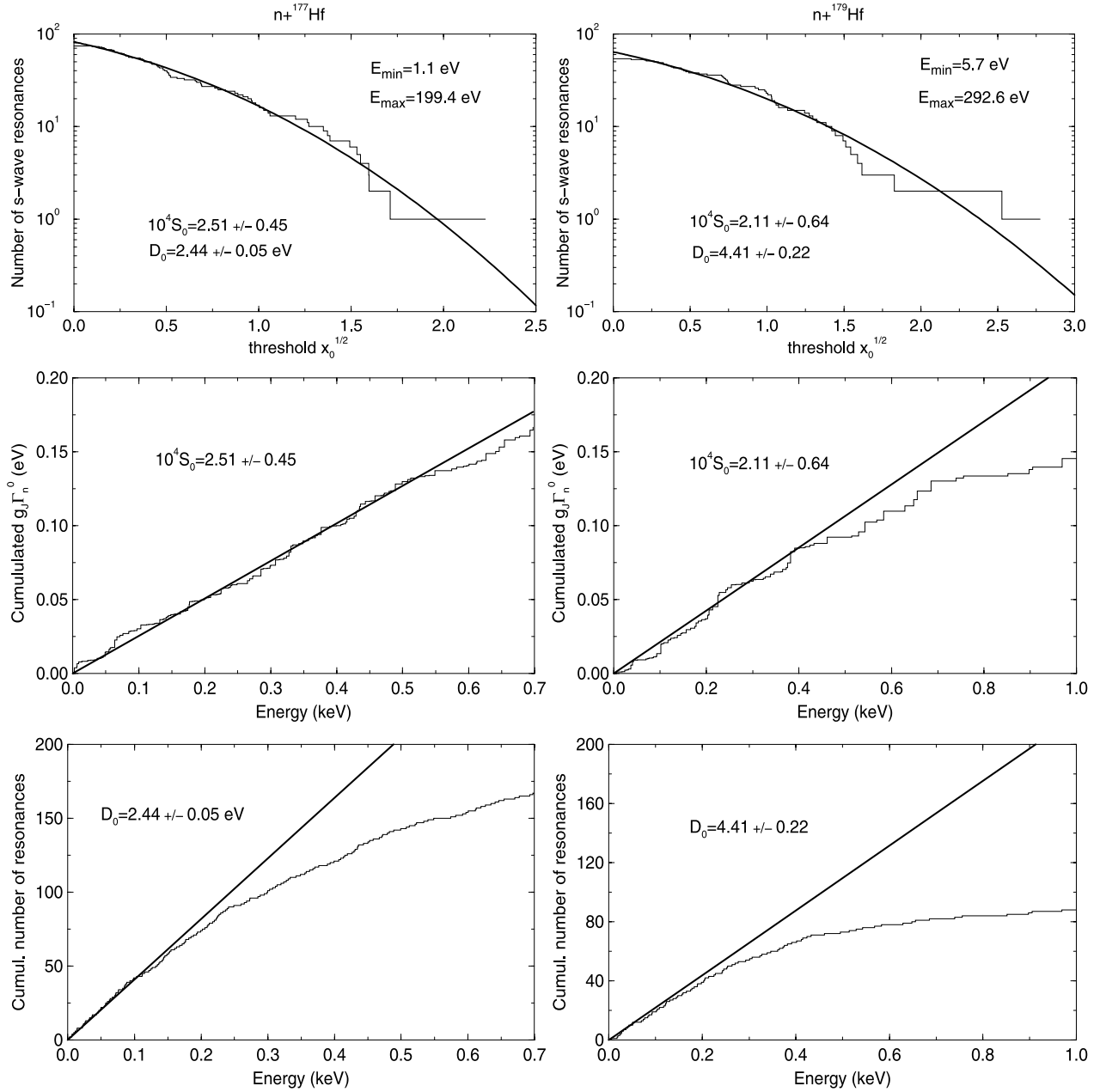


Fig. 9. Comparison of the $^{177,179}\text{Hf}$ ESTIMA results with the Porter–Thomas integral distributions (top plots), the staircase plots of the s -wave reduced neutron widths (middle plots) and the cumulative number of s -wave resonances (bottom plots). E_{\min} and E_{\max} stand for the lower and upper limit of the energy range within which the average resonance parameters have been obtained (see Eq. (13)).

5.3. s -wave mean level spacing

For the compound systems $n+^{177}\text{Hf}$ and $n+^{179}\text{Hf}$, D_0 values have been estimated with the ESTIMA method (see Section 5.2). Results are reported in Fig. 9. For the even/even hafnium isotopes, ESTIMA parameters were fine tuning in order to converge to S_0 values consistent with results reported in Table 7. This methodology was successfully applied on our ^{174}Hf and ^{178}Hf resonance parameters. ESTIMA analysis suggested that all the levels observed below 200 eV and 1 keV respectively are s -wave resonances. For $n+^{180}\text{Hf}$, the statistical analysis was performed up to 5 keV with a Bayesian criteria $P(l=1|g_J \Gamma_n) > 0.5$. Among the 57 observed levels, ESTIMA suggested that 31 resonances are s -wave and 26 resonances could be p -wave.

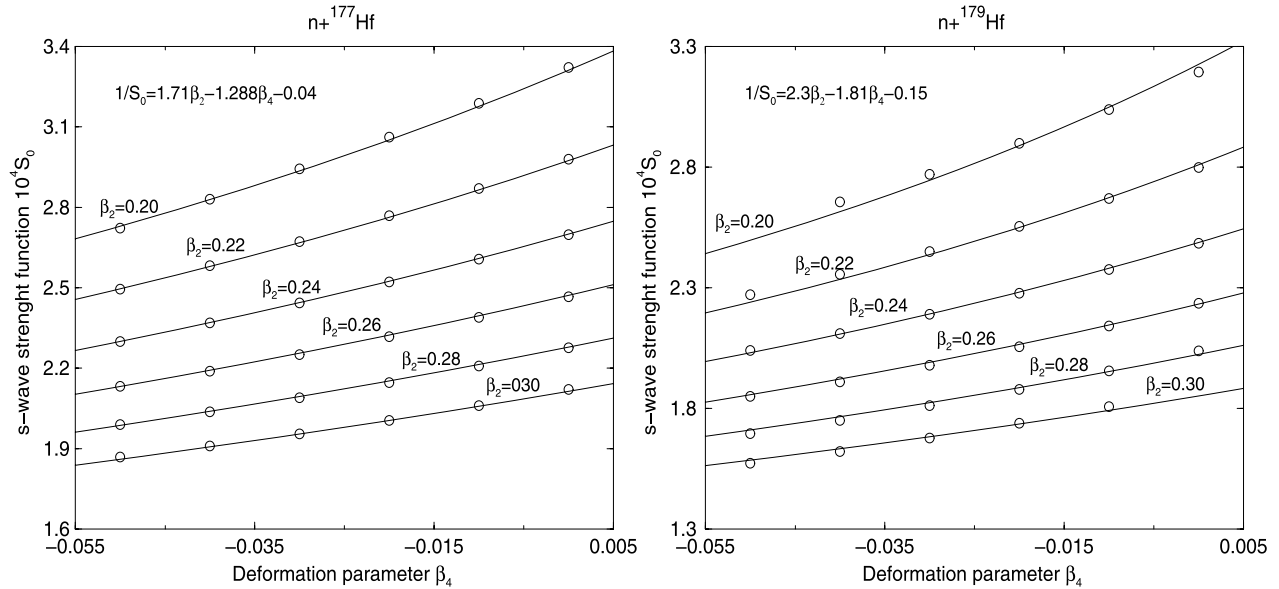


Fig. 10. Systematic behavior of the $^{177,179}\text{Hf}$ neutron strength functions with respect to the deformation parameters β_2 and β_4 .

The same methodology fails to provide a consistent set of D_0 and S_0 values for the compound system $n+^{176}\text{Hf}$. We tried to solve this difficulty by using the systematic behavior of the s -wave gamma-ray strength function S_γ . At low energy, the latter can be explicitly defined as follow:

$$S_\gamma = \frac{\langle \Gamma_\gamma \rangle}{D_0} \quad (15)$$

Assuming that only s -wave contributes, S_γ may alternatively be obtained by integrating the γ -ray transmission coefficients for multipolarity $E1$ over the density of final states (including discrete states) that may be reached in the first step of the γ -ray cascade. For $n+^{176}\text{Hf}$, we have:

$$S_\gamma \simeq N \int_0^{S_n} [\rho_{1/2-}(S_n - E_\gamma) + \rho_{3/2-}(S_n - E_\gamma)] f_{E1}(E_\gamma) E_\gamma^3 dE_\gamma, \quad (16)$$

in which f_{E1} stands for the energy-dependent spectral factor for $E1$ transition and N represents a normalization factor. In the present work, the latter factor was deduced from the S_γ values of the $n+^{174,178,180}\text{Hf}$ compound systems by calculating the giant dipole resonance shape f_{E1} with the standard Brink–Axel Lorentzian form [47,48] and with the incoherent sum of two generalized Lorentzian terms as proposed by Kopecky and Uhl [49]. Results given in Fig. 11 were produced without introducing in the calculations systematic uncertainties on the giant dipole resonance parameters. The least squares fit of our experimental values with the Kopecky–Uhl and Brink–Axel shapes provided a γ -ray strength function for the compound system $n+^{176}\text{Hf}$ equal to $10^{-4} S_\gamma = 16.3 \pm 0.9$. The quoted uncertainty is mainly due to the discrepancy observed between the Brink–Axel and Kopecky–Uhl models. The latter discrepancy ranges from 2% for $n+^{180}\text{Hf}$ to 8% for $n+^{174}\text{Hf}$. By combining this S_γ result with the $n+^{176}\text{Hf}$ average radiation width reported in Table 6, we obtained a s -wave mean level $D_0 = 33.9 \pm 2.4$ eV.

Results obtained for the s -wave mean level spacing of interest for this work are summarized in Table 9. For the $n+^{174}\text{Hf}$, $n+^{178}\text{Hf}$ and $n+^{180}\text{Hf}$ nuclear systems, the agreement between the D_0 values obtained with the ESTIMA method (by fine tuning to the S_0 value, see Table 7) and

Table 7

Model parameters established with the SPRT analysis: β_i ($i = 2, 4$) stand for the deformation parameters, S_l ($l = 0, \dots, 3$) are the neutron strength functions, R_l^∞ ($l = 0, \dots, 3$) represent the distant level parameters, R' is the potential scattering length and a_c is the so-called channel radius.

	n+ ¹⁷⁴ Hf	n+ ¹⁷⁶ Hf	n+ ¹⁷⁷ Hf	n+ ¹⁷⁸ Hf	n+ ¹⁷⁹ Hf	n+ ¹⁸⁰ Hf
β_2	0.246 ± 0.033	0.239 ± 0.032	0.239 ± 0.032	0.240 ± 0.032	0.240 ± 0.032	0.241 ± 0.033
β_4	-0.0149 ± 0.0021	-0.0264 ± 0.0038	-0.0264 ± 0.0038	-0.0340 ± 0.0049	-0.0344 ± 0.0050	-0.0408 ± 0.0059
$10^4 S_0$	2.18 ± 0.38	2.09 ± 0.38	2.48 ± 0.35	2.20 ± 0.29	2.15 ± 0.38	1.93 ± 0.40
$10^4 S_1$	1.17 ± 0.54	1.01 ± 0.44	0.94 ± 0.38	0.93 ± 0.38	0.97 ± 0.44	0.95 ± 0.50
$10^4 S_2$	3.42 ± 0.35	3.42 ± 0.34	2.97 ± 0.36	3.08 ± 0.42	3.20 ± 0.38	3.01 ± 0.29
$10^4 S_3$	1.26 ± 0.43	1.12 ± 0.36	1.01 ± 0.62	1.05 ± 0.40	1.10 ± 0.44	1.05 ± 0.38
R_0^∞	-0.032	-0.020	0.042	-0.011	0.012	0.005
R_1^∞	0.068	0.076	0.074	0.093	0.084	0.098
R_2^∞	0.039	0.012	0.035	0.081	0.020	-0.027
R_3^∞	0.201	0.207	0.262	0.242	0.267	0.226
a_c (fm)	7.64	7.67	7.68	7.69	7.71	7.72
R' (fm)	7.89 ± 0.03	7.82 ± 0.02	7.36 ± 0.62	7.74 ± 0.04	7.61 ± 0.17	7.76 ± 0.02

Table 8
Comparison of the neutron strength functions and potential scattering length.

Nuclear systems	Parameters	Mughabghab [39]	RIPL-2 [40]	This work
n+ ¹⁷⁴ Hf	$10^4 S_0$	2.8 ± 1.8	2.6 ± 0.6	2.18 ± 0.38
	R' (fm)	7.5 ± 0.6		7.89 ± 0.03
n+ ¹⁷⁶ Hf	$10^4 S_0$	2.6 ± 0.3	1.7 ± 0.4	2.09 ± 0.38
	$10^4 S_1$	0.87 ± 0.07		1.01 ± 0.44
	$10^4 S_2$	2.0 ± 0.2		3.42 ± 0.34
	R' (fm)	7.6 ± 0.7		7.82 ± 0.02
n+ ¹⁷⁷ Hf	$10^4 S_0$	2.60 ± 0.25	2.6 ± 0.3	2.48 ± 0.35
	$10^4 S_1$	1.00 ± 0.05		0.94 ± 0.38
	$10^4 S_2$	2.10 ± 0.07		2.97 ± 0.36
n+ ¹⁷⁸ Hf	$10^4 S_0$	2.2 ± 0.7	2.1 ± 0.3	2.20 ± 0.29
	$10^4 S_1$	0.51 ± 0.03		0.93 ± 0.38
	$10^4 S_2$	1.66 ± 0.11		3.08 ± 0.42
	R' (fm)	7.5 ± 0.7		7.74 ± 0.04
n+ ¹⁷⁹ Hf	$10^4 S_0$	1.74 ± 0.18	2.5 ± 0.4	2.15 ± 0.38
	$10^4 S_1$	0.83 ± 0.10		0.97 ± 0.44
	$10^4 S_2$	2.10 ± 0.17		3.20 ± 0.38
n+ ¹⁸⁰ Hf	$10^4 S_0$	1.9 ± 0.6	1.9 ± 0.6	1.93 ± 0.40
	$10^4 S_1$	0.44 ± 0.05		0.95 ± 0.50
	$10^4 S_2$	1.8 ± 0.1		3.01 ± 0.29
	R' (fm)	8.0 ± 0.7		7.76 ± 0.02

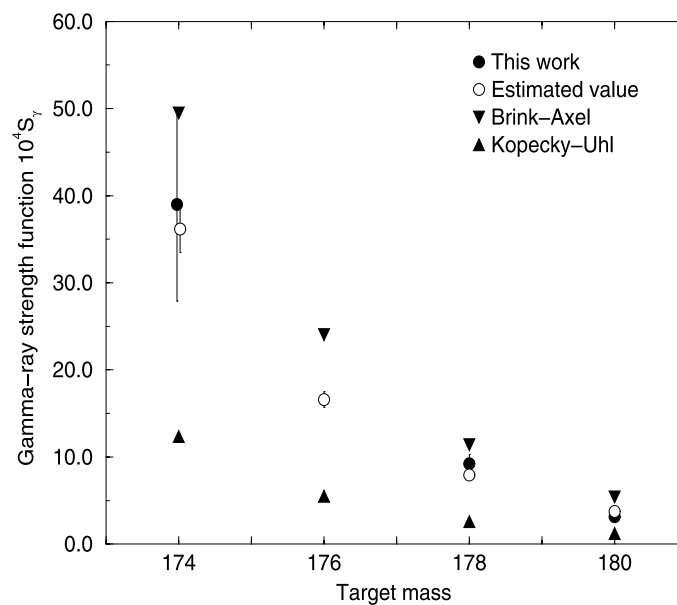


Fig. 11. Comparison of our experimental γ -ray strength functions with the systematic trends for the standard (Brink–Axel) and generalized (Kopecky–Uhl) Lorentzian shapes calculated with the TALYS code [20]. The estimated S_γ values were deduced from the normalized theoretical values (Brink–Axel and Kopecky–Uhl).

deduced from the γ -ray strength function (by using our $\langle \Gamma_\gamma \rangle$ results, see Table 6) remains within the limit of the uncertainties.

Fig. 12 compares the experimental trends (deduced from the resolved resonance range) with the theoretical curves (deduced from the systematics). As expected, the larger discrepancies can be observed on the “staircase” plots of the reduced neutron widths for the compound sys-

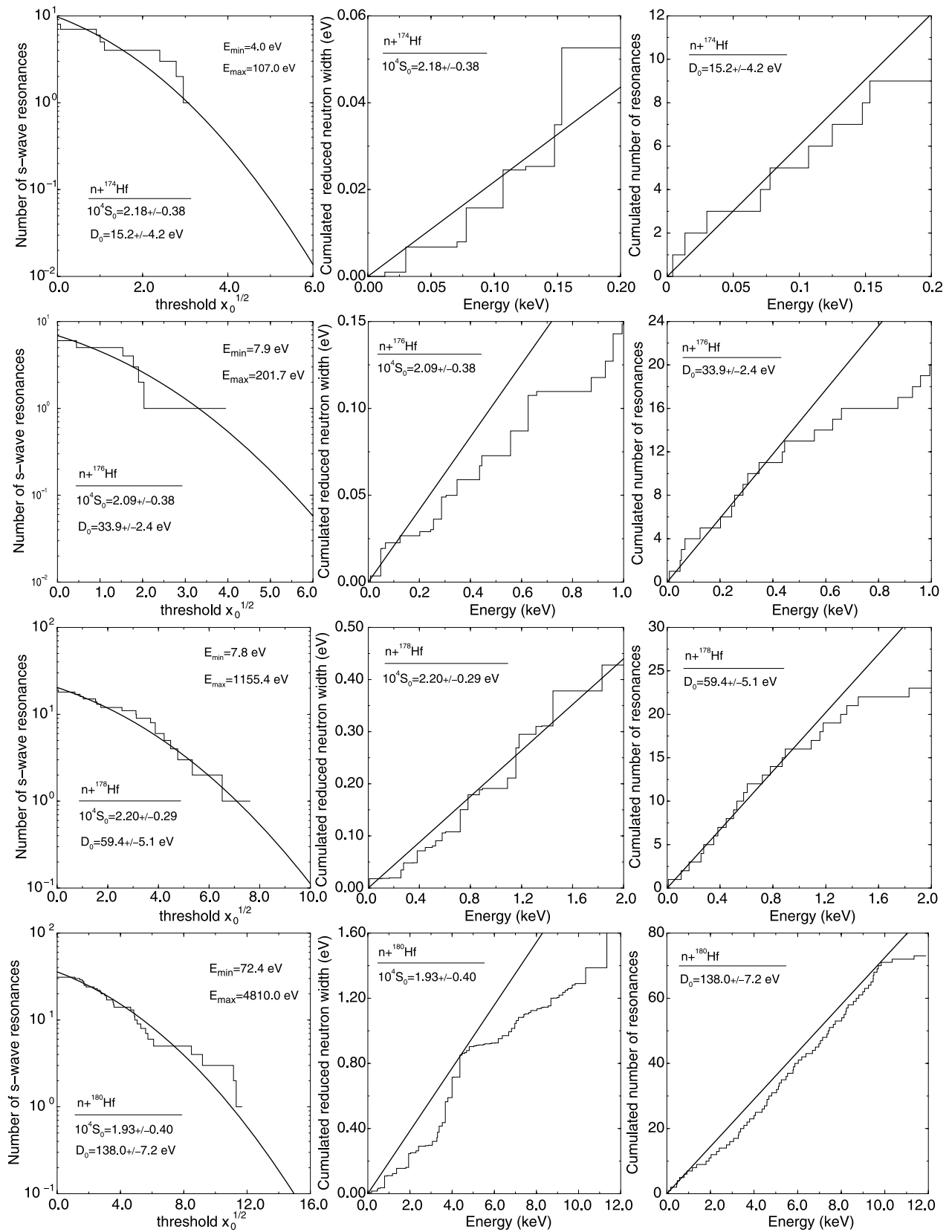


Fig. 12. Comparison of the $^{174,176,178,179}\text{Hf}$ ESTIMA results with the Porter–Thomas integral distributions (left hand plots), the staircase plots of the s -wave reduced neutron widths (middle plots) and the cumulative number of s -wave resonances (right hand plots). E_{\min} and E_{\max} define the energy range of interest for the ESTIMA method (see Eq. (13)).

Table 9

s-wave mean level spacing (in eV) for the nuclear systems of interest for this work. For the even/even isotopes, results obtained with the ESTIMA method are compared with those deduced from the radiative strength.

Nuclear system	Mughabghab [39]	RIPL-2 [40]	ESTIMA	From S_γ
n+ ¹⁷⁴ Hf	21.5±5.0	18.0±5.0	15.2±4.2	16.4±1.5
n+ ¹⁷⁶ Hf	29.0±3.0	30.0±7.0		33.9±2.4
n+ ¹⁷⁷ Hf	2.4±0.3	2.4±0.3	2.4±0.1	
n+ ¹⁷⁸ Hf	44.1±2.9	57.0±6.0	59.4±5.1	68.7±5.2
n+ ¹⁷⁹ Hf	4.1±0.3	4.6±0.3	4.4±0.2	
n+ ¹⁸⁰ Hf	94.0±11.0	94.0±15.0	138.0±7.2	115.2±22.0

tems n+¹⁷⁶Hf and n+¹⁸⁰Hf. Missing resonances and incorrect isotopic assignments of several weak resonances could explain the deviation of the experimental results from the systematic. For n+¹⁸⁰Hf, similar conclusions arise when we compare our results with those reported in the literature (Table 9). New time-of-flight measurements on isotopically enriched hafnium samples are needed to solve these ambiguous results.

5.4. Level density parameters

The unresolved resonance range is characterized by a weak energy dependence of the model parameters. Therefore, if the energy dependence of the level density parameter a is neglected, the continuum spectra of the compound nucleus can be adequately described by the semi-empirical composite level density formula of Gilbert and Cameron [50]. The adopted expression can be written as follows:

$$\rho_J(E) = \rho(E) \frac{2J+1}{4\sigma^2(E)} \exp\left(-\frac{(J+1/2)^2}{2\sigma^2(E)}\right) \quad (17)$$

with

$$\sigma^2(E) = 0.0888A^{2/3} \sqrt{a(E-\Delta)} \quad (18)$$

On both sides of the matching energy E_m , behavior of the lower levels is described by the constant temperature approximation ($E < E_m$) and the Fermi-gas model ($E > E_m$):

$$\rho(E) = \begin{cases} \frac{1}{T} \exp\left(\frac{E-E_0}{T}\right) & E < E_m \\ \frac{\exp(2\sqrt{a(E-\Delta)})}{12\sqrt{2}a^{1/4}(E-\Delta)^{5/4}\sigma(E)} & E > E_m \end{cases} \quad (19)$$

The matching energy E_m , corrected for pairing energy Δ , can be calculated as follow [51,52]:

$$E_m = \frac{T}{2} (aT - 3 + \sqrt{aT(aT - 6)}) + \Delta \quad (20)$$

The energy shift E_0 is given by:

$$E_0 = E_m - T \ln\left(\frac{T \exp(2\sqrt{a(E_m - \Delta)})}{12\sqrt{2}a^{1/4}(E_m - \Delta)^{5/4}\sigma(E_m)}\right) \quad (21)$$

Assuming equal probability for both parities (+ and -), the level density parameter a can be determined by solving transcendental equations that depend of the ground state spin I of the target nucleus:

$$1/D_0 = \begin{cases} \frac{1}{2}\rho_{1/2}(B_n) & I = 0 \\ \frac{1}{2}\rho_{J-1/2}(B_n) + \rho_{J+1/2}(B_n) & I \neq 0 \end{cases} \quad (22)$$

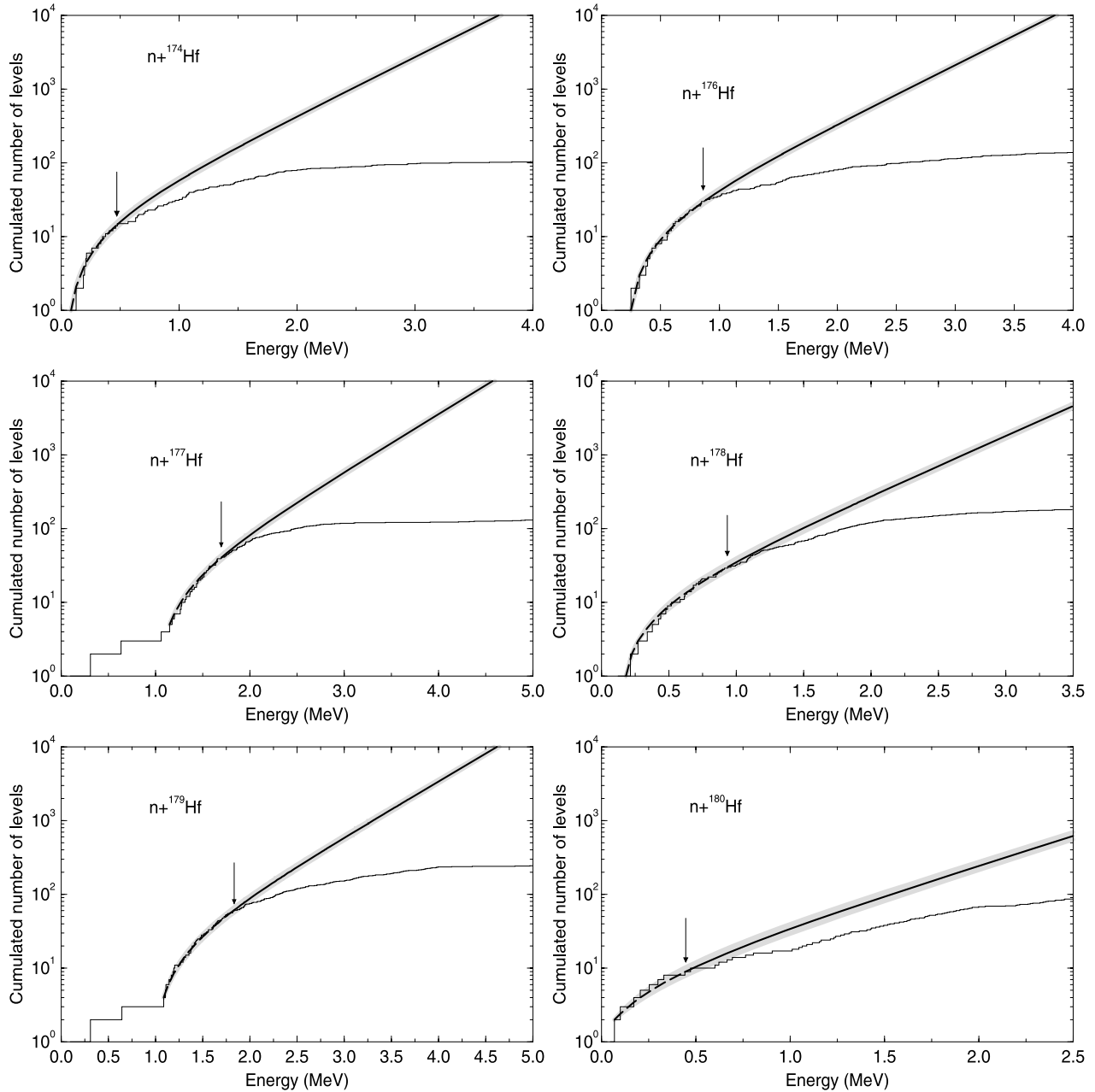


Fig. 13. Comparison of the experimental cumulated number of levels [40] with the constant temperature model (Eq. (19)) for the compound nuclei of interest for this work. The energy E_d where the level continuum was supposed to start is marked by an arrow (see Table 10).

Nuclear level density parameters and matching conditions established in the frame of the Gilbert–Cameron model are reported in Table 10. For the nuclear temperature T , values ranging from 0.53 MeV to 0.57 MeV were determined by fitting the cumulative numbers of low-lying nuclear levels (Fig. 13). The mean value of T is close to 0.549 MeV and the standard deviation is about 0.014 MeV (2.5%). Nuclear temperatures with variations in the same order of magnitude (0.52 MeV–0.54 MeV) are compiled in RIPL-2 [40]. However, a closer inspection of the major discrepancy of about 7% between the temperature obtained for the $n+^{178}\text{Hf}$ and $n+^{179}\text{Hf}$ nuclear systems provides clear evidence of the dependence of T with the E_d threshold of the fitting region and with the number of missing levels. The degree of completeness of the discrete level

Table 10

Level density parameters established in the frame of the Gilbert–Cameron formula [50]. The accuracies quoted for the nuclear temperature T , the energy shift E_0 and the matching energy E_m are fit uncertainties.

	$n+^{174}\text{Hf}$	$n+^{176}\text{Hf}$	$n+^{177}\text{Hf}$	$n+^{178}\text{Hf}$	$n+^{179}\text{Hf}$	$n+^{180}\text{Hf}$
D_0 (eV)	15.17 ± 4.24	33.90 ± 2.40	2.44 ± 0.05	59.41 ± 5.12	4.41 ± 0.23	137.96 ± 7.21
D_1 (eV)	3.22 ± 0.54	11.67 ± 0.83	1.27 ± 0.03	20.47 ± 2.80	2.28 ± 0.12	47.60 ± 2.49
D_2 (eV)	3.33 ± 0.93	7.47 ± 0.54	0.90 ± 0.06	13.12 ± 1.80	1.61 ± 0.08	30.60 ± 0.61
D_3 (eV)	2.61 ± 0.74	5.88 ± 0.42	0.74 ± 0.02	10.35 ± 1.43	1.31 ± 0.07	24.24 ± 1.28
a (1/MeV)	22.39 ± 0.71	21.83 ± 0.16	22.32 ± 0.05	21.60 ± 0.34	21.71 ± 0.11	21.22 ± 0.12
σ	5.62 ± 0.04	5.53 ± 0.01	5.65 ± 0.01	5.46 ± 0.02	5.58 ± 0.01	5.35 ± 0.01
E_m (MeV)	5.78 ± 0.11	5.61 ± 0.10	6.88 ± 0.11	5.33 ± 0.16	7.13 ± 0.11	5.31 ± 0.20
E_0 (MeV)	-1.31 ± 0.07	-1.17 ± 0.07	-0.55 ± 0.07	-1.00 ± 0.10	-0.77 ± 0.07	-0.98 ± 0.13
T (MeV)	0.545 ± 0.005	0.545 ± 0.005	0.555 ± 0.005	0.535 ± 0.008	0.575 ± 0.005	0.540 ± 0.010
N_d	15	32	41	30	61	8
E_d (MeV)	0.475	0.883	1.698	0.936	1.839	0.329

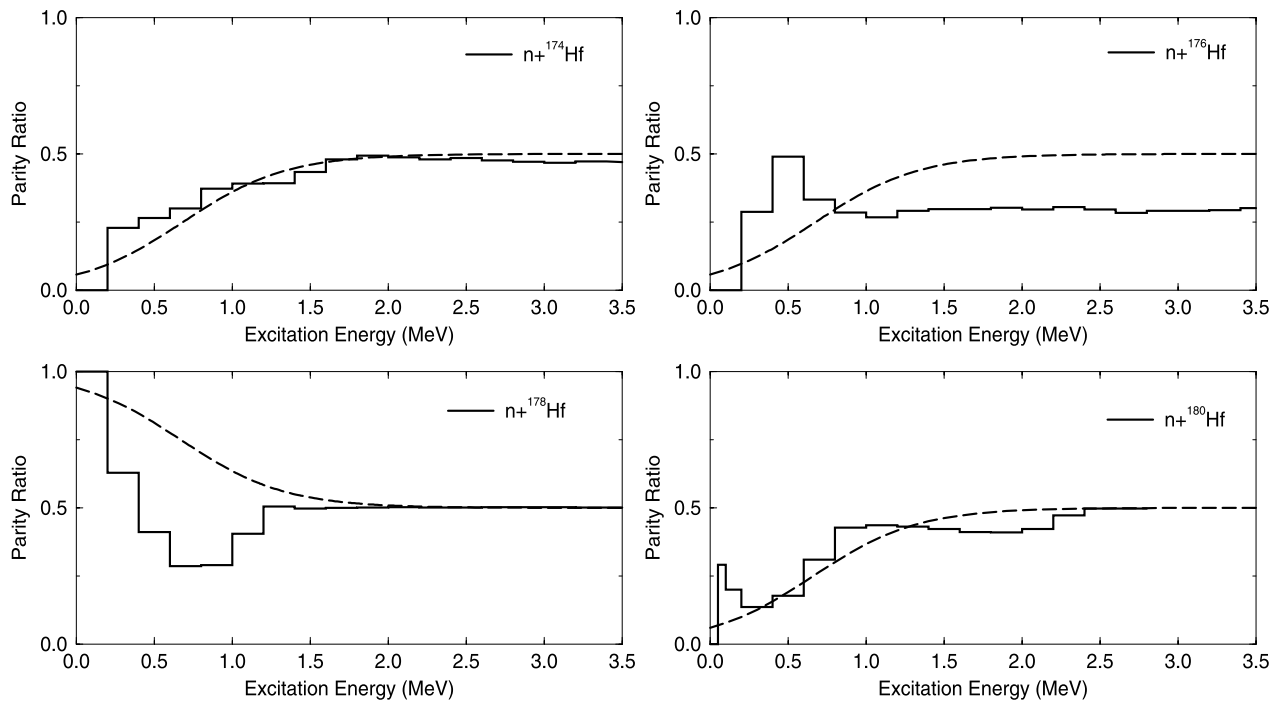


Fig. 14. Parity ratio (Eq. (23)) as a function of the excitation energy for the even/even Hf isotopes. The dashed line are systematics calculated with parameters reported in Ref. [46].

schemes adopted for the even/even Hf isotopes has been investigated by checking the smooth behavior with the excitation energy of the parity ratio parameter:

$$\pi(E) = \frac{\rho_+(E)}{\rho_+(E) + \rho_-(E)} \quad (23)$$

Fig. 14 shows the parity ratio constructed by calculating the ratio of the number of positive parity levels to the total number of levels in that bin. Comparisons with systematics taken from Ref. [46] show the reasonable behavior of the $n+^{174}\text{Hf}$ and $n+^{180}\text{Hf}$ discrete level schemes, while discrepancies observed for the $n+^{176}\text{Hf}$ and $n+^{178}\text{Hf}$ nuclear systems suggest missing experimental information in the level schemes adopted in this work. Therefore, an improved

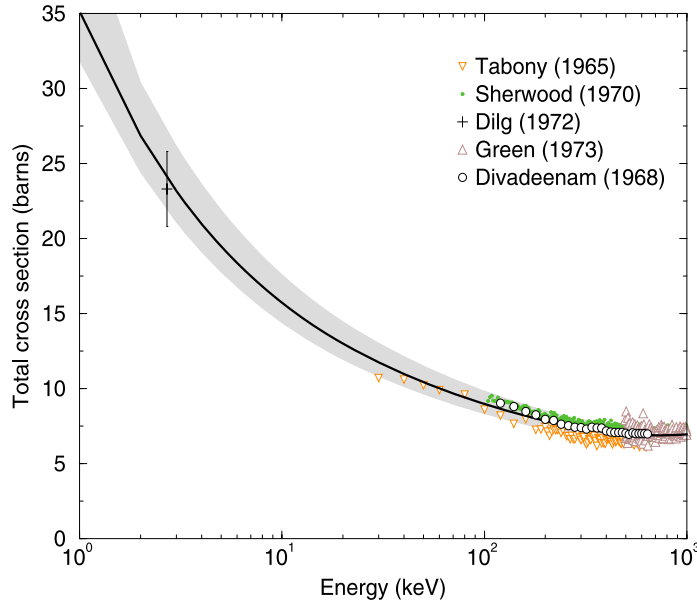


Fig. 15. Natural hafnium total cross section calculated from the CONRAD results obtained for each Hf isotope. The experimental data were retrieved from EXFOR [19].

methodology is needed to account for these poorly known sources of experimental uncertainties during the adjustment of the nuclear temperature.

6. Modeling of the neutron cross sections

The focus of this section is to describe the neutron induced reactions within the energy limit of the unresolved resonance range of the Hf isotopes. In the present work, the upper limit of this energy range was extended up to 1 MeV.

Average parameters determined in this work (see Tables 6, 7 and 10) were introduced in the CONRAD code. The corresponding total and capture cross sections were compared with results obtained from two independent calculations. The first one is based on ECIS and TALYS using the optical model parameters established by Morillon et al. [12,13]. The second calculation uses a local approach as given in Ref. [15] with ECIS results based on deformed optical model parameters of Young. In both cases, ECIS calculations were performed by using $\beta_{i=2,4}$ values of Table 7.

ECIS and CONRAD basically share the same formalism to calculate the total, shape elastic and reaction cross sections. In ECIS, elements of the collision matrix are calculated from a given phenomenological optical model potential, while CONRAD uses an average formulation of the R-Matrix theory parameterized in terms of l -dependent neutron strength function S_l and distant level parameters R_l^∞ [53,54]. Figs. 15 and 16 compare the CONRAD results with experimental total cross sections retrieved from EXFOR [19]. The uncertainties on the calculated total cross sections (gray zones) were deduced from the accuracy of the deformation parameters reported in Table 7. Measurements for each Hf isotope and for the natural element are well reproduced by the theoretical curves. A closer inspection of the CONRAD and ECIS results indicates that the discrepancies with the calculations based on the optical model parameters of Morillon et al. [12,13] remain below 5% at 1 MeV. The total cross section obtained with the optical model parameters of Young (see Ref. [15]) remains within the limit of the theoretical uncertainties.

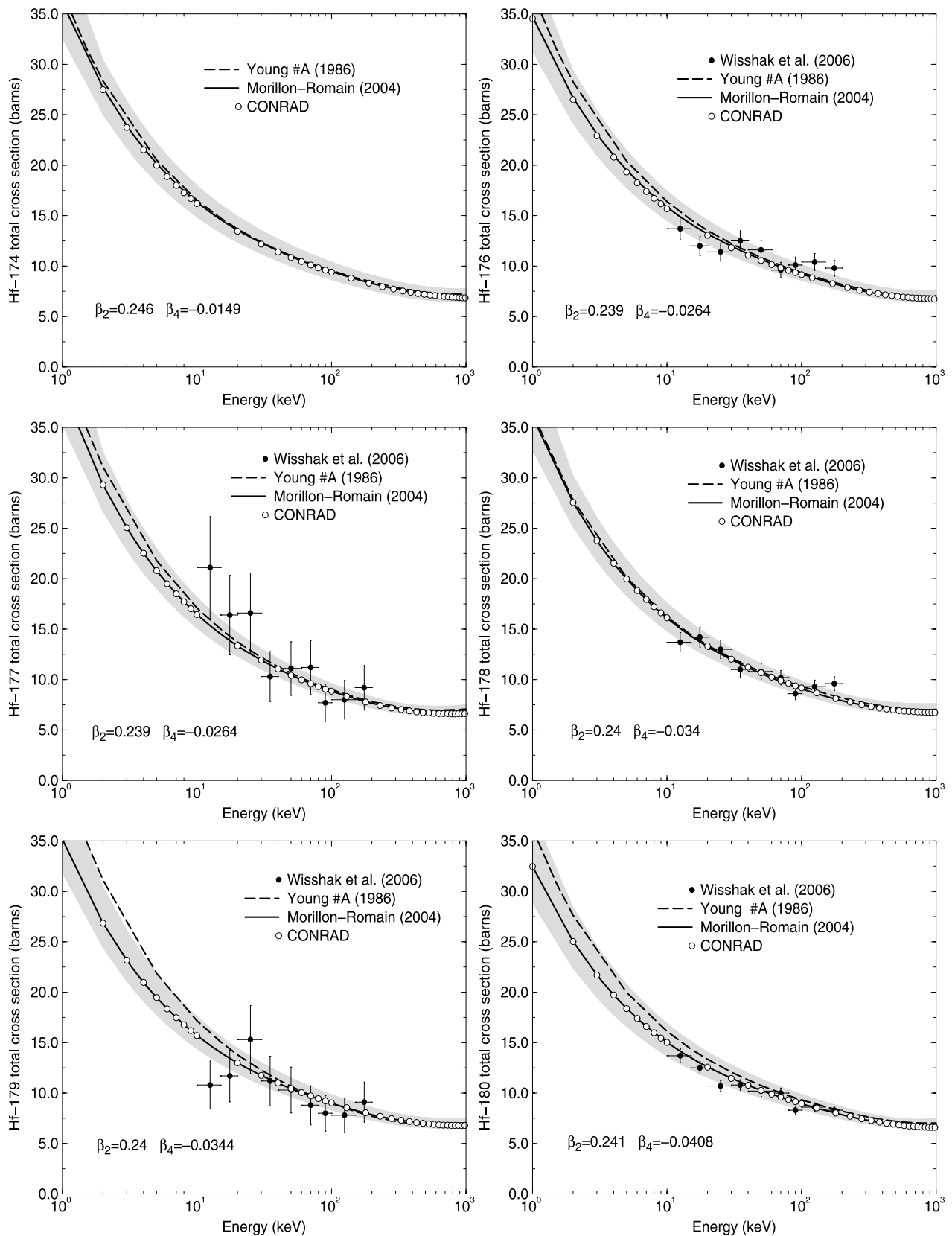


Fig. 16. CONRAD results compared with ECIS calculations based on the optical model parameters of Morillon et al. [12,13] and Young (see Ref. [15]) using deformation parameters from Table 7. Experimental data were measured at the VdG facility of Karlsruhe with the time-of-flight technique [19].

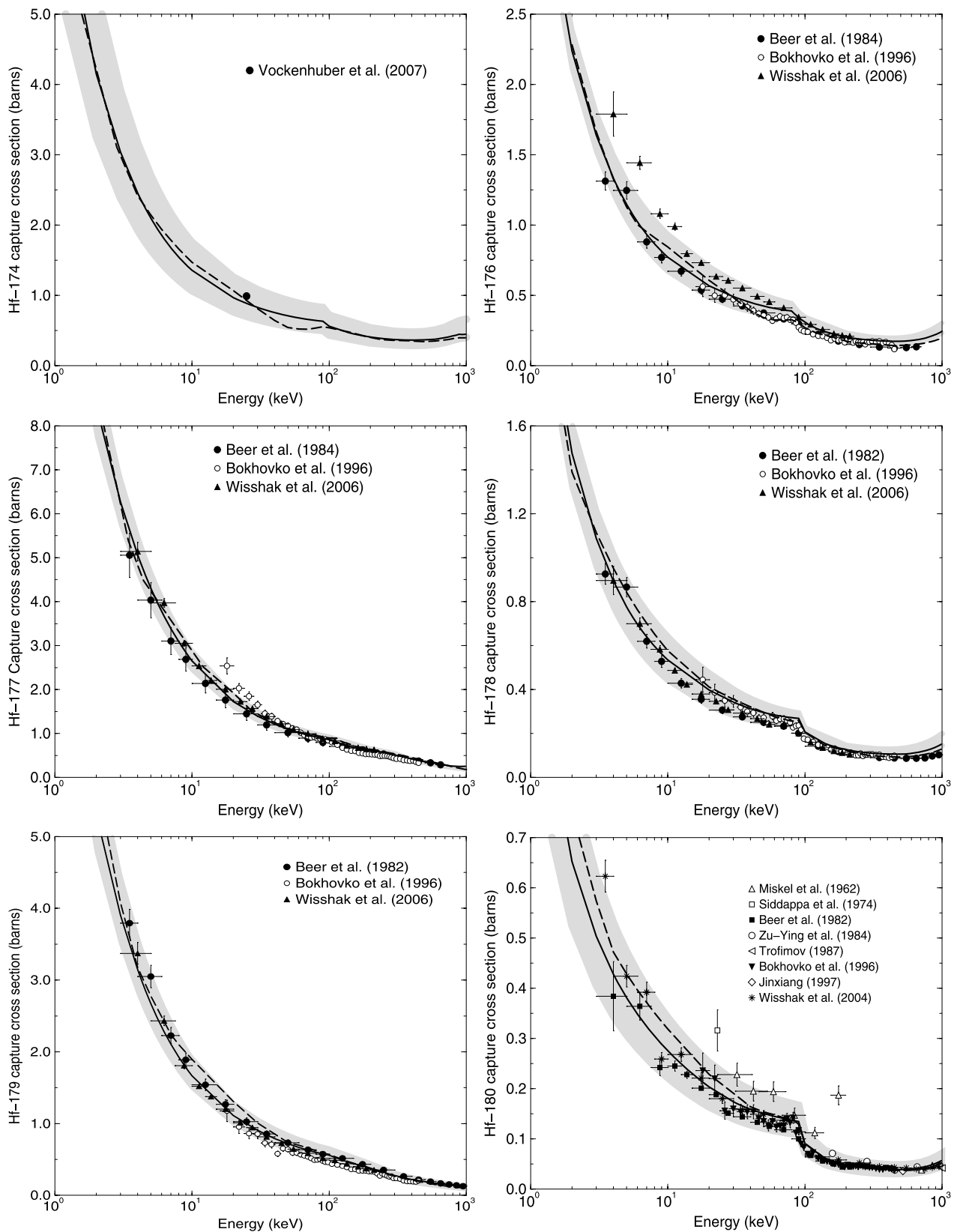


Fig. 17. CONRAD results (solid line) and uncertainties (gray zones) obtained by using the average parameters and the uncertainties reported in Tables 6, 7 and 10. They are compared with calculations (dashed line) based on the local approach and parameters given in Section 3.2.4 of Ref. [15] with the average radiation widths from Table 6 of this work. The experimental data were retrieved from EXFOR [19].

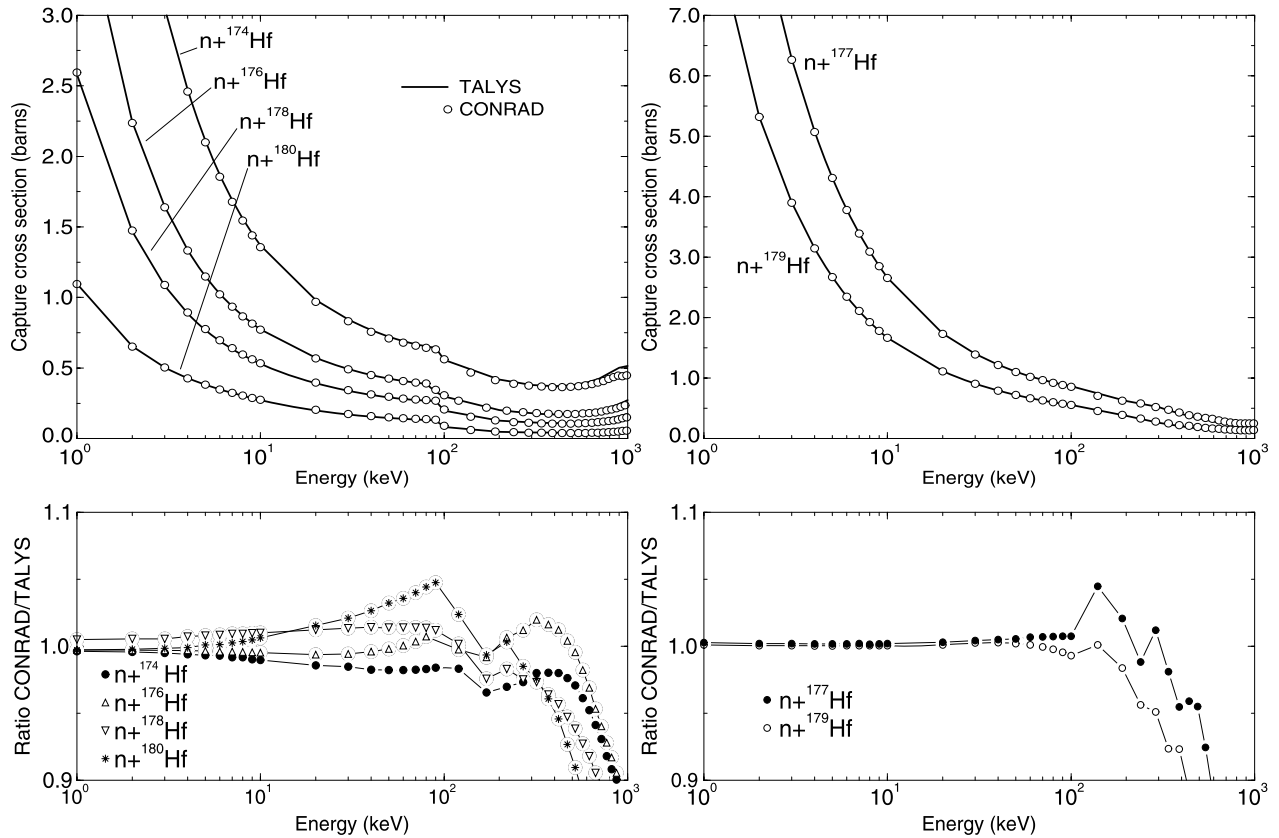


Fig. 18. Comparison of the capture cross sections produced by the CONRAD and TALYS codes.

For the modelling of the partial cross sections, CONRAD uses the Hauser–Feshbach formalism with width fluctuations corrections based on the Moldauer’s prescriptions [55]. For the capture cross section, the treatment of the γ -ray strength function is somewhat simpler than the models included in high energy codes. CONRAD takes only into account the electric- and magnetic-dipole transmission coefficients for multipolarity $l = 1$. The $E1$ radiation is described in the form of a Brink–Axel Lorentz line [47,48], while the energy dependence of the $M1$ γ strengths is given by a simple model as proposed by Blatt and Weisskopf [56]. Parameters of the photon transmission coefficients are taken from Ref. [57]. The consistency of the average radiation widths (Table 6) and of the level density parameters (Table 10) obtained in this work was verified with capture cross sections retrieved from EXFOR. As shown Fig. 17, agreements between the CONRAD results (solid line) and the experimental data remain within the limit of the theoretical uncertainties (gray zones). An overall good agreement is also obtained with the capture cross sections (dashed line) based on the local approach of Ref. [15]. In the latter approach, the energy-dependent spectral factor for $E1$ transition $f_{E1}(E_\gamma)$ has been obtained by means of a modified energy-dependent Breit–Wigner (EDBW) model [58,59]. Systematic correction factors F_{SR} within the EDBW formula were obtained by using the average radiation widths $\langle \Gamma_\gamma \rangle$ of the s -wave neutron resonances given in Table 6, and assuming that $F_{SR} = \langle \Gamma_\gamma \rangle / \Gamma_\gamma^{EDBW}$. Actually, the $f_{E1}(E_\gamma)$ thus obtained have been checked within the calculations of capture cross sections of Hf, Ta, and W isotopes in the neutron energy range from keV to 2–3 MeV (Refs. [14,15] as well as the present work), by using the OMP and nuclear level density parameters described above and global estimations [60] of the γ -ray strength functions for multipoles $\lambda \leq 3$.

As CONRAD and TALYS use the same statistical formalism to describe the compound nucleus reactions, results produced by the two codes are compared in Fig. 18. For the TALYS

calculations, the γ -ray strength function model for $E1$ radiation is based on the Kopecky–Uhl Lorentzian form [49]. The Brink–Axel shape is used for all transition types other than $E1$. The Giant Dipole Resonance parameters are taken from RIPL-2. In the lower energy part of the unresolved resonance range, where S_γ is nearly constant, values of the Hf capture cross sections calculated via the average parameters are close to those provided by the TALYS calculations. The increasing discrepancies observed above few hundreds of keV (~ 300 keV) mainly depend on the parameterization of the giant dipole resonance shape used in both codes.

7. Conclusion

This paper reports a consistent set of l -dependent model parameters for the Hf isotopes (γ -strength function, neutron strength function, potential scattering, distant level parameters, level density parameters). It was established by merging results provided by the statistical analysis of the resolved resonance range (ESTIMA approach) with results given by a generalized formulation of the conventional SPRT method. The average value of the parameters was mainly deduced from recent time-of-flight measurements performed at the GELINA facility and from the smooth behavior of the deformation parameters around $A = 177$ proposed by Moller and Nix. As suggested in previous works, we have obtained β_2 values close to 0.24 and β_4 values ranging from -0.015 to -0.04 . These results lead to neutron strength functions for s - and p -waves close to 2.1×10^{-4} and 1.0×10^{-4} respectively. For S_2 , values higher than 3.0×10^{-4} are confirmed by the present work.

These Hf model parameters were successfully used in the cross section models of CONRAD (average R-Matrix formalism and Hauser–Feshbach calculations) to accurately reproduce experimental data within the unresolved resonance range. Our study has demonstrated the need to merge conventional resonance shape analysis with systematics to determine reliable normalization factors for the ^{176}Hf capture cross section. Additional calculations have also shown that the CONRAD code provides cross section values consistent with those calculated by the sequential application of the ECIS and TALYS codes. Discrepancies remain below 5% up to few hundreds of keV (~ 300 keV).

Parallel studies were performed to provide reliable uncertainties on the model parameters. In a first approximation, the present work confirms the magnitude of the $\langle \Gamma_\gamma \rangle$ and D_0 uncertainties recommended by Mughabghab in his Atlas of Neutron Resonances. However, for the neutron strength functions and deformation parameters, the method used for the statistical analysis of the resolved resonance parameters represents the main source of uncertainties. Additional works are needed to reduce this contribution in order to favorize impact of the well known experimental uncertainties inherent to time-of-flight measurements.

Acknowledgements

Thanks are addressed to Arjan Koning for the valuable discussions and its relevant advices on using TALYS. We also express our gratitude to M. Moxon and T. Ware for the help in the correction of this work. This work was also partly supported by the CNCSIS-Bucharest project No. ID_43/2008 and the European Commission within the Sixth Framework Program through NUDAME (EURATOM contract No. FP6-516487).

References

- [1] T. Fuketa, J.A. Harvey, Report ORNL-3778, Oak Ridge National Laboratory, 1965.

- [2] T. Fuketa, J.E. Russell, R.W. Hockenbury, Report RPI-328-68, Rensselaer Polytechnic Institute, 1966.
- [3] M.C. Moxon, et al., Report AERE-R7864, Harwell laboratory, 1974.
- [4] H.I. Liou, et al., Phys. Rev. C 11 (1975) 2022.
- [5] G. Rohr, H. Weigmann, Nucl. Phys. A 264 (1976) 93.
- [6] M.J. Trbovich, et al., Nucl. Sci. Eng. 161 (2009) 303.
- [7] N.M. Larson, et al., in: O. Bersillon, et al. (Eds.), Proceedings of the International Conference on Nuclear Data for Science and Technology, Nice, France, 2007, EDP Science, 2008, p. 641.
- [8] P. Siegler, K. Dietze, P. Ribon, J. Nucl. Sci. Tech. Suppl. 2 (2002) 940.
- [9] G. Noguere, et al., in: Proceedings of PHYSOR-2006 Topical Meeting on Reactor Physics, Vancouver, Canada, 2006, American Nuclear Society, 2006.
- [10] G. Noguere, et al., in: O. Bersillon, et al. (Eds.), Proceedings of the International Conference on Nuclear Data for Science and Technology, Nice, France, 2007, EDP Science, 2008, p. 301.
- [11] M.C. Moxon, J.B. Brisland, Report CBNM/ST/90-131/1, Harwell Laboratory, 1990.
- [12] B. Morillon, P. Romain, Phys. Rev. C 70 (2004) 014601.
- [13] B. Morillon, P. Romain, Phys. Rev. C 74 (2006) 014601.
- [14] V. Avrigeanu, et al., NEA Nuclear Data Services document EFFDOC-928, 2005.
- [15] V. Avrigeanu, et al., Nucl. Phys. A 765 (2006) 1.
- [16] J. Raynal, in: Proceedings of the Specialists' Meeting on the Nucleon Nucleus Optical Model up to 200 MeV, Bruyeres-le-Chatel, France, 1996, Nuclear Energy Agency, 1997.
- [17] E. Fort, J.P. Doat, Report NEANDC-161U, NEA Nuclear Data Committee, 1983.
- [18] E. Rich, et al., Nucl. Sci. Eng. 162 (2009) 76.
- [19] H. Henriksson, et al., in: O. Bersillon, et al. (Eds.), Proceedings of the International Conference on Nuclear Data for Science and Technology, Nice, France, 2007, EDP Science, 2008, p. 737.
- [20] A.J. Koning, S. Hilaire, M.C. Duijvestijn, in: R.C. Haight, et al. (Eds.), Proceedings of the International Conference on Nuclear Data for Science and Technology, Santa Fe, New Mexico, 2004, American Institute of Physics, 2005, p. 1154.
- [21] C. De Saint Jean, et al., in: O. Bersillon, et al. (Eds.), Proceedings of the International Conference on Nuclear Data for Science and Technology, Nice, France, 2007, EDP Science, 2008, p. 251.
- [22] G. Noguere, Report CEA-R-6071, CEA/DEN Cadarache, 2005.
- [23] C. Coceva, A. Magnani, Report GE/R/ND/06/96, Institut for Reference Material and Measurements, 1996.
- [24] M. Flaska, et al., Nucl. Instrum. Methods A 531 (2004) 392.
- [25] V. Gressier, Report DAPNIA/SPHN-99-04T, CEA/DSM Saclay, 1999.
- [26] W.E. Lamb, Phys. Rev. 55 (1939) 190.
- [27] H.J. Stone, et al., J. Appl. Phys. 98 (2005) 064905.
- [28] N.M. Wolcott, in: Proceedings of the Conference de physique des basses temperature, Paris, 1955, Centre National de la Recherche Scientifique, 1956, p. 286.
- [29] G.D. Kneip, et al., Phys. Rev. 130 (1963) 1687.
- [30] J.O. Betterton, J.O. Scarbrough, Phys. Rev. 168 (1968) 715.
- [31] S.A. Ostanin, V.Yu. Trubitsin, Comput. Mater. Sci. 17 (2000) 174.
- [32] H.X. Gao, L.-M. Oeng, Acta Cryst. 55 (1999) 926.
- [33] I.D. Feranchuk, A.A. Minkevich, A.P. Ulyanekov, Eur. Phys. J. Appl. Phys. 19 (2002) 95.
- [34] C. Kittel, Introduction to Solid State Physics, 7th ed., Wiley, New York, 1995.
- [35] G. Noguere, et al., Nucl. Sci. Eng. 160 (2008) 108.
- [36] C. De Saint Jean, et al., Nucl. Sci. Eng. 161 (2009) 363.
- [37] G. Noguere, Report NT-SPRC/LEPH-9/208, CEA/DEN Cadarache, 2009.
- [38] A. Santamarina, et al., JEFF Report 22, NEA Nuclear Data Services, 2009.
- [39] S.F. Mughabghab, Atlas of Neutron Resonances, 5th ed., Elsevier, Amsterdam, 2006.
- [40] T. Belgya, et al., Report IAEA-TECDOC-1506, IAEA Nuclear Data Services, 2005.
- [41] P. Moller, et al., At. Data Nucl. Data Tables 59 (1995) 185.
- [42] J.-P. Delaroche, Ch. Lagrange, J. Salvy, Report IAEA-190, IAEA Nuclear Data Services, 1976.
- [43] M. Herman, Report BNL-NCS-44945-05-Rev, Brookhaven National Laboratory, 2005.
- [44] F. Gunsing, et al., Phys. Rev. C 61 (2000) 054608.
- [45] S. Marrone, Phys. Rev. C 73 (2006) 034604.
- [46] S.I. Al-Quraishi, et al., Phys. Rev. C 67 (2003) 015803.
- [47] D.M. Brink, Nucl. Phys. 4 (1957) 215.
- [48] P. Axel, Phys. Rev. 126 (1962) 671.

- [49] J. Kopecky, M. Uhl, *Phys. Rev. C* 41 (1990) 1941.
- [50] A. Gilbert, A.G.W. Cameron, *Can. J. Phys.* 43 (1965) 1446.
- [51] G. Vladuca, et al., *Nucl. Phys. A* 720 (2003) 274.
- [52] G. Vladuca, et al., *Nucl. Phys. A* 740 (2004) 3.
- [53] A.M. Lane, R.G. Thomas, *Rev. Mod. Phys.* 17 (1960) 563.
- [54] F.H. Frohner, *Nucl. Sci. Eng.* 103 (1989) 119.
- [55] P. Moldauer, *Phys. Rev.* 123 (1961) 968.
- [56] J.M. Blatt, V.F. Weisskopf, *Theoretical Nuclear Physics*, John Wiley and Sons, New York, 1952.
- [57] J.A. Holmes, et al., *At. Data Nucl. Data Tables* 15 (1976) 306.
- [58] D.G. Gardner, F.S. Dietrich, Report UCRL-82998, LLNL-Livermore, 1979.
- [59] M. Avrigeanu, V. Avrigeanu, G. Cata, M. Ivascu, *Rev. Roum. Phys.* 32 (1987) 837.
- [60] C.H. Johnson, *Phys. Rev. C* 16 (1977) 2238.